General Disclaimer

One or more of the Following Statements may affect this Document

- This document has been reproduced from the best copy furnished by the organizational source. It is being released in the interest of making available as much information as possible.

- This document may contain data, which exceeds the sheet parameters. It was furnished in this condition by the organizational source and is the best copy available.

- This document may contain tone-on-tone or color graphs, charts and/or pictures, which have been reproduced in black and white.

- This document is paginated as submitted by the original source.

- Portions of this document are not fully legible due to the historical nature of some of the material. However, it is the best reproduction available from the original submission.

STD RESEARCH CORPORATION
BOX 4127, CATALINA STATION • PASADENA, CALIFORNIA 91106
TELEPHONE: (213) 684-1771

Contract No. NAS 2-3580

STD-69-1

DETERMINATION OF ENERGY-LOSS FACTORS FOR SLOW ELECTRONS IN HOT GASES

FINAL REPORT

Covering the period 28 April 1966-15 August 1969

Prepared for

National Aeronautics and Space Administration
Ames Research Center
Magnetoplasmadynamics Branch
(Howard Stine, Technical Monitor, Mail Station N-229)
Moffett Field, California 94035

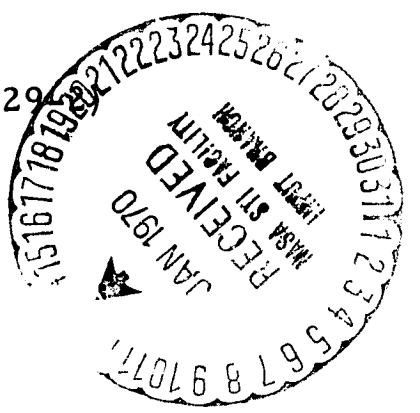

15 August 1969

CONTENTS

LIST OF FIGURES

LIST OF TABLES

LIST OF SYMBOLS

A_r	Cross sectional area of waveguide
A_{nm}	Einstein coefficient for spontaneous emission of radiation for transition from state n to state m
$\vec{B}$	Magnetic induction
B	Half-power width of a waveguide resonance, equation B2
c	Speed of light in vacuum
e	Elementary charge. Charge of electron is -e
E	Applied (rf) electric field, $\vec{E}$ = electric field vector
E_o	Amplitude of applied (rf) electric field
$\vec{E}'$	$\vec{E}' \equiv \vec{E} + \vec{U} \times \vec{B}$
f	Frequency (Hertz)
f_{o1}	Oscillator strength, equation G9
h	Planck constant
H_o	Stagnation enthalpy
I_2	Intensity of nitrogen afterglow, equation C5
I_4	Intensity of air afterglow, equation C7
I_ν	Intensity of spectral line with frequency ν. In appendix G, I_o is the intensity of a particular line with frequency ν_o
I_{ν_o}	Total intensity, integrated over the full line width $\Delta\nu$, of a spectral line with frequency ν; equation G2
I	Current in the Langmuir probe. In appendix D, I_o and I' are particular values of the current
I_e	Electron current in the Langmuir probe. I_{esat} is the electron saturation current
I_i	Ion current in the Langmuir probe. I_{isat} is the ion saturation current
j_{esat}	Electron saturation current density at Langmuir probe
j_{isat}	Ion saturation current density at Langmuir probe
$\vec{J}_e$	Total electron current

k	Boltzmann constant
k_1	Reaction constant, equation 43
k_ν	Absorption coefficient, equation G5
k_o	Defined in equation G9
K_{nm}	Collisional transition rates in argon, level n to level m; appendix F
ℓ	Unit distance in which argon plasma properties are constant, appendix G
L_E	Electron energy relaxation length
m_e	Mass of the electron
m_i	Mass of an ion
m_κ	Mass of a molecule of species κ
n_a	Neutral particle number density
n_e	Electron number density
n_i	Ion number density
n_κ	Number density of species κ
n_o	Number density of absorbing ground state argon atoms, equation G9
p	Pressure
p	In appendix B, the longitudinal eigennumber of a waveguide mode
p_e	Pressure of the electron gas
P	Applied rf power
P_1	Power associated with a forward propagating wave
P_2	Power associated with a backward propagating wave
$\vec{q}_e$	Energy flux vector for electrons, equation 8
Q_{ea}	Collision cross section for momentum transfer between electrons and neutral particles of species a
$Q_{e\kappa}$	Effective cross section for momentum transfer between electrons and species κ
Q_L	Quality factor of microwave cavity under load
Q_o	Quality factor of microwave cavity, uncoupled
Q_c	Quality factor of coupling element

Q	Quality factor, general, appendix B
$Q(\epsilon)$	Monoenergetic collision cross section for vibrational excitation or de-excitation of nitrogen by electrons of energy ϵ. Total cross section is $Q_{e_{N_2}, ex}(T_e)$ or $Q_{e_{N_2}, de}(T_e)$
r	Radius of the plasma jet
$R_e^{(2)}$	Collisional energy exchange integral
$\dot{R}$	Radiative energy loss rate (erg sec^{-1} cm^{-3})
R	Power reflection coefficient of microwave cavity
R_1, R_2	Value of the two resistances which make up the voltage divider in the Langmuir probe circuit
R_s	Resistance of the shunt resistor in the Langmuir probe circuit
R_{ex}	Normalized rate of nitrogen vibrational excitation by electron collision
R_{de}	Normalized rate of nitrogen vibrational de-excitation by electron collision
s_i	Rate of reaction i (sec^{-1} cm^{-3}), equation 9
$\dot{S}$	$\dot{S} \equiv \sum_i s_i \epsilon_i$
S	Standing wave ratio of microwave cavity
t	Time
Δt	Unit interval of time, equation D1
t_E	$t_E = L_E/U$
T	Temperature
T_e	Electron temperature
ΔT_e	Increment of electron temperature
T_a	Temperature of neutral species
T_i	Ion temperature
T_κ	Temperature of species κ; T_g = effective gas temperature
T_{trans}	Temperature associated with translational motion, T_{tr}
T_{rot}	Temperature of rotational degrees of freedom
T_{vib}	Temperature of vibrational degrees of freedom
T_o	Stagnation Temperature
T_{elec}	Temperature of electronic degrees of freedom
$T_{\kappa, s}$	$T_{\kappa, tr}$, $T_{\kappa, rot}$, or $T_{\kappa, vib}$ (see equation 9)
T_n	Reference temperature, equation 10

T_{eff}	Effective temperature for ionization ($T_{eff, ion}$) or recombination ($T_{eff, rec}$)
u	Defined in equation E12
u_o	The value of u when $T_{vib} = T_e$
$\vec{U}$	Mass average velocity of gas; velocity magnitude is U
v	In appendix E, the vibrational quantum number of the nitrogen molecule
v	In appendix G, the velocity of absorbing argon atoms in the rest frame
v_{ea}	Mean electron velocity, $(8kT_e/\pi m_e)^{1/2}$, for a Maxwellian distribution
V	Measured Langmuir probe bias voltage, V_o is a particular value of V
V_d	Voltage across the divider circuit in figure 1
V_P	Voltage from the probe to ground in figure 1. V_P' results from fluctuations in the current I_o
V_s	Langmuir probe bias at electron saturation
V_e	Effective volume from which electrons are collected by Langmuir probe, equation D1
V_i	Effective volume from which ions are collected by Langmuir probe
$\vec{w}_e$	Particle velocity (drift) relative to mass average velocity
$\vec{W}_e$	Average of $\vec{w}_e$ over velocity distribution, $\vec{W}_e = \langle \vec{w}_e \rangle$
W	Local power density in microwave cavity
x	Coordinate along direction of flow; Δx is an interval in the x-direction
X	Ratio of argon number density to seed number density in the application of the mixture rule, appendix A
Z	Waveguide impedance
α	Defined in equation G8
δ_κ	Energy loss factor, average fraction of energy lost per collision between an electron and a molecule of species κ
$\delta_{\kappa, s}$	Energy loss factor for the s class of energy states (translational, rotational or vibrational) for species κ

δ_{eif}	Effective energy-loss factor for a gas mixture. $\delta_{eff} \equiv \sum_{\kappa} \sum_{s} \delta_{\kappa, s} \cdot (\tau_{e, \kappa}^{-1}/\nu_t)(T_e - T_{\kappa, s})/(T_e - T_n)$
ϵ_i	Energy per reaction, equation 2
ϵ_v	Transition energy from one nitrogen vibrational level to the next successive level
ϵ	Electron energy, equation E11
θ	Characteristic temperature for vibration excitation, equation E12
λ	Wavelength, $\lambda_o = 1038$ Å in appendix G
λ_r	Photon mean-free-path
$\nu_{e, \kappa}$	Collision frequency for electrons with molecules of species κ
ν_t	$\nu_t \equiv n_a Q_{ea} (8kT_e/\pi m_e)^{1/2}$
ν	Photon frequency, spectral line frequency
$\Delta\nu$	Full width of spectral line
$\Delta\nu_D$	Doppler width of spectral line
$\overleftrightarrow{\pi}_e$	Electron pressure tensor, $\overleftrightarrow{\pi}_e = \rho_e \langle \vec{w}_e \vec{w}_e \rangle$
ρ	Density
ρ_o	Density at STP
ρ_κ	Density of species κ
$\sigma_{\delta_{eff}}$	Standard deviation on measurements of δ_{eff}
$\sigma_{\Delta T_e}$	Standard deviation on measurements of ΔT_e
$\tau_{e, \kappa}$	Effective collision time for momentum transfer between electrons and particles of species κ, $(4/3)\tau_{e, \kappa} = 1/\nu_{e, \kappa}$
$\overleftrightarrow{\tau}_e$	Viscous stress tensor
ϕ	$-\phi$ is the first term of $R_e^{(2)}$, defined in equation E2
ϕ_s	Contribution to ϕ from the s class of energy states (translational, rotational, vibrational)
ω	$\omega \equiv 2\pi f$
ω	Quantity defined by equation G7
$\dot{\Omega}$	Ohmic heating, equation E4

Subscripts

$( )_e$	Quantities associated with electrons
$( )_s$	Quantities associated with the s class of energy states; s identifies the translational, rotational, or vibrational degrees of freedom
$( )_\kappa$	Quantities associated with species κ
$( )_{el}$	Values for elastic collisions
$( )_{inel}$	Values for inelastic collisions
$( )_E$	Values in the presence of an (rf) E field (except L_E, τ_E)
$( )_{E=0}$	Values in the absence of an (rf) E field

DETERMINATION OF ENERGY-LOSS FACTORS FOR SLOW ELECTRONS IN HOT GASES

by S. T. Demetriades and C. D. Maxwell
STD Research Corporation, Pasadena, California 91106

SUMMARY

The energy-loss factor for slow electrons of essentially Maxwellian energy distribution has been determined in a number of pure gases and gas mixtures as a function of electron temperature and gas enthalpy. The method used to make these measurements employed a high-frequency (2.45 GHz) electric field to elevate the temperature of the free electrons above the temperature of the arc-heated gas and a Langmuir probe to determine the electron temperature. The electron energy-loss factor is then obtained by measuring the rate of change of the electron temperature with the high frequency power used to illuminate the plasma.

Electron energy-loss factors δ_κ or δ_{eff} were obtained for pure argon, helium and nitrogen and binary mixtures of nitrogen, oxygen, carbon monoxide, carbon dioxide, nitric oxide and helium with argon. The mixture results were analyzed by means of a single mixture rule and the energy-loss factors for the pure constituent gases were thus derived. The argon-helium and argon-nitrogen mixture results yielded values of δ_κ for the pure gases that were in close agreement with the values obtained for δ_κ in pure nitrogen and helium. In addition, the δ_κ obtained for the pure gases by analyzing the mixture results were independent of the relative concentrations of the gases in the mixture (except in the case of nitric oxide).

In the course of these experiments values of δ_κ for helium and argon were obtained, under certain conditions, that were lower than the elastic values. This effect was ascribed to superelastic collisions between electrons and excited (e.g. metastable) states of these gases.

It is concluded that the results obtained in these investigations are of sufficient accuracy to be of use in the study of the detailed mechanisms and rates of electron energy relaxation in plasmas.

INTRODUCTION

Previous investigations (refs. 1 and 2) have demonstrated the feasibility and fundamental advantages of a novel method for determining the electron energy-loss factor in hot gases and have provided a detailed discussion of the theory on which this method is based as well as a description of the apparatus built to carry out the required measurements. The method can be briefly summarized as follows: It can be shown that the temperature of the free electrons in a weakly ionized gas is increased by illumination with a microwave field of relatively low power, and that the ratio of the microwave power to the temperature increment is proportional to the energy-loss factor for the electrons in the gas for a range of plasma parameters (ionization, enthalpy, density, etc.) and microwave parameters (frequency and power) that is relatively easy to achieve and determine in the laboratory. Moreover, the two primary variables, electron temperature and microwave power, lend themselves to precise measurement. Consequently the energy-loss factor can also be computed with corresponding precision.

In this investigation, the elevation of the temperature of the free electrons as a function of microwave illumination power, arc-heated gas enthalpy and composition is obtained for some pure gases (argon, helium and nitrogen) and for several mixtures of gases (argon-nitrogen, argon-oxygen, argon-helium, argon-carbon monoxide, argon-carbon dioxide and argon-nitric oxide. Electron energy-loss factors are then obtained from these results by means of the theory presented in reference 2 that relate the measured quantities to the energy-loss factor δ_κ for pure gases and δ_{eff} for gas mixtures.

The results obtained for the loss factor δ_κ of the pure constituent gases from the gas-mixture experiments are in excellent agreement with the results obtained from the pure-gas experiments and are independent of the relative concentrations of the gases in the mixture, except in the case of nitric oxide which apparently dissociates when heated in the presence of an excess of argon.

At the beginning of these experiments it was doubtful whether the measurements could be made sensitive enough over a broad microwave

power range to resolve the competing effects of electron energy gain due to superelastic collisions and energy loss due to radiation that appear (and become dominant in different gas enthalpy and electron temperature ranges) in the full electron energy balance equation given in reference 2. However, the precision of the measurements turned out to be such that these effects are readily observed for diatomic (nitrogen) as well as monatomic (argon and helium) gases. In fact, the precision of the measurements is such that deviations from the linear behavior expected on the basis of the first-order theory [equations (19) or (20) of reference 2] became readily apparent, and required the application of the more sophisticated non-linear theory [equations (16b) and (17a) of reference 2] for proper interpretation. In addition, the resolution afforded by the measurements made it necessary to develop more refined diagnostic methods for the determination of other plasma parameters, such as the species concentration and the population of particular excitation states or the energy state of the gas.

This report presents first the experimental results obtained in the course of this investigation. This presentation is followed by a discussion and interpretation of the observed behavior of the data in the light of the available theory and diagnostic information. This discussion advances the point that all observed phenomena can be explained on the basis of available information. However, the precise quantification of some of the observed phenomena (i.e., superelastic energy exchange with monatomic gases at low rf power and inelastic energy losses at high rf powers) must await more precise and reliable information on the mechanisms and cross sections for these processes. This lack of information (which is required to enable us to separate a priori and quantify the energy exchange mechanisms due to various processes at the two extremes of the electron energy or rf power range for all gases) dictates the order of presentation of our findings in this report, but in no way detracts from the usefulness of the data since, after all, the data yield the bulk (or global equivalent) energy exchange factor δ_{eff} for all energy exchange between electrons and all other species due to all processes as outlined in reference 2. In fact we may conclude that this investigation, perhaps for the first time, presents simultaneously, a consistent and detailed accounting of most of the important energy exchange

processes that occur between electrons and heavy species in a low temperature plasma and opens up a veritable Pandora's box of possibilities for studies of the detailed mechanisms and rates of electron energy relaxation and energy exchange between electrons and heavy particles in hot, excited gases, that may yield results pertinent to an astonishing variety of applications.

EXPERIMENTAL RESULTS

The primary measurements consist of the determination of the free electron temperature in the plasmajet by the Langmuir probe techniques described in reference 2 as a function of the applied rf illumination power. Several modifications of the Langmuir probe circuits described in reference 2 were devised in an attempt to improve the signal-to-noise ratio. Although this ratio was significantly improved by circuits such as the one shown in figure 1, the measured electron temperature elevation as a function of rf power is essentially the same for all probe circuits.

In the attempt to display δ_κ or δ_{eff} as a function of the electron temperature, the question arises whether it is better to calculate δ_{eff} for each measurement of P and ΔT_e and to fit a polynomial to these computed δ_{eff} points or to fit a polynomial to all the data for P and ΔT_e and then compute δ_{eff} from the points on the curve. The difficulty with the first approach is that the standard deviations of the δ_{eff} points* are often different by an order of magnitude, and a complicated statistical fit involving non-measured weighting factors would be required.

The superior method (from the point of view of convenience, at least as far as the pure gas experiments are concerned) is to fit a curve to the data for P and ΔT_e before δ_{eff} is computed. Since all of the ΔT_e have the same standard deviation (because all temperatures we measure have approximately the same experimental error, e.g. $\pm$ 100 ^{o}K) a simple polynomial fit (i.e., one without weighting factors) can be very accurate.

*The standard deviations of δ_{eff} points are given by $\sigma_{\delta_{eff}} = \delta_{eff}(\sigma_{\Delta T_e}/\Delta T_e)$, where $\sigma_{\Delta T_e} \approx$ standard error on ΔT_e.

Finally, δ_κ or δ_{eff} is computed as a function of T_e from the resulting polynomial by means of the relation

$$\delta_{eff}(T_e) = \frac{e^2}{3km_e\omega^2}\left(\frac{4Z}{A_r}\right)\frac{P}{T_e - T_{e,\,E=0}} = 0.287\,\frac{P}{\Delta T_e} \qquad (1)$$

given in reference 2, where P is in watts and ΔT_e in ^oK. Note that, strictly speaking, the symbol δ_κ is appropriate for the electron energy-loss factor of a pure monatomic gas with only one significant temperature T_g or for a polyatomic gas where $T_g = T_{trans} = T_{rot} = T_{vib} = \text{etc.}$ whereas the symbol δ_{eff} is appropriate either for a gas mixture or for a polyatomic gas where there is more than one significant temperature, $T_{trans} \neq T_{vib}$.

This method is followed in the determination of energy-loss factors in pure gases. For the binary mixtures, where molecular concentrations are often varied to test the validity and consistency of the data, it is more convenient to treat each measurement of P and ΔT_e separately to obtain a δ_{eff} since the solution of the mixture rule depends on molecular concentrations (see Appendix A). No attempt is made in that case to carry out the statistical fit necessary to arrive at a smooth curve for the energy-loss factors of the pure gases computed from the δ_{eff} of the mixture.

A computer was extensively used in this work to reduce the data whenever possible, to obtain least square fits, etc.

Determination of Loss Factors in Pure Gases

For argon, helium and nitrogen a quadratic curve can be fitted by least squares to the measured data points of electron temperature increment versus applied rf power and the corresponding energy loss factor for each electron temperature T_e (attained upon illumination of the plasma by an rf power P) can be computed from it.

Figures 2 and 3 present such data for argon. Figure 2 reveals two very interesting features, namely an elevation of the electron temperature that is initially, at very low rf powers, higher than the value specified by the first-order (linear) theory for an elastic energy-loss factor $\delta_{A,\,el} =$

2.727×10^{-5} and an elevation that becomes lower than the first-order theory for $\delta_{A,el} = 2.727 \times 10^{-5}$ above approximately 0.7 watts of illuminating rf power. When the first-order theory is used to analyze these data we obtain the $\delta_{A,eff}$ results shown in figure 3. Since the correct value, consistent with the theory of reference 2, for δ_A is $\delta_{A,el}$ it is clear that some process or processes are taking place at low rf powers that cause the electrons to gain additional energy, over and above the energy they gain from the rf electric field, while at higher rf powers (and higher electron temperatures) something is taking place that causes the electrons to lose more energy than they lose in elastic collisions.

Since the same general behavior was observed with helium (see figures 4 and 5), and, at least at high rf powers, perhaps even with nitrogen (see figures 6, 7 and 8) we can rule out a systematic experimental error. Rather, we must seek an explanation in the violation of some of the constraints (ref. 2) within which the simple first-order theory is valid.

A careful examination of these constraints reveals, as discussed in a later section, that at least for argon and helium the simple first-order theory is not valid except in a very limited range of rf powers. When the full non-linear theory of reference 2 is used and corrections are made for energy gains by the electrons from energy-storing species and energy losses due to radiation the elastic electron energy-loss factors for argon and helium may be recovered with great accuracy, as explained in a later section.

Figures 6 and 7 present the measured electron temperature increment as a function of applied rf power for nitrogen at two values of the gas enthalpy. Figure 8 presents the corresponding energy loss factors. In a later section it is shown that the difference in the results for each enthalpy level can be easily explained on the basis of an increase in the population of the vibrationally excited states of nitrogen with an increase in gas enthalpy. To understand why the energy loss factor for nitrogen decreases at a given T_e with an increase in enthalpy, note that if a minor correction is introduced in these results to account for the increase in energy gain of the electrons due to collisions with the vibrationally excited nitrogen molecules,

whose concentration increases at the higher enthalpy, we can shift the higher enthalpy curve of figure 8 higher so that the two curves coincide and the energy loss factor continues to rise with an increase in T_e, as it should, if the concentration of vibrationally excited nitrogen molecules remains constant with an increase in enthalpy. Eventually, all or nearly all the molecules are vibrationally excited to some level or other as the enthalpy increases and from that point on the electron temperature influence on the energy loss factor is predominant and δ_{N_2} increases steeply with electron temperature since, at that enthalpy level, the initial electron temperature $T_{e, E=0}$ is also quite high (because it is coupled to T_{vib} which is approximately equal to 80% of the stagnation temperature T_o). Thus from limited data in the enthalpy range from 4×10^6 joules/kg to 6×10^6 joules/kg we have found that δ_{N_2} is of the order of 10^{-2} at $T_{e, E=0} \approx 5,000\ ^oK$ and $T_e \approx 5,500\ ^oK$.

Since with the present rf generator (maximum useful illumination $\approx$ 50 watts) we cannot easily attain the required electron temperature elevation to achieve high precision at these high initial electron temperatures, we have limited our investigations with nitrogen to a maximum enthalpy of 3×10^6 joules/kg.

Determination of Loss Factors in Mixtures and Derivation of the Loss Factor in Pure Gases From These Results

The simple relationship given by equation (1) can be used to obtain an accurate determination of δ_{eff} for a mixture of gases in the absence of electron energy gain due to superelastic collisions, $\dot{S}$, and radiation losses, $\dot{R}$, or other complicating factors as explained in reference 2. These results of δ_{eff} for mixtures can then be processed, by use of a simple mixture rule in the manner indicated in Appendix A, to yield the energy loss factor δ_κ for the pure gases. This approach is justified (a) by the fact that some gases cannot be conveniently handled or heated in the arcjet in the pure state without excessive dissociation and other complications but can be investigated with greater ease and accuracy when mixed as diluents

in a carrier gas (argon in this case) of known properties, (b) by the fact that some of the gases of interest have energy loss factors that are so high that the maximum available rf power of illumination of approximately 50 watts is inadequate to produce an easily measurable ΔT_e and (c) by the need to gain confidence in this method for the determination of energy-loss factors by obtaining the same results for the pure gases whether the primary measurements are carried out in pure gases or in gas mixtures of various concentrations.

Thus mixtures are employed to determine the electron energy-loss factor in difficult gases such as oxygen, carbon monoxide, carbon dioxide and nitric oxide. The carrier gas is argon in all these cases. In addition, the determination of the loss factors for pure nitrogen and helium is carried out by analyzing the results for ΔT_e vs. P obtained in (a) nitrogen-argon mixtures and (b) helium-argon mixtures. These results are then compared with the results obtained in the pure gas measurements reported in the preceding section.

Tables I through IV present the results of ΔT_e vs. P obtained for various concentrations of CO, He, N_2 and NO, respectively, mixed with argon. The energy loss factors derived from the data of tables I through IV for these gases in the pure state are shown in figures 9 (for CO), 10 (for He), 11 (for N_2), and 12 (for NO), as a function of the electron temperature for various concentrations. It is evident from figures 9 through 12 that the derived energy-loss factors for these pure gases are independent of their concentration in the mixture, except for nitric oxide which undergoes significant dissociation that depends strongly on its initial concentration (ref. 3). The scatter in the CO data is due to a rapid coating process that is found to cover the tungsten Langmuir probe with carbon and to change its surface characteristics soon after injection of CO in the argon plasmajet. It is also evident from figure 10 that the energy loss factors obtained for pure He from measurements in mixtures with argon are in close agreement with the results of figure 5 obtained from measurements in pure helium. These results are in agreement with the transport property theory for mixtures.

Figures 13 and 14 present the results obtained for ΔT_e vs. P and the energy loss factor of CO_2 as a function of T_e, respectively, for various

CO_2 concentrations in argon. The intermingling of data for different concentrations of CO_2 in figure 14 demonstrates the independence of measured energy-loss factors to CO_2 concentration.

Figures 15 and 16 present the results obtained for ΔT_e vs. P and the energy-loss factor of O_2 as a function of T_e, respectively, for various O_2 concentrations in argon. It is clear from figure 16 that the loss factor obtained for pure O_2 by measurements in mixtures with argon is also independent of the concentration of O_2.

Figures 17 and 18 present the results obtained for ΔT_e vs. P and the energy loss factor of N_2 as a function of T_e, respectively, for various N_2 concentrations in argon. It is clear from figure 18 that the loss factor obtained for pure N_2 by measurements in mixtures with argon is also independent of the concentration of N_2. Also included in figure 18 for purposes of comparison are the results obtained by measurements in pure nitrogen and first presented in figure 8.

It is evident from figures 10 and 18 that the mixture rule and analysis of Appendix A is valid. It can be clearly seen that the data points of figures 9, 10, 11, 14, 16 and 18, measured under widely varying conditions have in effect a very small dispersion and therefore we may conclude that the mixture method is valid and applicable over a range of almost four orders of magnitude in δ_{eff}.

Finally, figure 19 summarizes all energy-loss factor data obtained in the course of this investigation and, supported by the interpretation and discussion of the results that follows, demonstrates that a simple, reliable and direct method for the measurement of the loss factor in hot gases has been developed and has been effectively used to measure δ_{eff} in hot gases. The results are presented in a concise and convenient form that should prove useful to many other investigators in a diversity of fields.

The gas enthalpy and electron temperature range of these measurements can be greatly increased and the accuracy of the measurements can be considerably improved by using the full non-linear theory of reference 2 and the diagnostic techniques developed in the course of this investigation to interpret future experiments. This is discussed in the following section.

INTERPRETATION AND DISCUSSION OF RESULTS

It became apparent during the course of this investigation that the observed behavior of the data, e.g. the change of ΔT_e with rf power and of δ_{eff} with gas enthalpy and T_e, could not be explained on the basis of the simple linear theory summarized by equation (1). For example, in the careful study of the elevation of the free electron temperature in argon plasmas performed prior to the initiating of the series of mixture experiments with argon as the carrier gas, it was observed that ΔT_e did not increase linearly with P even at the very low rf powers, electron temperatures and gas enthalpies that we were able to investigate. A reduced rate of increase of ΔT_e with rf power below the linear rate specified by the elastic electron energy-loss factor in argon, $\delta_{A,el} = 2.727 \times 10^{-5}$, when inserted in equation (1) in place of δ_{eff}, was expected due to radiation losses ($\dot{R}$) from the gas. However, we were not prepared for the large increase of ΔT_e with P, at low P, above the linear rate specified by equation (1), when evaluated with the elastic energy loss factor, that we encountered first for argon (figure 2) and later for helium (figure 4), even under conditions where radiation was negligible. This implied a decrease of δ_{eff} for these gases below the elastic value.

Also, in analyzing the behavior of δ_{eff} for nitrogen as a function of gas enthalpy and T_e we were perplexed by the seeming decrease of δ_{eff} with increasing gas enthalpy at a constant T_e (figure 8).

Finally, the rate of increase of δ_{eff} for N_2 and T_e at constant gas enthalpy (figure 8) and the role of dissociation and other composition changes on all the results were suspect. While on a different plane, that was more connected with theory than with experiment, the relationship between T_n, T_{vib} that characterize the state of excitation of the gas and $T_{e,E=0}$ appeared to deserve additional critical scrutiny.

At first suspicion was directed towards the microwave system and its ability to illuminate the plasma with the TE_{10} mode in the manner predicted in reference 2 so that the simple relationship between illumination power P, where P = (waveguide power input + waveguide power output)/2, and electric field in the plasma given in reference 2 applies.

The results of a careful investigation of the performance of the entire microwave illumination system are given in Appendix B. The conclusion of this investigation was that the microwave system was performing as designed and there was no likelihood of experimental error due to its performance.

Then suspicion was directed at the possibility of changes in the gas composition in the arcjet due to dissociation, ionization, etc. A careful study of the species concentrations was performed in nitrogen and nitrogen-oxygen mixtures as described in Appendix C. Although these investigations proved that the energy-loss factor results for nitrogen-oxygen mixtures presented in reference 2 were indeed subject to a correction, due to the presence of nitric oxide in the mixture, that could be as large as a factor of $(2)^{-1}$ at the moderate and lower concentrations of O_2 (i.e., the results for δ_{eff} for pure O_2 reported in reference 2 on the basis of measurements in N_2-O_2 mixtures should be divided by 2 in the mole fraction range below $[O_2]/\{[O_2] + [N_2]\} \approx 0.3$), they failed to show any significant effect due to atomic nitrogen in the pure nitrogen results at the higher enthalpies and electron temperatures presented in references 1 and 2 and figure 8. For example, even when $[N]/[N_2] = 5/95$, the presence of nitrogen atoms depresses the energy-loss factor of the mixture by only 2% to 4% below the value of energy-loss factor for pure nitrogen. Therefore the dissociation of nitrogen is insufficient to explain the behavior, with increased enthalpy, of δ_{eff} for N_2 shown in figure 8, since at these enthalpies the fraction $[N]/[N_2]$ is less than 4% for the arcjet plasma generator system used in these experiments.

A study of the ion concentration in the plasmas used in these experiments confirmed that the ion densities and electron-ion recombination times are such that they could not possibly account for the observed super-elastic energy loss factors or any of the other phenomena in question. Typical electron concentrations are shown in Appendix C as a function of the gas enthalpy for nitrogen at a tank pressure of approximately 600 microns.

Another interesting result of the study of species concentration presented in Appendix C is the verification of strong non-equilibrium concentrations of dissociated and ionized species in the jet. These concentrations

are considerably higher than even the equilibrium concentrations at stagnation conditions. For example, in the nitrogen plasmajet that we have used in these investigations, the electron concentration at a stagnation temperature of 2000 ^{o}K and a stagnation pressure of 0.5 atmospheres, corresponds to the electron concentration at equilibrium with T_o = 4500 ^{o}K and the same pressure. The nitrogen atom concentration at the same stagnation temperature and pressure of 2000 ^{o}K and 0.5 atmospheres, corresponds to the atom concentration at equilibrium with T_o = 4800 ^{o}K and the same pressure. This departure from equilibrium becomes less pronounced at the higher stagnation temperatures and pressures so that at the stagnation temperature of 5000 ^{o}K and stagnation pressure of 0.78 atmospheres the observed ionization and dissociation levels are at equilibrium with T_o = 5600 ^{o}K and the same pressure. These results indicate that the gas in the plasmajet is in a highly excited state.

Finally, additional measurements of the rotational and vibrational temperatures in the nitrogen plasmajet were carried out as a function of gas stagnation enthalpy to settle the questions concerning (a) the appropriate value of the reference gas temperature T_n and (b) the closeness of the coupling of $T_{e, E=0}$ with T_{vib}. The results of these measurements are presented in Appendix D. They indicate that in the range of enthalpies and other conditions of interest in our experiments the free electron and nitrogen vibrational temperatures in the jet are very closely coupled and that the proper reference temperature T_n to use with nitrogen is T_{vib}.

The Need to Use the Complete Electron Energy Balance Equation to Interpret the Results

Failure of all these investigations, as described in the preceding discussion, to trace the cause of the behavior to some of the data to the suspected experimental reasons, permits the focusing of attention on the theory used to interpret the experiments and reduce the data. This approach promises to explain all observed phenomena, even at the extremes of the electron and gas energy ranges of interest, for both monatomic and poly-

atomic gases.

For example, it is now clear that the observed behavior of ΔT_e vs. rf power of illumination P for argon heated to these initial temperatures by an arc should be expected. As demonstrated in what follows, reduction of the data by the simple theory of reference 1 should indeed yield lower-than-elastic energy-loss factors at low ΔT_e and P, that become increasingly higher-than-elastic as ΔT_e and P increase.

The reasons for this behavior are: (a) The argon plasmajet consists of an afterglow plasma that is a tightly coupled kinetic system. It contains a large concentration of metastables and other energy-storing species such as ions and all energy exchange processes in it are very sensitive to variations in the electron temperature. (b) The simple electron energy balance equation of reference 1 neglects (or lumps together in the energy-loss factor it describes) "second-order" or superelastic impacts (that result in the transfer of the energy of an excited particle to the incoming electron) and radiation losses (that tend to transfer energy from the electrons to the gas in inelastic collisions and from the gas through radiation to the surroundings so that any equilibrium between electron temperature and excited optical states of the atoms is upset). The influence of these effects on the "lumped" energy-loss factor of reference 1 is indeed such that at low electron temperatures (and at low ΔT_e or the low rf power used to generate it) superelastic collisions tend to lower the "lumped" energy-loss factor below the elastic value whereas at higher electron temperature (and high ΔT_e) the radiation losses predominate and they tend to increase the "lumped" energy-loss factor above the elastic value. (c) The electron energy-loss factor in argon is small to start with (equal to the elastic energy-loss factor within the framework of the theory of reference 2, because argon does not possess rotational and vibrational energy-absorbing degrees of freedom) and therefore it is much more sensitive to superelastic and radiation effects.

Obviously, as we can see from the theory of reference 2, the magnitude of the electron energy-loss factor depends strongly on the use of the correct theoretical expression to reduce the data. Only through use of the

full electron energy balance, given in reference 2, can one explain all the observed effects in a consistent and meaningful manner. A simplified version of the complete electron energy balance equation is given in reference 2 in the form

$$\vec{J}_e \cdot \vec{E}' = \frac{3}{2} k n_e \nu_t \delta_{eff} (T_e - T_n) + \dot{R} + \sum_i s_i \epsilon_i \qquad (2)$$

where the term on the left of the equality sign is the ohmic heating. The first term on the right is the term that gives the difference between the average electron internal energy and the heavy particle internal energy (which, as explained in reference 2, involves only translational, rotational and vibrational degrees of freedom and therefore in the case of argon $T_n \equiv T = T_{tr}$). The second term on the right is the radiation energy loss rate from the plasma (which is usually equal to the energy lost by the electrons in exciting electronic levels of the heavy particles that are available for optical transitions). The third term on the right is a term that describes electron energy losses or gains that arise from actual changes in plasma composition through chemical reactions in which the electrons are energy-partners (i.e., ionization by electron impact, recombination where the electron is a third body, de-excitation of metastables where the electron carries off the energy, etc.). Note that the sign of $\sum_i s_i \epsilon_i$ depends on whether the electron loses energy (+) or whether it gains energy (-).

When, in the absence of electric currents, we can neglect $\sum_i s_i \epsilon_i$, we see that for argon it is possible to obtain

$$T_e = T - \frac{2\dot{R}}{3 k n_e \nu_t \delta_{eff}} \qquad (3)$$

i.e., the electron temperature can (and must) fall below the gas temperature because of radiation.

Under the same conditions but with electric currents present, we see that, even when δ_{eff}, n_e and ν_t do not change with T_e,

$$\delta_{eff} = \left(\frac{\Delta(\vec{J}_e \cdot \vec{E}') - \Delta\dot{R}}{\Delta T_e} \right) \cdot \frac{2}{3 k n_e \nu_t} \qquad (4)$$

and therefore, if $\Delta\dot{R}/\Delta T_e$ is neglected, we obtain δ_{eff} from the measured $\Delta(\vec{J}_e \cdot \vec{E}')/\Delta T_e$ (or the inverse of the rate of change of electron temperature with rf power) that is given by

$$\delta'_{eff} = \frac{\Delta(\vec{J}_e \cdot \vec{E}')}{\Delta T_e} \cdot \frac{2}{3kn_e\nu_t} \tag{5}$$

Equation (5) corresponds to the simple theory for obtaining δ_{eff} given in reference 1 and we see that when $\Delta\dot{R}/\Delta T_e$ cannot be neglected, then $\delta'_{eff} > \delta_{eff}$ or the real δ_{eff} is lower than the δ'_{eff} obtained from the data by the simple theory. This explains the behavior of the observed data at high rf illumination powers and high ΔT_e or T_e.

At low rf powers and low gas temperatures $\dot{R}$ is negligible and we can write, in the absence of an electric field,

$$T_e = T - \frac{2\sum_i s_i \epsilon_i}{3kn_e\nu_t\delta_{eff}} \tag{6}$$

i.e., the electron temperature will rise above the gas temperature when $s_i\epsilon_i$ is negative (e.g. when the energy-storing species concentration decreases and the electron average energy increases) and will again fall below the gas temperature when $s_i\epsilon_i$ is positive (e.g. when the energy-storing species concentration increases and the electron average energy decreases).

When $s_i\epsilon_i$ terms are important in the presence of $\vec{J}_e \cdot \vec{E}'$ and δ_{eff}, n_e and ν_t do not change with T_e, we obtain

$$\delta_{eff} = \left(\frac{\Delta(\vec{J}_e \cdot \vec{E}') - \Delta(\Sigma s_i\epsilon_i)}{\Delta T_e} \right) \cdot \frac{2}{3kn_e\nu_t} \tag{7}$$

and we see that if the rate of change with time of the number density of energy-storing species decreases with temperature, i.e., if $\Delta(\Sigma s_i\epsilon_i)/\Delta T_e < 0$, the correct δ_{eff} will be higher than the value computed from equation (5) while if the rate of change of concentration of these species increases with temperature, the correct δ_{eff} will be lower than the value computed from equation (5).

The situation is somewhat similar with nitrogen except that because

the metastable energy level in the nitrogen molecule (first vibrational level of the electronic ground state) is much lower (~ 0.3 ev) than the metastable levels in argon (~ 11 ev) and the energy-loss factor for N_2 is much higher than for A (because of possible excitation of rotational and vibrational degrees of freedom), superelastic effects should not be as pronounced in nitrogen as they are in argon and the loss factor for nitrogen should never even approach, much less fall below, the elastic value.

These considerations point out the need for using the complete electron energy balance equation to interpret the results of these experiments.

Interpretation and Discussion of Results Within the Framework of the Complete Electron Energy Balance Equation

A discussion of some of the terms appearing in the complete electron energy balance equation of reference 2 is presented first, in order to clarify and emphasize the significance of each of these terms and avoid ambiguities in their use.

It can be shown (ref. 2) that the energy balance equation for electrons is given by

$$\frac{\partial}{\partial t}\left(\frac{3}{2} p_e\right) + \nabla \cdot \left(\frac{3}{2} p_e \vec{U} + \vec{q}_e\right) + \overleftrightarrow{\pi}_e : \nabla \vec{U}$$

$$= \rho_e \vec{W}_e \cdot \left[\frac{e}{m_e}\left(\vec{E} + \vec{U} \times \vec{B}\right) - \frac{d\vec{U}}{dt}\right] + R_e^{(2)} \tag{8}$$

where the collisional energy exchange integral $R_e^{(2)}$ is given by

$$R_e^{(2)} = -\frac{3}{2} k n_e \sum_{\kappa} \sum_{s} \delta_{\kappa, s}(T_e - T_{\kappa, s}) \tau_{e, \kappa}^{-1} - \dot{R} - \sum_i s_i \epsilon_i \tag{9}$$

or the equivalent form

$$R_e^{(2)} = -\frac{3}{2} k n_e \nu_t \delta_{eff}(T_e - T_n) - \dot{R} - \sum_i s_i \epsilon_i \tag{10}$$

and the other notation is defined in the list of symbols.

The form of the collisional energy exchange integral given by equation (9) is the result of some deliberation and it is appropriate to elaborate somewhat here on its origin.

The quantity $R_e^{(2)}$ contains all energy exchange terms, elastic and inelastic, between the electron and its surroundings.

The term $\dot{R}$ is most generally defined to represent energy lost from the system containing the electrons (e.g. a plasma) to the surroundings, provided it is understood that this energy originated from the electrons. For example, that part of the radiant energy lost from the system that comes from the excitation of electronic states of the heavy particles by electronic impact followed by spontaneous emission is contained in the term $\dot{R}$, since this energy originated from the electrons. This term also contains energy radiated directly from the electrons (bremsstrahlung) but does not contain energy that the electrons lose in creating ions, free radicals, metastables or other relatively long-lived species.* Additional reasons for considering this term separately are (1) that it may be a function of geometry (through self-absorption of radiation in the plasma) and (2) that usually it involves processes that have a very small time scale or lifetime (of the order of 10^{-7} sec or even less) compared to the processes accounted for by the other two terms on the right-hand side of equation (9). This comes about because $\dot{R}$ depends on spontaneous emission that does not directly depend on temperature or particle density. Therefore the emission of radiation that makes up $\dot{R}$ can be considred instantaneous for all practical purposes, i.e., there is no significant time lag between the moment of impact when the electron loses some energy in exciting the heavy particle and the moment when the heavy particle loses this energy by spontaneous radiation to the surroundings.

In considering $\dot{R}$, however, we must never lose sight of the fact that it is only a manifestation of an energy exchange process between electrons and heavy particles, namely the excitation of the heavy particle, that is very difficult to follow or measure directly. Thus although the conversion of electron energy to radiant energy may be an almost instantaneous process, the redistribution of energy among the electrons, i.e., the cooling

*It also contains that part of the radiant energy from resonant levels that is not trapped in the system but leaks from it.

of the electron gas, is not necessarily equally rapid. Nevertheless, use can be made of the fact that in most plasmas of interest to this investigation the optically excited levels of atoms or molecules are generally in instantaneous equilibrium with the free electrons. In these plasmas, while the electrons and other plasma components experience energy exchange among one another, the ultimate loss of energy from the system is due to radiation. Therefore, the appropriate portion of the collisional energy losses from the free electrons (i.e., that portion of the energy lost by an electron upon impact with an atom or molecule that goes into exciting electronic levels of the heavy particle) can be usually equated to the radiative losses $\dot{R}$ from excited states of the heavy particles at the electron temperature (ref. 4).

The other two terms on the right-hand side of equation (9) represent energy lost (or gained) by the electrons that remains in the system or, in some cases, originates outside the system but is passed on to the electrons in the system by collisions with the heavy particles. Usually both of these terms involve processes that have a time scale or lifetime that can be anywhere from much shorter to very much longer than 10^{-7} sec. In addition, the magnitude of the characteristic times for the processes described by these two terms is usually a direct function of temperature and/or particle density and neither of the two exhibits a marked geometrical dependence.

Despite these similarities it is found necessary to separate the processes described by these terms into two different categories depending on whether they represent energy exchange between the electron and the physical degrees of freedom, with well-defined temperatures, of the heavy particle or energy exchange associated with chemical or chemical-like change. Thus the term containing $\delta_{\kappa, s}$ accounts for all electron-heavy particle interactions that involve exchange of energy between the electron and the various degrees of freedom of the heavy particle. These degrees of freedom of the heavy particle are primarily translational, rotational and vibrational and their excitation by electron impact does not result in any energy leaving the system directly, unlike the excitation of electronic (or optical) degrees of freedom which, as we have seen, is a "leaky" energy exchange mechanism and has to be treated separately. The characteristic times for these processes also can be extremely fast. Thus the characteristic times

for excitation and relaxation of translational and rotational energy can be of the same order as the characteristic times for electronic excitation and radiation. Although the characteristic times for excitation and relaxation of vibrational energy can be several orders of magnitude slower (depending on temperature and pressure) it still makes sense to define a temperature for this, as well as the other degrees of freedom. Hence the definition of $T_{\kappa, s}$: It is the temperature that describes the level of excitation of the degree of freedom s of the heavy particle or component κ and since we have excluded electronic excitation, s stands for the remaining degrees of freedom, e.g. translational, rotational and vibrational. Therefore the important characteristic of this term is that it can be conveniently expressed in terms of the difference between the electron temperature and the temperature $T_{\kappa, s}$.

Again we must point out that although an electronic (or optical) excitation temperature T_{elec} can also be easily defined (and measured) to describe the excitation of electronic degrees of freedom, we have chosen to exclude this energy exchange process from the term containing $\delta_{\kappa, s}$ and prefer to split it into two parts, one that has to do with energy leaking from the system, $\dot{R}$, and the other, that has to do with energy remaining in the system, contained, among many other sources and sinks of electron energy, in the term

$$\dot{S} \equiv \sum s_i \epsilon_i \tag{11}$$

where ϵ_i can be positive or negative depending on whether the electrons lose or gain energy by the process i.*

The term $\dot{S}$ accounts for all energy exchange processes between electrons and heavy particles that are associated with chemical or chemical-like changes. For example, electron energy losses that lead to dissociation or ionization (or electron energy gains that are associated with ion or free-radical recombination) are accounted for in this term. Since metastables (or trapped resonant levels) can be considered as chemically different species as a consequence of their relatively long lifetimes and some

*Therefore $\dot{S}$ also describes energy exchange between electrons and resonant levels under conditions of strong trapping of resonant radiation.

chemical-like properties (e. g. a very slow metastable atom or molecule can pull out an electron from a solid surface whereas a slow atom or molecule in the ground state cannot), this term also describes all electron-metastable interactions that result in electron energy changes, or electron-atom interactions that lead to the creation of metastables (and therefore with electron energy changes that remain in the system).* In addition $\dot{S}$ can describe electron energy changes that are produced by energy that originates outside the system (e. g. elevation of the electron temperature by recombination, with electrons acting as third bodies, of ions that were produced through photoionization, or by de-excitation, due to electron impact, of electronically excited atoms produced by photo-excitation).

Another important characteristic of this term is that, unlike the term containing $\delta_{\kappa, s}$, it cannot conveniently be expressed in terms of a difference between the electron temperature and some temperature $T_{i,\epsilon}$ (appropriate to process i resulting in an electron energy exchange ϵ_i) since the resulting parameters would be very difficult to measure even if we assume that they can be consistently defined. Finally, of all the terms on the right-hand side of equation (9) this is the one that can be the slowest since it involves chemical reaction rates and energy exchange with species with very long lifetimes.

To summarize, $\dot{R}$ represents a fast "leak" of energy from the system caused mainly by the exchange of energy between electrons and heavy particles inside the system that results in a net loss of energy to the electrons in the system. The other two terms on the right-hand side of equation (9) describe changes of the energy of the electrons in the system. The term containing $\delta_{\kappa, s}$ represents a change of the energy of the electrons in the system due to electron collisions that result in physical changes of the components κ within the system that have an easily described temperature $T_{\kappa, s}$. The term $\dot{S}$ represents a change of energy of the electrons in the system due to electron collisions that result in chemical-like changes (relatively long-lived species) within the system.

---

*Since trapped resonance levels are effectively long-lived they can be described by $\dot{S}$ and treated as "pseudometastables."

One of the advantages of this formulation is the relative ease with which the various quantities making up the collisional energy exchange integral, equation (9), can be determined in our experiments.

To demonstrate this, note that under steady-state conditions ($\partial p_e/\partial t = 0$, $\partial \vec{U}/\partial t = 0$) in a flow field with negligible axial velocity and electron concentration and temperature gradients, i.e., when $\nabla \cdot [(3 p_e \vec{U}/2) + \vec{q}_e] + \overleftrightarrow{\pi} : \nabla \vec{U} = 3 \vec{U} \cdot \nabla k n_e T_e/2 + 3 p_e \nabla \cdot \vec{U}/2 + \nabla \cdot \vec{q}_e + p_e \nabla \cdot \vec{U} - \overleftrightarrow{\tau}_e : \nabla \vec{U} \approx 0$ since $\partial n_e/\partial x = \partial T_e/\partial x = \partial u_x/\partial x \approx 0$, the electron energy balance equation, equation (8) becomes

$$\vec{J}_e \cdot (\vec{E} + \vec{U} \times \vec{B}) = \frac{3}{2} k n_e \nu_t \delta_{eff} (T_e - T_n) + \dot{R} + \dot{S} \qquad (12)$$

where T_n is any convenient reference temperature that characterizes the energy level of the gas as described in reference 2.

Using equation (12) and the methods of Ginzburg and Gurevich (ref. 5) it can be shown that in a high-frequency electric field ($E = E_o \cos \omega t$, $\omega = 2\pi f$), when $\vec{B} = 0$, the difference between the electron temperature T_e and the reference temperature T_n is given by

$$T_e - T_n = \frac{e^2 E_o^2}{3 k m_e \delta_{eff} (\omega^2 + \nu_t^2)} - \frac{2}{3 k n_e \nu_t \delta_{eff}} [\dot{R} + \dot{S}] \qquad (13)$$

where the first term on the right contains only two variables, δ_{eff} and ν_t, dependent on gas properties and the second term at least three. Then if we illuminate the plasma with a high frequency electric field such that $\omega^2 \gg \nu_t^2$, the effective energy-loss factor δ_{eff} can be obtained by operating in a regime where either the magnitude or the change of $\dot{R} + \dot{S}$ with electron temperature is negligible or can be deteremined independently.

For example, let us consider our experiments with nitrogen. Assuming $\dot{R} + \dot{S}$ is negligible in these experiments (since the temperatures are relatively low) we can write equation (13) in the form

$$T_{e,\,E=0} - T_n = 0 \qquad (14)$$

when $E_o = 0$ (i.e., with rf power off), and since T_n does not change significantly with rf power, we can write equation (13) in the form

$$T_e - T_{e,E=0} = \frac{e^2 E_o^2}{3 k m_e \omega^2 \delta_{eff}} \tag{15}$$

when $E_o \neq 0$ and $\omega^2 >> \nu_t^2$. Therefore, since $E_o = (4 PZ/A_r)^{1/2}$ in our experiment (ref. 2), the effective energy-loss factor at T_e and a reference gas temperature $T_g = T_n$ which describes the energy state of the gas, is given by

$$\delta_{eff} = \left(\frac{e^2}{3 k m_e \omega^2}\right)\left(\frac{4Z}{A_r}\right)\frac{P}{T_e - T_{e,E=0}} \tag{16}$$

where, as we have already explained, δ_{eff} contains translational, rotational, and vibrational contributions to the energy loss factor.

In these experiments it is an observed fact that $T_{e,E=0} \approx T_{vib}$, as clearly indicated by the experimental results plotted in figures 1 and 2 of Appendix D. This evidence is in agreement with the theoretical result (see, e.g., ref. 6) that the free electrons in the plasma are closely coupled energetically with the vibrational mode of the gas molecule and are therefore very nearly at equilibrium with the vibrational temperature of the nitrogen molecules. Further experimental evidence is reported in reference 7 for shock-heated mixtures of argon and 1% N_2.

In our experiments this coupling occurs for the following reasons: In the absence of electron energy sources due to recombination of ions or other species ($\dot{S} = 0$), the electron temperature relaxes very rapidly and reaches its steady-state value (which in the absence of an electric field is T_n) almost immediately. [The relaxation time in that case can be computed by the methods of reference 5 and is equal to $1/\nu_t \delta_{eff}$. This is also clear from equations (8) and (10) above.] Consequently, use of the steady-state approximation, equation (12), to obtain the electron temperature, is justified. In addition, in our experiments with N_2, $\dot{R}$ is negligible (see discussion in reference 2) and $\dot{S}$ is negligible for the reasons given in

Appendix E. When $\dot{R}$ and $\dot{S}$ are negligible and we make use of the definition of δ_{eff} [compare equations (9) and (10)] equation (12) in the absence of electric and magnetic fields reduces to

$$\delta_{N_2, tr}(T_{e, E=0} - T_{N_2, tr}) + \delta_{N_2, vib}(T_{e, E=0} - T_{N_2, vib}) + \delta_{N_2, rot}(T_{e, E=0} - T_{N_2, rot}) = 0 \quad (17)$$

But under the conditions of these experiments ($T_e \geq 2000\ ^{o}K$, $n_{N_2} \approx 10^{22}$ particles/m^3) the data of Engelhardt et al. (ref. 8) prove that even at $T_e \approx 2000\ ^{o}K$ the fractional power input due to collisions of electrons with N_2 molecules that result in elastic scattering of the electron (and contribute to the translational degree of freedom of the molecule) and rotational excitation of the N_2 molecule is of the order of 2% or less of the total power that the electron loses in elastic and inelastic collisions. Therefore, since under the conditions of reference 8, $T_g = T_{N_2, rot} = T_{N_2, vib} = T_{N_2, tr}$, we obtain,

$$\frac{(\delta_{N_2, tr} + \delta_{N_2, rot})(T_e - T_g)}{(\delta_{N_2, tr} + \delta_{N_2, rot} + \delta_{N_2, vib})(T_e - T_g)} \approx 0.02 \quad (18)$$

in the range of T_e of interest to us. Then, since in our experiments $T_{N_2, rot} = T_{N_2, tr}$, a combination of equations (17) and (18) yields

$$\frac{T_{N_2, vib} - T_{e, E=0}}{T_{e, E=0} - T_{N_2, tr}} \approx \frac{1}{49} \quad (19)$$

For our experiments, where $T_{e, E=0} \approx 2000\ ^{o}K$ and $T_{N_2, tr} \approx 350\ ^{o}K$, equation (19) yields

$$T_{N_2, vib} - T_{e, E=0} \approx 35\ ^{o}K \quad (20)$$

We conclude that our experimental observation that $T_{e, E=0}$ is approximately equal to $T_{N_2, vib}$ is in agreement with theory. Therefore, since

vibrational relaxation of the nitrogen is slow (and the vibrational temperature in the jet is frozen at or close to the nozzle throat temperature), it is clear that the electron temperature in the jet in the absence of an electric field will also be frozen at the relatively high value of the vibrational temperature at the throat; this also is in agreement with experiment

Finally, we must point out, that instead of invoking the data of reference 8, we can invoke the second law of thermodynamics to prove that the dominant process for energy input to the electrons must be a coupling with the vibrational temperature of the nitrogen since the measured $T_{N_2, rot} = T_{N_2, tr}$ is far below the measured $T_{N_2, vib}$ and the measured $T_{e, E=0}$ is close to the measured $T_{N_2, vib}$ in all enthalpy ranges studied. For this reason elastic and rotational processes of energy exchange must result in losses of electron energy. Moreover, these losses must be small, despite the large temperature difference $T_{e, E=0} - T_{N_2, tr}$, because if they were large they would have to be balanced by an energy input from a large $T_{N_2, vib} - T_{e, E=0}$ (and this temperature difference is measured to be small), or from a large energy input from $\dot{S}$ (and the recombination of ions or atoms with electrons acting as the third body at the required rate is unlikely). Again we conclude that the observation $T_{N_2, vib} \approx T_{e, E=0}$ is in agreement with the steady-state theory and equation (12) with $\vec{E} = \vec{B} = 0$ and $\dot{R} + \dot{S} = 0$. We may also conclude from this discussion that for these experiments the appropriate reference temperature to use in equation (12) is $T_n = T_{N_2, vib}$.

The assumption that $\dot{R}$ and $\dot{S}$ are negligible for these relatively low-temperature experiments in nitrogen is therefore supported by the observations. However, as either T_e or T_{vib} are increased (by increasing the rf power or the plasma enthalpy, respectively) there will come a point where the terms $\dot{R}$ and/or $\dot{S}$ can no longer be neglected and will have to be added to equations (15) and/or (16). Otherwise, i.e. if we keep using equations (15) or (16) rather than equation (13) to determine δ_{eff}, there will result a serious over- or under-estimation of the electron energy-loss factor. This point has been illustrated by our experiments (see figures 2-5 and 20).

Fortunately, contributions to the electron energy equation such as

$\dot{R}$ and $\dot{S}$ can be easily determined by measuring the change of either $\dot{R}$ or $\dot{S}$ with electron temperature, provided T_e can be manipulated in such a way that the effect on n_e, n_a and δ_{eff} is either small or predictable. Our method of heating the electrons of a hot and fast jet of plasma comes very close to satisfying these conditions because the hot gas does not reside in the region of rf illumination long enough to cause a significant increase in electron number density or a significant change of n_a and the heating of the gas due to the rf field is negligible. Therefore, if $\dot{R}$ and $\dot{S}$ can be measured by independent means, our experiment can also be used as a method for determining the influence of various mechanisms on the relaxation of electron temperature. Such independent measurements of $\dot{R}$ and $\dot{S}$ are relatively simple: $\dot{R}$ can be determined by measuring the radiation emitted from the hot gas as a function of T_e and $\dot{S}$ can be determined by measuring changes in composition as a function of T_e. These tasks are made easier by the requirement that the determination of changes in $\dot{R} + \dot{S}$ with T_e will usually suffice.

To demonstrate the advantages of this formulation in the presence of significant contributions from $\dot{R}$ and $\dot{S}$ let us consider our experiments concerned with heating the electrons in an argon plasmajet with rf power with the results summarized in figure 20.

In this case, since the static temperature of the jet is $T_g = T_{tr} \approx 100\ ^oK$ and we observe that $T_{e,E=0} >> 100\ ^oK$, it is clear that energy must be going to the free electrons in the jet, to keep their temperature high, from some source $\dot{S}$ (since rotational and vibrational modes do not exist and the electronic or optical modes contained in $\dot{R}$ can only represent energy losses). Therefore we cannot use the method for computing the relaxation time given in reference 5. Instead we must use the method given in reference 9.

A computation of the electron energy relaxation length L_E or relaxation time $t_E = L_E/U$ by the methods of reference 9, using a value for the characteristic energy ϵ_i of 10 ev and assuming an instantaneous process (equivalent to the instantaneous Saha equilibrium assumed in reference 9) — an assumption that is justified if electron impact by a single

electron rather than three-body recombination is the energy source — results in a very long relaxation time and again justifies the use of the steady state approximation of the electron energy equation, equation (12). In the absence of an electric field and when $\dot{R}$ is negligible, (i.e. at low arcjet powers), we obtain from equation (13)

$$T_{e,E=0} - T_n = -\frac{2}{3kn_e\nu_t\delta_{eff}}\dot{S}_{E=0} \tag{21}$$

and when an rf field is present, with $\omega^2 >> \nu_t^2$, and $\dot{R}$ is still negligible, we obtain

$$T_{e,E} - T_n = \frac{e^2E_o^2}{3km_e\omega^2\delta_{eff}} - \frac{2}{3kn_e\nu_t\delta_{eff}}\dot{S}_E \tag{22}$$

For argon $\delta_{eff} \equiv \delta_{A,el} = 2.727 \times 10^{-5}$ since there are no rotational or vibrational modes and the appropriate reference gas temperature to use in these experiments is the static temperature so that $T_n = T_g = T_{tr} \approx 100\ ^oK$. The glowing outline of the argon plasmajet is barely distinguishable in the tank under these conditions and therefore, at least for low electron temperatures, $\dot{R}$ can be neglected ($T_{elec} \approx T_e \approx 2000\ ^oK$).

The pressure in the vacuum tank in these experiments is 0.51×10^{-3} atm and therefore the number density of argon atoms in the jet is $n_A = p/kT_g = 3.7 \times 10^{22}$ per m^3. (Note that T_g can be measured very accurately with the electron beam device.) From an independent determination of the collisional cross-sections for momentum transfer (ref. 10) we have $Q_{eA} = 4.48 \times 10^{-21}\ m^2$ at $2083\ ^oK$ and $Q_{eA} = 9.32 \times 10^{-21}\ m^2$ at $3568\ ^oK$. Using typical experimental results we see that when $T_{e,E=0} = 2083\ ^oK$ and $P = 0.085$ w we obtain $\Delta T_e = 1485\ ^oK$ or $T_e = 3568\ ^oK$. The electron number density in these experiments with argon is estimated to be approximately $10^{16}/m^3$ (it can be measured quite accurately using the Langmuir probe).

Thus we have all the necessary ingredients to determine $\dot{S}$ as a function of T_e from equations (21) and (22). Actually, as we shall see, at this point we have several choices concerning the dependent variable (or what we can choose as an unknown).

The collision frequencies ν_t [$\nu_t(T_e) \equiv \frac{4}{3} n_a Q_{ea} (8kT_e/\pi m_e)^{1/2}$] become

$$\nu_t(2083) = \frac{4}{3} \times 3.7 \times 10^{22} \times 4.48 \times 10^{-21} \times 6.213 \times 10^{3} \times 45.6$$

$$= 6.26 \times 10^{7} \text{ sec}^{-1} \tag{23}$$

and

$$\nu_t(3568) = \frac{4}{3} \times 3.7 \times 10^{22} \times 9.32 \times 10^{-21} \times 6.213 \times 10^{3} \times 59.75$$

$$= 1.707 \times 10^{8} \text{ sec}^{-1} \tag{24}$$

In addition we have use for the following numerical values:

$$\frac{3k\delta_{eff}}{2} = 5.645 \times 10^{-28}, \quad \frac{2}{3k} = 0.4829 \times 10^{+23} \tag{25}$$

$$\frac{e^2}{2m_e\omega^2} = 5.947 \times 10^{-29}, \quad \omega = 1.5393 \times 10^{10} \tag{26}$$

and, for $Z = 387$ ohms and $A_r = 1.548 \times 10^{-2}$ m^2

$$E_o^2 = \left(\frac{4Z}{A_r}\right) P = 1.0 \times 10^{5} P \tag{27}$$

Therefore, if we consider $\delta_{eff} = 2.727 \times 10^{-5}$ a <u>known</u> quantity, we obtain, from equations (21) and (22)

$$\dot{S}_{E=0} = - \left(\frac{3k\delta_{eff}}{2}\right)\left(n_e \nu_t\right)_{E=0}\left(T_{e,\,E=0} - T_n\right) \tag{28}$$

and

$$\dot{S}_E = - \left(\frac{3k\delta_{eff}}{2}\right)\left(n_e \nu_t\right)\left(T_{e,\,E} - T_n\right) + \left(\frac{e^2}{2m_e\omega^2}\right)\left(n_e \nu_t\right) E_o^2 \tag{29}$$

or, if we assume that n_e remains nearly constant at 10^{16} m^{-3},

$$- \dot{S}_{E=0} = 5.645 \times 10^{-28} \times 10^{16} \times 6.26 \times 10^{7} \times 1983 = 0.701 \text{ watts/m}^3 \tag{30}$$

and

$$- \dot{S}_E = 5.645 \times 10^{-28} \times 10^{16} \times 1.707 \times 10^{8} \times 3468$$

$$- 5.947 \times 10^{-29} \times 10^{16} \times 1.707 \times 10^{8} \times 10^{5} \times 0.085 = 2.48 \text{ watts/m}^3 \quad (31)$$

We can now use equations (28) and (29) in several ways. For example, from our measurements we can deduce the dependence of $\dot{S}_E$ on T_e. One possible such deduction is that the quantity $\dot{S}_E$ can be expressed by

$$\dot{S}_E = \left(\frac{T_{e,E}}{T_{e,E=0}} \right)^{5/2} \dot{S}_{E=0} \quad (32)$$

since this relationship fits all available data. For example, substituting the appropriate values for $T_{e,E} = 3568\ ^{o}K$, $T_{e,E=0} = 2083\ ^{o}K$ and $\dot{S}_{E=0} = 0.701$ watts/m^3, yields $\dot{S}_E = 2.68$ watts/m^3, i.e., within 8% of the value from equation (29). To check the accuracy of equation (32) we note that equations (28) and (29) then yield

$$\delta_{eff} = \frac{e^2}{3 k m_e \omega^2} \left(\frac{4Z}{A_r} \right) P \cdot \Delta^{-1} \quad (33)$$

where

$$\Delta \equiv \left(T_{e,E} - T_n \right) - \left(T_{e,E=0} - T_n \right) \left(\frac{T_{e,E}}{T_{e,E=0}} \right)^2 \left(\frac{n_{e,E=0}}{n_{e,E}} \right) \frac{Q_{eA,E=0}}{Q_{eA,E}} \quad (34)$$

For these conditions, and assuming $n_{e,E=0} = n_e$, we obtain

$$\delta_{eff} = 3.58 \times 10^{-5}$$

or a δ_{eff} overestimated by 31%. However, note that if a slight increase in the electron number density occurs due to the rf power (e.g. if the recombination is slowed down some so that n_e in the test section becomes higher by almost 10% as observed), i.e., if $n_{e,E} = 1.08\ n_{e,E=0}$, we obtain

$$\delta_{eff} = 2.75 \times 10^{-5}$$

in excellent agreement. Under different conditions, when $P = 0.15$ watts, $T_{e,E=0} = 2083\ ^{o}K$, $T_{e,E} = 4503\ ^{o}K$ (and $Q_{eA} = 1.276 \times 10^{-20}$ m^2) we obtain $\delta_{eff} = 3.8 \times 10^{-5}$ with $n_{e,E} = n_{e,E=0}$ or $\delta_{eff} = 2.727 \times 10^{-5}$ when

$n_{e,E} = 1.14\, n_{e,E=0}$ as observed.

An alternative approach is to deduce from the experiments that a relationsip of the form

$$\dot{S} = s_1 \epsilon_1 = -1.4 \times 10^{-8}\, n_e \nu_t \epsilon_1 T_e^{1/2} \tag{35}$$

holds instead of equation (32). This approach, in combination with equations (28) and (29), leads to the expression

$$\delta_{eff} = \frac{0.287\, P}{(T_e - T_n) - (T_{e,E=0} - T_n)(T_{e,E}/T_{e,E=0})^{1/2}} \tag{36}$$

Equation (36) gives $\delta_{eff} = 2.727 \times 10^{-5}$ at $P = 0.085$ watts in excellent agreement with the theoretical value.

The "success" of both expressions, equations (32) and (35) demonstrates the non-uniqueness of empirical fits of this type. Nevertheless, the "success" or failure of these particular computations is not the important result. The important result is that use of equations (33) and (34) to interpret the experimental data allows us to determine precisely the power law that governs the electron temperature dependence of S if we first obtain $n_{e,E=0}/n_{e,E}$. The derivation of an empirical relationship of this type should not be considered below our dignity because it is just about standard practice in reaction kinetics. It is important to note that <u>absolute</u> measurements of n_e <u>are not required.</u>

Alternately, use of equation (36) allows us to test the validity of the expression given by equation (35) — which reduces to a form very similar to equation (32) when the temperature dependence of the cross sections is taken into account. Thus for constant n_e and n_a equation (35) leads to

$$\frac{\dot{S}_E}{\dot{S}_{E=0}} = \frac{Q_{eA,E} v_{eA,E}}{Q_{eA,E=0} v_{eA,E=0}} \left(\frac{T_{e,E}}{T_{e,E=0}}\right)^{1/2}$$

$$= \frac{Q_{eA,E}}{Q_{eA,E=0}} \cdot \frac{T_{e,E}}{T_{e,E=0}} \left(\frac{T_{e,E}}{T_{e,E=0}}\right)^{2.5} \tag{37}$$

More generally, the use of equations (28), (29) or (33) and (34) allows us (a) to determine a precise relationship between $\dot{S}_E$ and $\dot{S}_{E=0}$ and the electron temperature if $n_{e,E=0}/n_{e,E}$ is known and (b) to obtain an expression for $\dot{S}$ if n_e is known. These relationships can be of great value in the study of the kinetics and transport properties of metastable and trapped-resonant level argon atoms.

An independent check of these results can be obtained by determining the number density n_{A*} of metastable and trapped-resonant level (= pseudo-metastables) argon atoms, i.e., by using the corresponding continuity equations rather than the electron energy equation. Note that by definition (ref. 2) and neglecting diffusive losses of metastables as well as losses due to metastable-metastable or metastable-own gas collisions†

$$\dot{S} \equiv s_1 \epsilon_1 \equiv \epsilon_1 \frac{d n_{A*}}{dt} \tag{38}$$

or the continuity equation for metastables and pseudometastables becomes

$$d n_{A*}/dt = \dot{S}/\epsilon_1 \tag{39}$$

and since the jet is essentially at a steady state and $U = \Delta x/\Delta t$, we obtain

---

†Coefficients for these losses which in any case do not depend on T_e have been determined for some gases by Phelps, A. V.: Phys. Rev. 99 (1955) p. 1307 and Phelps, A. V.; and Molnar, J. P.: Phys. Rev. 89 (1953) p. 1202 to be small for our conditions. Specifically the de-excitation or quenching cross section of argon metastables ($3P_2^o$) by argon atoms in the ground state is very small, of the order of 10^{-24} m^3 (Futch, A. H.; and Grant, F. A.: Phys. Rev. 104, No. 2 (1956) pp. 356-361). Therefore the quenching frequency or reaction rate for $A* + A \rightarrow 2A + h\nu$ is negligible compared to quenching by electrons since the speed of approach of these particles at 100 °K is 1.6×10^3 times lower than the electron-argon approach speed at T_e = 3600 °K. Thus the quenching frequency for $e + A*$ is about 140 times higher than the quenching frequency for $A* + A$ even though $n_e \approx 10^{-6}\, n_A$.

$$\dot{S} = \epsilon_1 \Delta n_{A^*} \cdot \frac{U}{\Delta x} \tag{40}$$

Therefore, if we determine the change in number density of metastables per unit length of the jet, we can obtain an independent measurement of $\dot{S}$. An estimate of the magnitudes involved can be obtained by using $U = 2000$ m/sec and $\epsilon_1 = 11 \text{ ev} \times 1.6 \times 10^{-19}$ joule/ev $= 1.76 \times 10^{-18}$ joules. Then from equations (30) and (40), without rf,

$$\frac{\Delta n_{A^*}}{\Delta x} = \frac{-0.701}{1.76 \times 10^{-18} \times 2000} = -2 \times 10^{14} \frac{\text{metastables}}{m^3} \cdot \frac{1}{m} \tag{41}$$

and from equations (31) and (40) with 0.085 watts rf

$$\frac{\Delta n_{A^*}}{\Delta x} = -7 \times 10^{14} \frac{\text{metastables}}{m^3} \cdot \frac{1}{m} \tag{42}$$

Now usually the number density of metastables for this type of plasma is of the order of 10% of the number density of ions (ref. 11). Therefore, if the ion number density is of the order of 10^{16}, the number density of metastables will be of the order of 10^{15} and equations (41) and (42) show that we can get a significant change (10% to 35%) of the number density of metastables within 0.5 meters of the arcjet exit. This change of n_{A^*} could be measured quite easily (ref. 12) and can be increased by increasing the rf power.

Note that we do not have to invoke reference 11 to obtain an estimate of the number density of metastables. The electron-metastable cross section for de-excitation Q_{eA^*} is of the order of $10\,Q_{eA}$ or higher (ref. 13). Therefore since for the process

$$A^* + e \xrightarrow{k_1} A + e^* \tag{43}$$

we have†

---

† $n_{A^*} k_1 \approx \nu_{eA^*, \text{quench}} = n_{A^*} Q_{eA^*} v_{eA}$, see Bennett, W. R. Jr.: Applied Optics, Supplement No. 1, "Optical Masers," (1962), pp. 32-33.

$$\dot{S} = \epsilon_1 \frac{dn_{A^*}}{dt} = \epsilon_1 k_1 n_{A^*} n_e = \epsilon_1 n_e (n_{A^*} Q_{eA^*} v_{eA}) \tag{44}$$

we obtain

$$n_{A^*} = \frac{\dot{S}}{\epsilon_1 n_e Q_{eA^*} v_{eA}} \leq \frac{\dot{S}}{10\, \epsilon_1 n_e Q_{eA} v_{eA}} \tag{45}$$

Therefore at $T_e = 2083\ ^oK$ and $n_e = 10^{16}$ [when $\dot{S} = 0.701$ watts m^3 from equation (30)] we obtain $n_{A^*} \leq 3.15 \times 10^{15}$ per m^3, and again we conclude that Δn_{A^*} is easily measurable.†

Thus by measuring Δn_{A^*} over a given Δx, with and without rf, we can obtain an independent measurement of $\dot{S}$ from equation (40) or by integrating equation (38). This second measurement can be used to verify the results we obtain from the electron energy equation, equations (28) and (29). Determination of Δn_{A^*} or the variation of n_{A^*} with T_e and n_e can also establish the precise form of the superelastic energy exchange (de-excitation) mechanism and the magnitude of the reaction rate constant k_1.

Note that in discussing the reason why T_e remains so much higher than $T_g = T_{tr}$ in the argon experiments we cannot use the same simple argument about entropy that we used in discussing the N_2 experiments. The reason for this is because we cannot <u>easily</u> define a temperature reservoir at some temperature higher than T_e from which the electrons gain energy. The higher temperature source in this case is the energy stored in the metastables.

---

† If equation (38) is a good approximation for n_{A^*} we should expect to obtain about the same n_{A^*} no matter which $\dot{S}$ (and T_e that goes with it) we use, since the first two of equations (44) are generally valid. Thus when we use $\dot{S}$ at 0.085 watts, i.e., $\dot{S} = 2.48$ watts/m^3 and $T_e = 3568\ ^oK$ we obtain $n_{A^*} \leq 4.07 \times 10^{15}$, in fairly good agreement with the result at E = 0 (the small difference could be due to a small change in n_e or a different dependence of Q_{eA^*} on T_e).

Finally let us consider if indeed the energy that goes into heating all the electrons that pass through the waveguide by ~ 600 ^{o}K (the temperature increment we ascribe to superelastic collisions with metastables at rf power of 0.085 watts, see figure 20) is indeed equal to the energy that the electrons pick up by collisions with metastables. In other words, let us examine whether the de-excitation of metastables by electron impact can provide the electrons with an amount of energy that is consistent with their superelastic heating.

As we have seen at P = 0.085 watts we obtain T_e = 3568 ^{o}K. Letting $n_e = 10^{16}$ per m^3 and $Q_{eA^*} = 10\, Q_{eA} = 9.32 \times 10^{-20}$ m^2 we obtain $n_{A^*} = 4 \times 10^{15}$ per m^3. Then the total number of superelastic electron collisions with metastables per m^3 in the waveguide is equal to $n_e n_{A^*} Q_{eA^*} v_{eA} = 1.38 \times 10^{18}$ m^{-3} sec^{-1}. The waveguide region where the temperature is elevated to that level is greater than approximately 0.1 m and the flow velocity is 2000 m/sec. Therefore during their time-of-flight through this region the number of electrons that experience superelastic collisions with metastables is 6.92×10^{13} per m^3. The total energy that these electrons pick up is therefore $6.92 \times 10^{13} \times 1.76 \times 10^{-18} = \underline{1.22 \times 10^{-4}\ \text{joules/m}^3}$. The energy required to raise 10^{16} electrons per m^3 by 600 ^{o}K is $(3/2) n_e k (600) = \underline{1.24 \times 10^{-4}\ \text{joules/m}^3}$, in close agreement. This shows that <u>all</u> the electrons passing through the waveguide can have their temperature elevated by 600 ^{o}K thanks to the superelastic collisions that a <u>few</u> of them undergo. Note that since the energy loss factor for electrons with electrons is 1/2, it takes only about 5 electron-electron collisions to decrease the temperature of a 100,000 ^{o}K electron to approximately 3000 ^{o}K. Since the electron-electron collision frequency in the waveguide is about 10^6 per sec, it will take less than about 10^{-5} sec for the electrons to thermalize, i.e., they will travel less than about 2 cm downstream. Therefore the temperature elevation due to superelastic collisions will indeed occur mostly within the waveguide without any significant lag. On the other hand, because the relaxation time for the electrons in the argon plasma is long compared to the time-of-flight, the temperature elevation will persist downstream and the electron number density will remain higher (because of slower recombination etc.) downstream than without rf, a fact that has

been observed experimentally (unlike the nitrogen plasma where theory predicts and experiment verifies that the elevation in T_e dies out rapidly downstream of the waveguide).

We conclude that careful measurements of $n_{e,E=0}/n_{e,E}$ or the absolute value of n_e can give us the ratio $\dot{S}_E/\dot{S}_{E=0}$ or the absolute value of $\dot{S}$, respectively, from the electron energy equation. These values can be checked by measuring the change of the number density of metastables with distance as a function of rf and using the continuity equation for metastables or other energy-storing species. Either one or both of these methods should yield very accurate measurements of $\dot{S}$ without any a priori assumption of a de-excitation or superelastic energy exchange mechanism. Once $\dot{S}$ is determined with confidence, we can proceed to establish the de-excitation mechanism (i.e., to decide whether equation (43) is true or, if it is not, what is the form of the reaction) by observing how Δn_{A^*} changes with x, T_e, n_e, etc. Once the form of the reaction kinetics is determined, we can proceed to establish values for k_1 and/or Q_{eA^*} by using the measurements of $\dot{S}$ and n_{A^*}, e.g. through the use of equations such as (44). Thus we have here a very powerful tool for determining not only the magnitude of $\dot{S}$ but also the basic reaction kinetics and the absolute magnitude of the metastable de-excitation cross section Q_{eA^*}.

So far we have limited our discussion to regions where $\dot{R}$ is negligibly small. However, it is a relatively simple matter to determine $\dot{R}$ also as a function of rf power by essentially similar reasoning as we have applied above and by use of the electron energy equation in regions where $|\dot{S}| \ll \dot{R}$, or by first determining $\dot{S}(T_e)$ or even $\dot{S}_{E=0}/\dot{S}_E$. From figure 20, for example, we can immediately see that $\dot{R} > |\dot{S}|$ for argon above 0.7 watts rf power: ΔT_e becomes smaller than the elastic value.

An independent measurement of $\dot{R}$ can be obtained (ref. 14) to check the validity of the determination of $\dot{R}$ from the electron energy equation. The magnitude of $\dot{R}$ should be of the order of 20 watts/m^3 or higher in the regions of interest. Since the volume of the plasma in the rf cavity is of the order of 100 cm^3, the power radiated should be of the order of 2×10^{-3} watts. Assuming a sensor located 30 cm away, we obtain

approximately 2×10^{-7} w/cm^2 at the sensor. Therefore the sensor should be capable of detecting changes of the order of 10^{-8} w/cm^2. Since we are talking about an essentially steady-state experiment (time constant of the order of 1 sec or more) and assuming an area of the detector (within the sensor) of 16 square mm, we see that the Havens detection limit is of the order of 1.2×10^{-11} watts. Therefore we should have no problem in measuring $\dot{R}$ with any number of commercially available devices (ref. 14) if the radiation is in the visible or infrared range. Corrections to $\dot{R}$ due to the particular geometry of the experiment can be carried out in such a way that the results can be presented in a form independent of geometry and universally valid for any geometry (ref. 15).

Part of $\dot{R}$ is the result of resonant radiation in the ultraviolet range of the spectrum. Since the plasma of our interest is far from equilibrium, we shall consider briefly the spectral distribution of the radiation from a recombining plasma.

In a low density recombining plasma, the ionization energy released when an ion and an electron recombine is either transmitted to the free electrons by collision or is lost from the system by radiation. The super-elastic electron collision results in a decrease of the rate at which the hot electrons relax toward the equilibrium temperature.

Radiation losses from transitions that do not involve the ground state (i.e., non-resonant radiation) can be measured by using standard spectroscopic or total radiation methods. The resonant radiation, on the other hand, is strongly absorbed and therefore requires special techniques. Because both resonant (the part that is not absorbed) and non-resonant radiation are included in $\dot{R}$, it is necessary either to calculate or to measure the ratio of resonant radiation to non-resonant radiation. As shown below, the calculation of the amount of resonant radiation that is lost is, at best, a very rough estimate.

For a simple estimate of the resonant radiation loss, we consider the electron-ion recombination model proposed by Byron (ref. 16) and applied to an argon plasma by Chen (ref. 17). In this model the electron is assumed to become bound to the ion at the highest energy levels and then

"cascade" through the lower levels to the ground state. This de-excitation process is by either super-elastic electron collisions or by radiation, and the recombination rate is found to be equal to the rate at which the electrons cascade past some critical energy level. The de-excitation of the critical energy level is slower than the de-excitation of any other level and constitutes the "bottleneck" for the cascading electrons of Byron's model. When radiation losses are important, the critical energy level is found as the level where the collisional and radiative de-excitation rates are equal. For argon, this radiation, as well as that involving transition to the lowest excited level, is primarily in the visible and easily measured.

From the above discussion, we can conclude that the radiant loss and the energy gained by the electrons from ion recombination are approximately equal, or, at least, of the same order of magnitude for the de-excitation of all levels above the metastable level. The lowest excited levels, the 4s configuration of the argon atom, consists of two metastable and two resonant levels at about 11.5 eV. Thus, most of the ionization energy is released by the transition from the lowest excited level to the ground state.

The lowest energy levels are also de-excited by collisions or by radiative transitions. Because of the large energy difference to the ground state, collisional de-excitation rates are very small, whereas the spontaneous transition probabilities are very large. The rate of the transition producing the ArI line at 1066 Å, for example, is about 10^6 times as large as the rate of de-exciting the level by electron collisions. (See Appendix F.) However, as mentioned previously, most of this radiation is reabsorbed, or "trapped," by adjacent ground state atoms and does not escape from the plasma.

An estimate of the resonant radiation loss may be obtained by calculating the photon mean-free-path for absorption of resonant lines. This calculation has been performed for the λ 1048 line, as shown in Appendix G, for a line shape appropriate to Doppler broadening. If the line shape remains constant throughout the plasma, the calculation indicates a photon mean-free-path λ_r of only 4.5×10^{-6} m. This would suggest that, under the assumptions of Appendix G, as far as the resonant radiation is con-

cerned, the plasma could be considered as an opaque cylinder from which radiation emmanates only from a cylindrical shell of thickness λ_r at the surface. The ratio, per unit length, of this escaping radiation to the total resonant radiation in the jet can be estimated simply by the area ratio $2\pi r\lambda_r/\pi r^2$ where r is the radius of the jet. Under the conditions of our experiment (see Appendix G) this ratio is found to be 4.5×10^{-4}. We remind the reader at this point that the part of resonant radiation which is self-absorbed does not, by definition, become part of $\dot{R}$. The above calculation shows that the resonant radiation that is part of $\dot{R}$, because it escapes, is 4 orders of magnitude smaller than the total resonant radiation. Thus, as shown in Appendix G, the resonant radiation loss from the surface of the jet can be expected to be of minor importance in the electron energy equation (under conditions similar to those under which the results shown on figure 20 were obtained). The same reasoning can be applied to any control volume under certain conditions, to determine the ratio of escaping to trapped resonant radiation. In any case the validity of this reasoning can be tested by measurements.

Although the validity of this reasoning and the results of Appendix G as well as inferences from it require further exhaustive examination, we consider it appropriate to mention some preliminary results of crude radiation measurements, using a borrowed CINTRA 101 digital radiometer with a Model 111N detector probe, that appear to give some partial support to our inferences.

These measurements were carried out by looking at a 6-cm long portion of the plasma jet from outside the vacuum tank with the radiation detector placed at a distance of 70 cm from the jet axis. The optical axis of the detector was perpendicular to the jet axis.

At 1 watt rf power we measured a total radiation flux of approximately 1.2×10^{-7} watts/cm^2 at the detector in the range from 4000 to 11,000 Å. This means that the total radiation from the 6-cm portion of the jet was approximately $1.2 \times 10^{-7} \times 4\pi \times (70)^2 \approx 6 \times 10^{-3}$ watts. Since the jet is approximately 120 cm long (before it is stopped at the heat exchanger) and the radiation intensity under these conditions can be

assumed to be constant along the flow direction, the total power radiated from the jet is approximately $6 \times 10^{-3} \times 120/6 = 0.12$ watts. Note that for argon jets under these conditions the theory predicts (and the experiments prove) that electron heating effects persist throughout the jet because of slow relaxation, radiation trapping, etc., although they are stronger close to the rf electron heater.

Let us now refer to the results presented in figure 20. We note that at P = 1 watt rf power (in the argon experiments under similar conditions), ΔT_e due to $\dot{R}$ (i.e., the difference between the curves labeled "Argon Experiment" and "Argon Elastic" in figure 20) is approximately 2000 ^{o}K. This ΔT_e corresponds (as seen from the "Argon Elastic" curve) to approximately 0.2 watts of power loss in the electron energy balance. If we assume that there is no energy input into the electrons due to metastables, this energy loss can be associated with $\dot{R}$. Under the circumstances this value must be considered in excellent agreement with the crude measurement of 0.12 watts mentioned above. Reasonable agreement was also obtained at other rf power levels. The main uncertainty in these measurements was whether the enthalpy and degree of ionization of the argon-jet was exactly the same as in the measurements of ΔT_e vs. P presented in figure 20 since the two experiments were not simultaneous.

Since a temperature profile exists in the jet, the lines from atoms near the axis of the jet are broader than the lines from atoms near the edge. This means that photons with frequencies near the line center will continue to be strongly absorbed, but those that contribute to the line wings will escape. Although the resulting "escape factor" is undoubtedly small, the loss could be significant because of the large transition probabilities of the resonant lines (ref. 18). The loss, if this mechanism is important, is a volume process, and not a "surface" process as would be predicted for the model in which the photon mean free path was found to be 4.5×10^{-6} m (Appendix G).

Because of the difficulty of estimating the resonant radiation loss, as we have mentioned above, the portion of $\dot{R}$ that consists of resonant radiation must be measured by vacuum spectroscopic techniques. Unfor-

tunately neither the funds nor the time were available for these important measurements and the data available in the literature has failed to yield estimates of $\dot{R}$ and $\dot{S}$ for the conditions and gases of interest.

CONCLUSIONS AND RECOMMENDATIONS

We may conclude from this discussion that the results of these experiments are inherently accurate as long as they are obtained under conditions such that $\dot{R}$ and $\dot{S}$ are negligibly small. The available theory is sufficiently powerful to yield equally accurate results for the electron energy-loss factor in the range of conditions where $\dot{R}$ and $\dot{S}$ are not negligible, provided measurements or estimates of $\dot{R}$ and $\dot{S}$ as a function of T_e are available for the gases and conditions of interest. This investigation yielded reliable measurements of the energy-loss factor for several gases at relatively high enthalpies.

Although it is a relatively simple matter to attain conditions where both $\dot{R}$ and $\dot{S}$ are negligible and all the other constraints on the experiment are met at the same time, by manipulating the arcjet flow rates and power level, the primary to secondary flow rate ratio, the stagnation pressure and expansion ratio etc., this procedure involves a considerable amount of preliminary exploration of the arcjet characteristics through careful diagnostics. Thus, future investigations of the energy-loss factor for electrons in arc heated gases by this method require detailed knowledge of the arc heater performance in terms of the detailed energy state and composition of the exhaust gas. It is indeed unfortunate that after all these years of arcjet development the exhaust characteristics of commercially available arcjet systems are not sufficiently well known for many gases in terms of these parameters. In fact, the diagnostic information obtained for the commercial arcjet system used in this study during the course of this work may be considered as one of the major contributions of this investigation.

The information on plasma parameters obtained during the course

of this work made it possible to study the behavior of the electron energy balance in detail that has seldom been achieved before and to identify mechanisms of excitation and de-excitation of atomic energy levels by electron impact that, with additional study, may find numerous useful applications.

It is therefore recommended that these well-proven techniques and existing facilities be used in two continuing programs, namely:

(1) extension of the measurement of electron energy-loss factors in hot gases over
   (a) a wider range of electron temperatures, gas enthalpies and excitation states of the gas, and
   (b) a wider range of gas composition, including mixtures representative of rocket exhausts, ablation products, combustion processes, re-entry wakes, etc.

and

(2) detailed investigation of the mechanisms and rates of electron energy relaxation in plasmas and excitation or de-excitation of excited atomic or molecular states by electron impact with the purpose of identifying means for selectively controlling their populations by manipulation of the electron temperature.

ACKNOWLEDGMENTS

The authors want to thank C. H. Deichler, J. C. Sutton, P. Dimotakis and G. Fonda-Bonardi of our laboratory, for outstanding performance in the design and fabrication of all the specialized apparatus used in these experiments and careful performance of some of the measurements reported here and Drs. G. S. Argyropoulos, John Thornton and F. Culick of our permanent and consulting staffs for many helpful suggestions and discussions. We also want to thank Mrs. Alrae Tingley, Mike Casteel, and Susan Hagen for reduction of much of the data presented in this and previous publications and Mrs. Ethel Valaer for typing much of the manuscript. Thanks are also due to Prof. S. L. Petrie for the design of the electron beam apparatus and to Dr. S. Schwartz for some of the measurements of T_{vib} reported here. Finally we want to thank Mr. Howard Stine of NASA/Ames for his patience, his constructive critical comments and his support in the course of this investigation.

REFERENCES

1. Demetriades, S. T.: Determination of Energy-loss Factors for Slow Electrons in Hot Gases. Phys. Rev., vol. 158, No. 2, June 1967, pp. 215-217.

2. Demetriades, S. T.: Novel Method for Determination of Energy-loss Factors for Slow Electrons in Hot Gases. Interim Report on Contract NAS 2-3580 (1 August 1968).

3. Demetriades, S. T.; and Aroeste, H.: Theoretical Studies on the Thermal Decomposition of Nitric Oxide in a Shock Tube. Guggenheim Jet Propulsion Center Report No. 3, Contract AF 18(603)-2, AFOSR-TN-56-335, ASTIA Doc. No. AD-95-211, June 1956.

4. Lutz, M. A.: Radiation and Its Effect on the Nonequilibrium Properties of a Seeded Plasma. AIAA J. vol. 5, No. 8, August 1967, pp. 1416-1423.

5. Ginzburg, V. L.; and Gurevich, A. V.: Nonlinear Phenomena in a Plasma Located in an Alternating Electromagnetic Field. Usp. Fiz. Nauk, vol. 70, No. 2, February 1960, pp. 201-246 [English transl.: Soviet Phys. - Usp., vol. 3, July-August 1960, pp. 115-147].

6. Hurle, I. R.: On the Thermal Energy Transfer Between Free Electrons and Molecular Vibration. J. Chem. Phys., vol. 41, 1964, pp. 3592-3603.

7. Hurle, I. R.; and Russo, A. L.: Spectrum-Line Reversal Measurements of Free-Electron and Coupled N_2 Vibrational Temperatures in Expansion Flows. J. Chem. Phys., vol. 43, No. 12, 1965, pp. 4434-4443.

8. Engelhardt, A. G.; Phelps, A. V.; and Risk, C. G.: Determination of Momentum Transfer and Inelastic Collision Cross Sections for Electrons in Nitrogen Using Transport Coefficients. Phys. Rev. vol. 135, No. 6A, September 1964, pp. A1566-A1574.

9. Lackner, K. ; Argyropoulos, G. S. ; and Demetriades, S. T. : Relaxation Effects in J × B Devices. AIAA J. vol. 6, No. 5, May 1968, pp. 949-951.

10. Demetriades, S. T. ; Argyropoulos, G. S. ; and Fonda-Bonardi, G. : Final Report, Contract AF 49(638)-1594, in process of preparation.

11. Mosburg, E. R., Jr. : Phys. Rev. vol. 152, 1960, pp. 166-176. He has observed values of n_{He^*}/n_e between 0. 1 and 0. 25. Argon should not behave very differently.

12. Kaminsky, Manfred: Atomic and Ionic Impact Phenomena on Metal Surfaces, see chapter on "De-excitation of Metastable Atoms and Ions on Metal Surfaces," Academic Press, New York (1965), pp. 292-299.

13. Sovie, Ronald J. ; and Dugan, J. V., Jr. : Effects of Metastable Atoms on Volume Ion Production in a Tenuous Helium Plasma. NASA TN D-3121, November 1965.

14. Locket, Arthur S. et al. : Guidance, in Principles of Guided Missile Design, Grayson Merrill (ed.), D. Van Nostrand Company, Inc., Princeton, New Jersey, 1955.

15. Cool, T. A. : Recombination, Ionization and Nonequilibrium Conductivity in Seeded Plasmas. Ph. D. Thesis, California Institute of Technology, 1965.

16. Byron, S. ; Stabler, R. C. ; and Bortz, P. I. Electron-Ion Recombination by Collisional and Radiative Processes. Physical Review Letters, vol. 8, 1962, pp. 376-379.

17. Chen, C. J. : Collisional-Radiative Electron-Ion Recombination Rate in Rare-Gas Plasmas. J. Chem. Phys., vol. 50, 1969, pp. 1560-1566.

18. Lawrence, G. M. : Radiance Lifetimes in the Resonance of Ar I. Phys. Rev. vol. 175, 1968, pp. 40-44.

Table Ia. Raw data for computing effective energy-loss factors in three mixtures of Carbon Monoxide and Argon

Run No.	Time	Enthalpy BTU/lb	rf power P_{av}	Electron Temperature, ^{o}K		
				no rf $T_{e, E=0}$	with rf $T_{e, rf}$	increment ΔT_e
210-C	16:08	532	.800	4430	7655	3225
210-C	16:11	532	.815	4820	7945	3125
210-C	16:12	532	.845	5330	7935	2605
210-C	16:14	532	.835	5620	8575	2955
210-D	16:20	536	.417	6020	8860	2840
210-D	16:27	536	.419	6250	8550	2300
210-F	16:41	534	.180	5610	6248	638

Table Ib. Collision cross sections, mixture ratios, and effective energy-loss factors used in the solution of the mixture equation for the energy-loss factor of pure CO

Run Time	$T_e(^{o}K)$	$Q_{e, A}$	$Q_{e, CO}$	Mixture Ratio n_A/n_{CO}	δ_{eff}	δ_{CO}
16:08	7655.	2.51E-20	1.87E-19	103.315	7.12E-05	6.82E-04
16:11	7945.	2.62E-20	1.85E-19	103.315	7.48E-05	7.75E-04
16:12	7935.	2.62E-20	1.85E-19	103.315	9.31E 05	1.06E-03
16:14	8575.	2.88E-20	1.80E-19	103.315	8.11E-05	9.71E-04
16:20	8860.	2.99E-20	1.78E-19	101.350	4.22E-05	2.97E-04
16:27	8550.	2.87E-20	1.80E-19	101.350	5.23E-05	4.58E-04
16:41	6248.	1.95E-20	1.95E-19	47.047	8.10E-05	3.34E-04

Table IIa. Raw data for computing effective energy-loss factors in two mixtures of Helium and Argon

Run No.	Time	Enthalpy BTU/lb	rf power P_{av}	Electron Temperature, °K: no rf $T_{e,E=0}$	with rf $T_{e,rf}$	increment ΔT_e
219-A	11:15	438	.823	2450	7300	4850
219-A	11:17	438	.422	2550	4198	1648
219-A	11:20	438	.419	2585	5405	2820
219-B	11:24	414	.340	2401	4602	2201
219-B	11:27	414	.331	2740	4151	1411
219-C	11:37	404	.254	2907	4887	1980
219-C	11:40	404	.184	2875	4204	1329
219-D	11:44	411	.089	2570	3157	587
219-H	12:05	402	.440	2640	4050	1410
219-H	12:08	402	.439	2604	4149	1545
220-A	14:43	413	.550	1001	3306	2305
220-A	14:47	413	.535	873	3543	2670

Table IIb. Collision cross sections, mixture ratios, and effective energy-loss factors used in the solution of the mixture equation for the energy-loss factor of pure He

Run Time	T_e(°K)	$Q_{e,A}$	$Q_{e,CO}$	Mixture Ratio n_A/n_{CO}	δ_{eff}	δ_{CO}
11:15	7300.	2.37E-20	6.26E-20	2.531	4.87E-05	6.93E-05
11:17	4198.	1.16E-20	6.48E-20	2.531	7.35E-05	9.45E-05
11:20	5405.	1.62E-20	6.41E-20	2.531	4.27E-05	5.26E-05
11:24	4602.	1.31E-20	6.46E-20	2.536	4.43E-05	5.31E-05
11:27	4151.	1.14E-20	6.49E-20	2.536	6.73E-05	8.53E-05
11:37	4887.	1.42E-20	6.44E-20	2.541	3.68E-05	4.22E-05
11:40	4204.	1.16E-20	6.48E-20	2.541	3.97E-05	4.55E-05
11:44	3157.	7.86E-21	6.53E-20	2.544	4.38E-05	4.88E-05
12:05	4050.	1.11E-20	6.49E-20	1.296	8.96E-05	1.03E-04
12:08	3306.	8.38E-21	6.52E-20	2.511	6.85E-05	8.18E-05
14:43	3306.	8.38E-21	6.52E-20	2.511	6.85E-05	8.18E-05
14:47	3543.	9.23E-21	6.52E-20	2.511	5.75E-05	6.83E-05

Table IIIa. Raw data for computing effective energy-loss factors in various mixtures of Nitrogen and Argon

Run No.	Time	Enthalpy BTU/lb	rf power P_{av}	Electron Temperature, ^{o}K		
				no rf $T_{e,E=0}$	with rf $T_{e,rf}$	increment ΔT_e
216-C	9:17	488	1.310	4710	6658	1948
218-A	10:22	449	2.560	4710	6475	1765
209-A	13:47	490	1.700	6020	7800	1780
213-A	13:51	489	.865	6640	7446	806
213-A	14:07	489	1.280	5460	6685	1225
213-A	14:09	489	2.155	5560	7490	1930
209-E	14:26	476	.870	3480	4169	689
209-F	14:38	487	2.625	3410	5240	1830
212-A	10:49	490	.865	5730	6419	689
212-A	10:51	490	1.355	5770	6329	559
212-A	10:53	490	1.705	6200	7057	857
212-B	11:00	510	2.525	6160	7650	1490
212-C	11:13	475	2.105	5630	6890	1260
212-E	11:30	408	2.535	5610	6534	924
213-A	13:51	489	1.585	2450	3710	1260
213-B	13:58	488	1.625	2385	3795	1410
213-B	14:01	488	1.600	2620	3812	1192
213-B	14:03	488	2.515	2789	4099	1310
213-B	14:06	488	2.560	2589	3969	1380
213-B	14:09	488	.865	2550	3391	841
213-D	14:14	425	.895	2470	3242	772

Table IIIb. Collision cross sections, mixture ratios, and effective energy-loss factors used in the solution of the mixture equation for the energy-loss factor of pure N_2

Run Time	$T_e(^oK)$	$Q_{e,A}$	$Q_{e,CO}$	Mixture Ratio n_A/n_{CO}	δ_{eff}	δ_{CO}
9:17	6658.	2.11E-20	1.58E-19	9.012	1.93E-04	3.93E-04
10:22	6475.	2.04E-20	1.56E-19	4.235	4.16E-04	6.32E-04
13:47	7800.	2.57E-20	1.66E-19	12.244	2.74E-04	7.41E-04
13:51	7446.	2.42E-20	1.64E-19	9.955	3.08E-04	7.21E-04
14:07	6685.	2.12E-20	1.58E-19	11.661	3.00E-04	7.27E-04
14:09	7490.	2.44E-20	1.64E-19	11.661	3.20E-04	8.29E-04
14:26	4169.	1.15E-20	1.21E-19	5.087	3.62E-04	5.24E-04
14:38	5240.	1.56E-20	1.39E-19	5.047	4.12E-04	6.29E-04
10:49	6419.	2.02E-20	1.55E-19	4.087	3.60E-04	5.37E-04
10:51	6329.	1.98E-20	1.54E-19	4.087	6.96E-04	1.05E-03
10:53	7057.	2.27E-20	1.61E-19	4.087	5.71E-04	8.84E-04
11:00	7650.	2.51E-20	1.65E-19	4.059	4.86E-04	7.69E-04
11:13	6890.	2.20E-20	1.60E-19	3.984	4.79E-04	7.28E-04
11:30	6534.	2.06E-20	1.56E-19	2.018	7.87E-04	9.90E-04
13:51	3710.	9.83E-21	1.14E-19	8.830	3.61E-04	6.16E-04
13:58	3795.	1.01E-20	1.15E-19	8.819	3.31E-04	5.66E-04
14:01	3812.	1.02E-20	1.15E-19	8.819	3.85E-04	6.64E-04
14:03	4099.	1.13E-20	1.20E-19	8.791	3.51E-04	9.82E-04
14:06	3969.	1.08E-20	1.18E-19	8.791	5.32E-04	9.38E-04
14:09	3391.	8.68E-21	1.09E-19	8.791	2.95E-04	4.83E-04
14:14	3242.	8.15E-21	1.07E-19	8.724	3.33E-04	5.36E-04

Table IVa. Raw data for computing effective energy-loss factors in three mixtures of Nitric Oxide and Argon

Run No.	Time	Enthalpy BTU/lb	rf power P_{av}	Electron Temperature, ^{o}K		
				no rf $T_{e, E=0}$	with rf $T_{e, rf}$	increment ΔT_e
240-A	13:38	304	1.695	1310	1495	185
240-A	13:41	304	4.305	1310	2150	840
240-A	13:44	304	4.360	1344	2369	1025
240-B	13:47	295	6.005	1344	3929	2585
240-B	13:54	295	5.945	1159	4099	2940
240-C	13:57	276	3.385	1260	2066	806
240-C	14:00	276	3.430	1160	2453	1293
235-A	15:11	373	2.610	2117	2705	588
235-B	15:22	369	4.400	1328	4546	3218
235-B	15:27	369	6.045	1291	2971	1680
235-C	15:32	398	6.055	1159	2671	1512
237-B	12:24	590	1.265	1191	4201	3010
237-B	12:26	590	.830	1310	4081	2771
237-B	12:29	590	.422	1225	3206	1981
237-C	12:34	674	.579	1412	3562	2150
237-C	12:35	674	.421	1428	2772	1344
237-C	12:37	674	.593	1175	3307	2132
237-D	12:39	669	.251	1092	2519	1427
237-D	12:45	669	.251	1109	2469	1360
237-D	12:47	669	.501	1025	3343	2318
237-E	12:53	671	.837	1529	4454	2925
237-E	12:57	671	1.635	1528	5948	4420

Table IVb. Collision cross sections, mixture ratios, and effective energy-loss factors used in the solution of the mixture equation for the energy-loss factor of Nitric Oxide.

Run Time	T_e (°K)	$Q_{e,A}$	$Q_{e,CO}$	Mixture Ratio n_A/n_{CO}	δ_{eff}	δ_{CO}
13:38	1495.	3.00E-21	1.70E-19	444.000	2.63E-03	2.31E-02
13:41	2150.	4.65E-21	1.98E-19	444.000	1.47E-03	1.65E-02
13:44	2369.	5.28E-21	2.04E-19	444.000	1.22E-03	1.49E-02
13:47	3929.	1.06E-20	2.04E-19	496.900	6.67E-04	1.72E-02
13:54	4099.	1.13E-20	2.02E-19	496.900	5.80E-04	1.59E-02
13:57	2066.	4.42E-21	1.96E-19	528.100	1.21E-03	1.53E-02
14:00	2453.	5.53E-21	2.06E-19	528.100	7.61E-04	1.12E-02
15:11	2705.	6.32E-21	2.09E-19	87.550	1.27E-03	4.58E-03
15:22	4546.	1.29E-20	1.96E-19	90.344	3.92E-04	2.57E-03
15:27	2971.	7.22E-21	2.10E-19	90.344	1.03E-03	4.16E-03
15:32	2671.	6.21E-21	2.09E-19	90.808	1.15E-03	4.18E-03
12:24	4201.	1.16E-20	2.01E-19	56.013	1.21E-04	4.24E-04
12:26	4081.	1.12E-20	2.02E-19	56.013	8.60E-05	2.68E-04
12:29	3206.	8.03E-21	2.10E-19	56.013	6.11E-05	1.34E-04
12:34	3562.	9.30E-21	2.07E-19	59.072	7.73E-05	2.10E-04
12:35	2772.	6.54E-21	2.09E-19	59.072	9.00E-05	2.06E-04
12:37	3307.	8.38E-21	2.09E-19	59.072	7.98E-05	2.04E-04
12:39	2519.	5.73E-21	2.07E-19	62.299	5.06E-05	9.10E-05
12:45	2469.	5.58E-21	2.06E-19	62.299	5.30E-05	9.65E-05
12:47	3343.	8.51E-21	2.09E-19	62.299	6.20E-05	1.50E-04
12:53	4454.	1.26E-20	1.97E-19	65.303	8.22E-05	3.11E-04
12:57	5948.	1.83E-20	1.78E-19	65.966	1.06E-04	6.44E-04

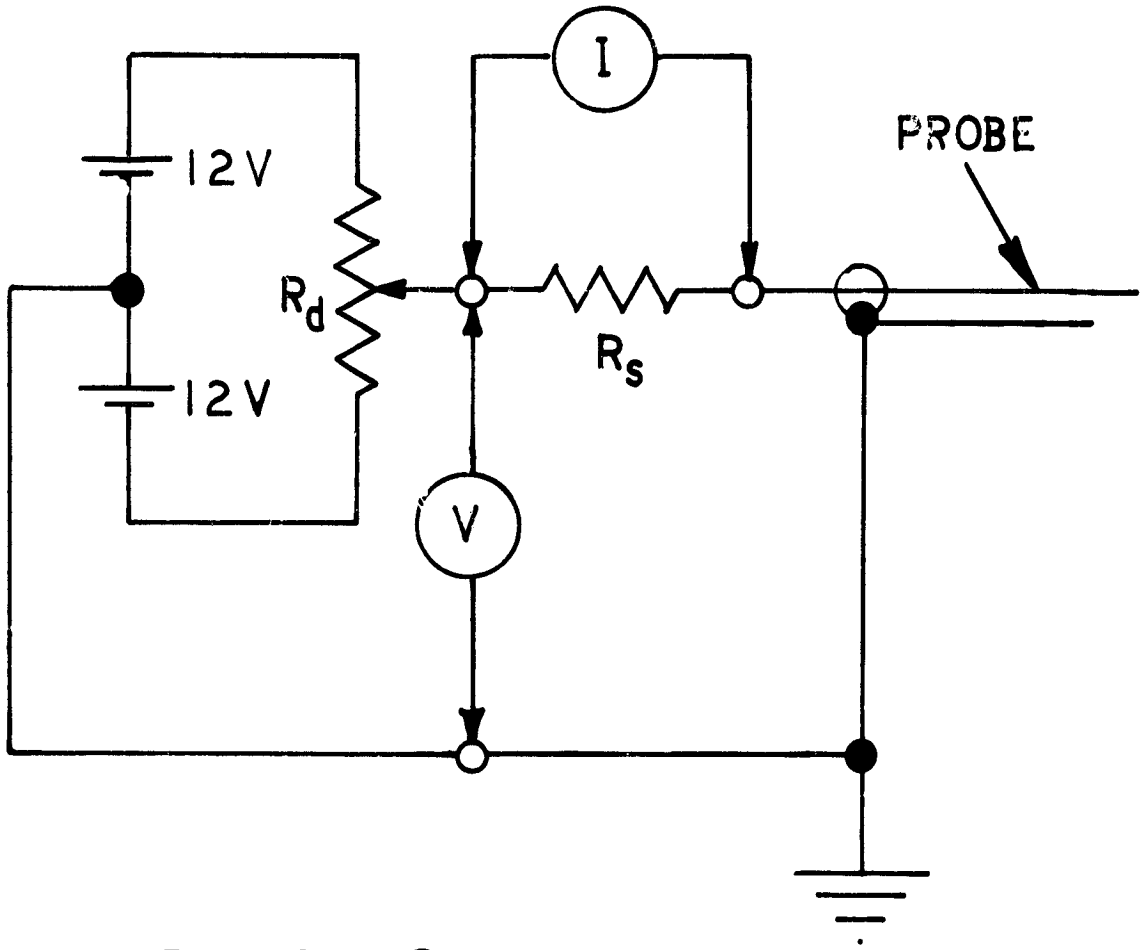

$R_d = 200\Omega$

$R_s = 10$ or 100Ω

Figure 1. Langmuir probe measurement circuit

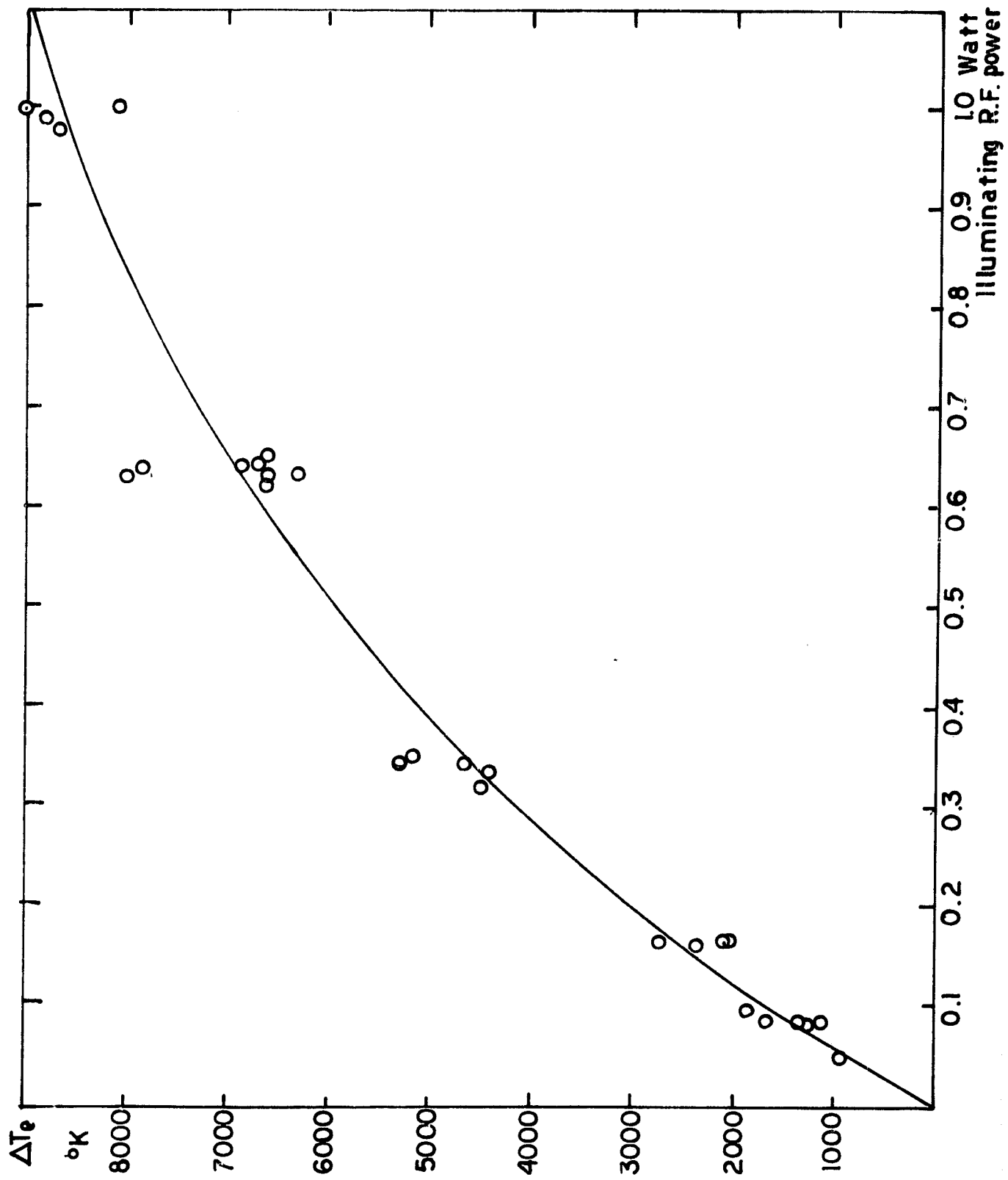

Figure 2. Measured electron temperature increment in pure argon as a function of applied microwave power.

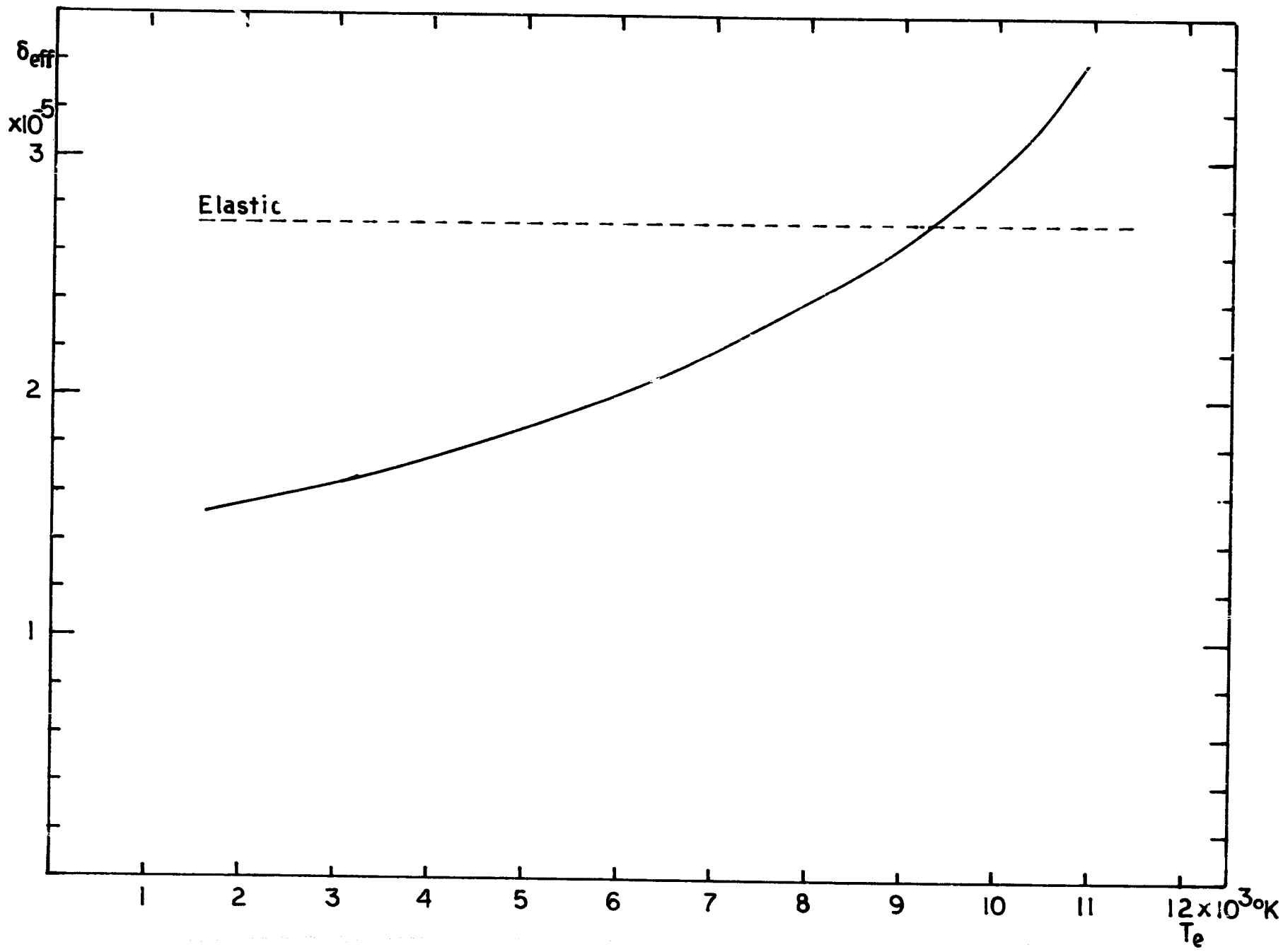

Figure 3. Electron energy-loss factor for pure argon as a function of electron temperature.

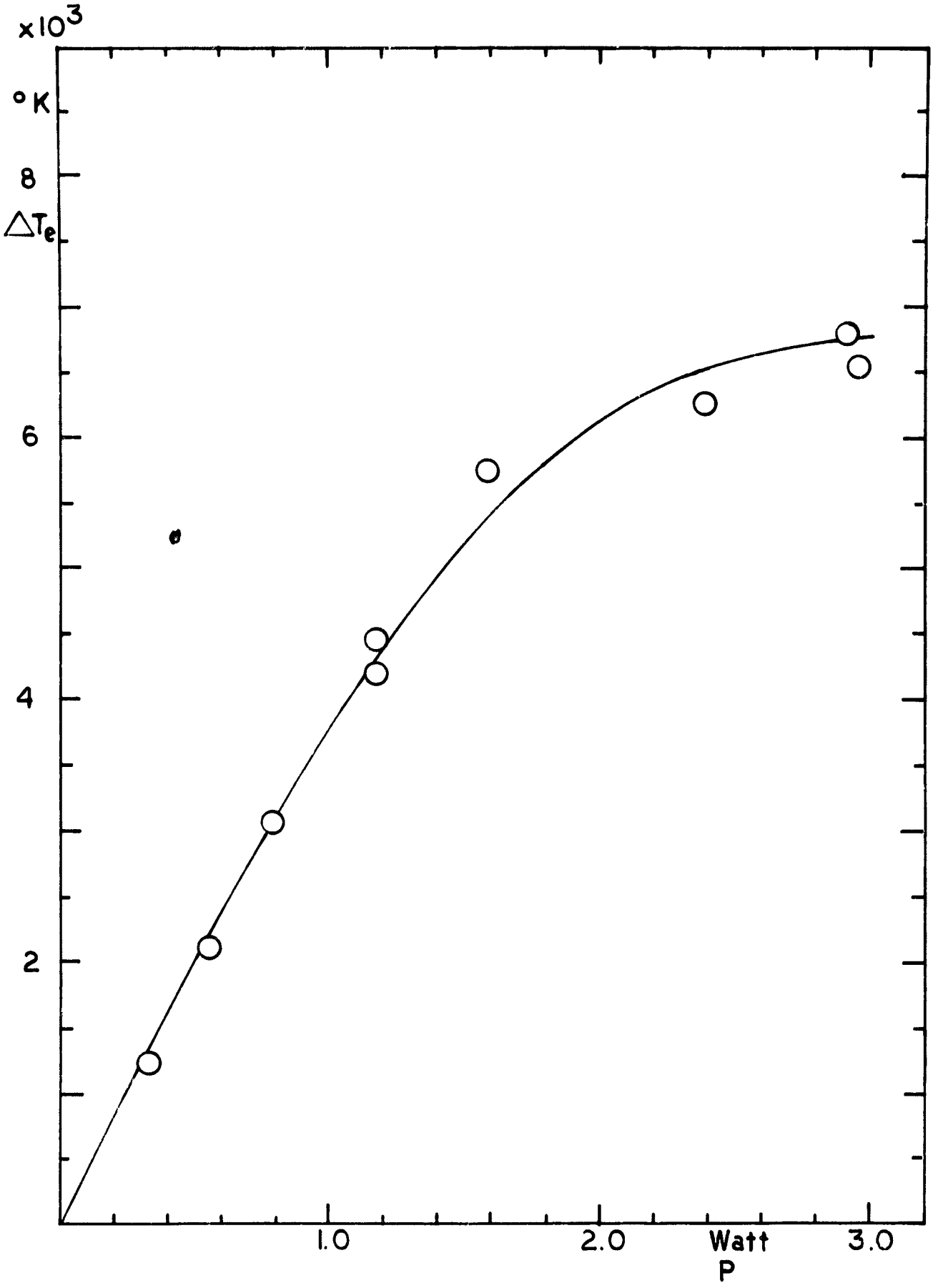

Figure 4. Electron temperature elevation in pure helium as a function of applied microwave power

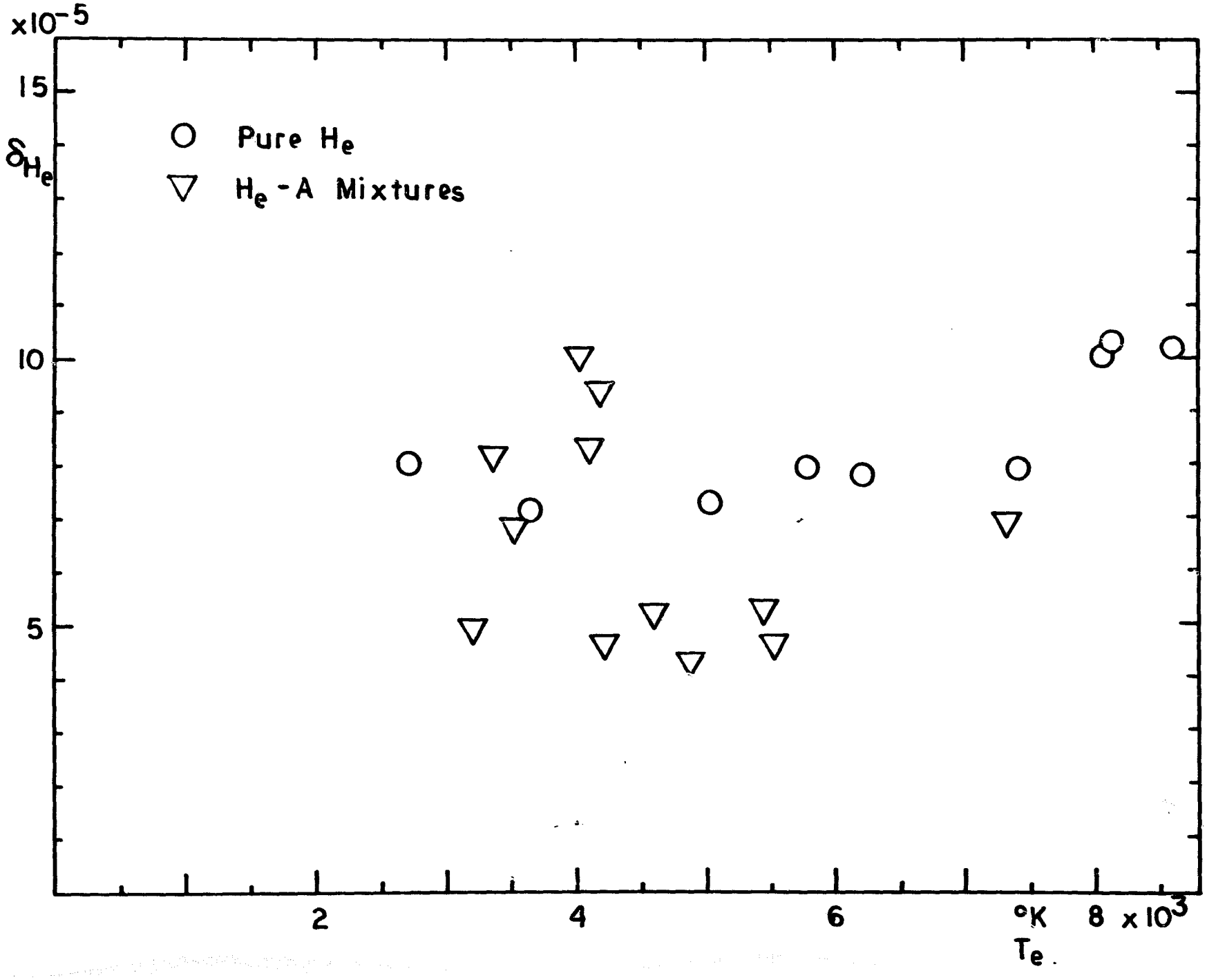

Figure 5. Electron energy-loss factor for helium as a function of electron temperature. Mixture-rule data and pure-helium data are shown together for comparison.

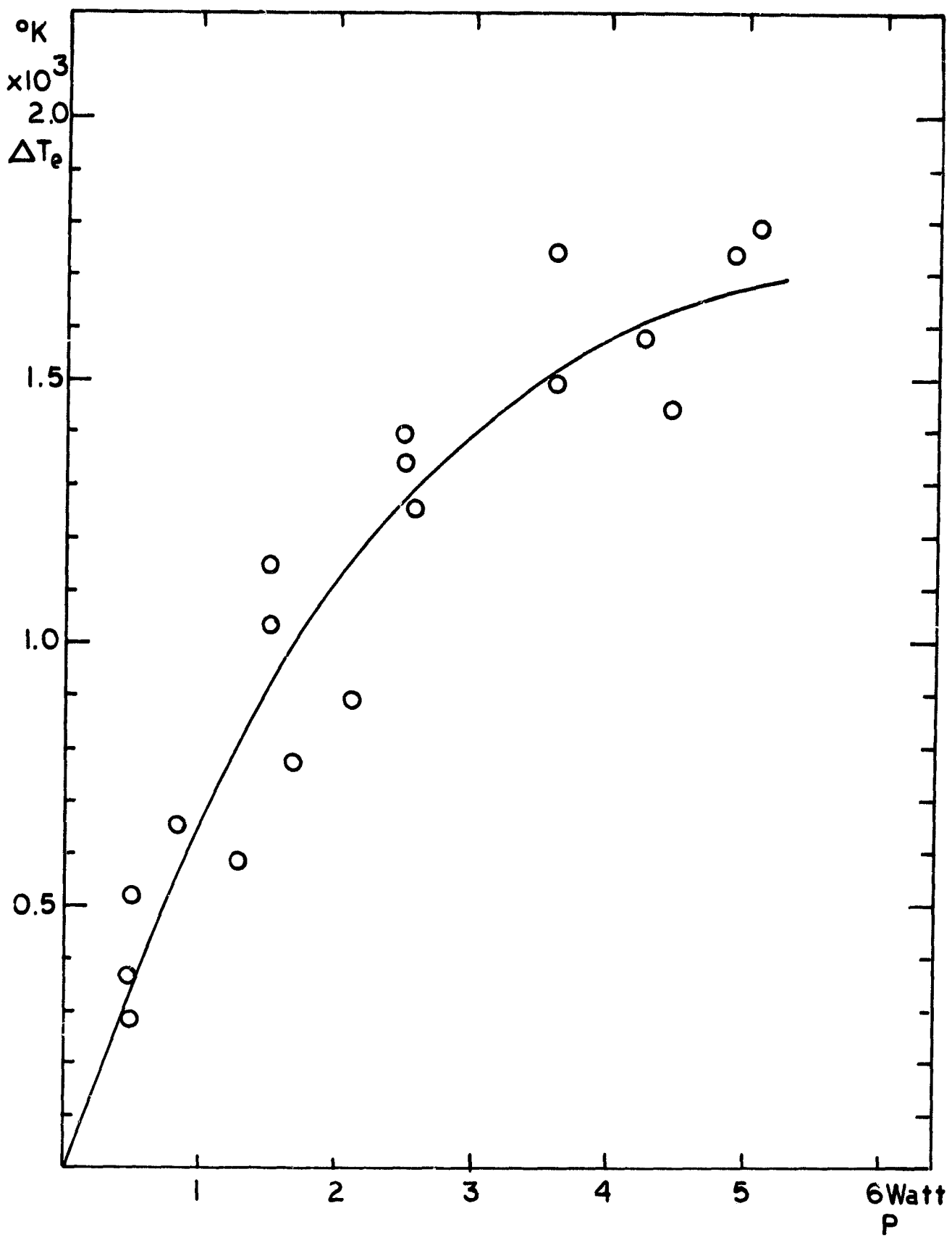

Figure 6. Measured electron temperature rise, ΔT_e, as a function of rf power in prepurified nitrogen plasmajet with $H_o \approx 1200$ BTU/lb produced by Thermal Dynamics 50-N arcjet

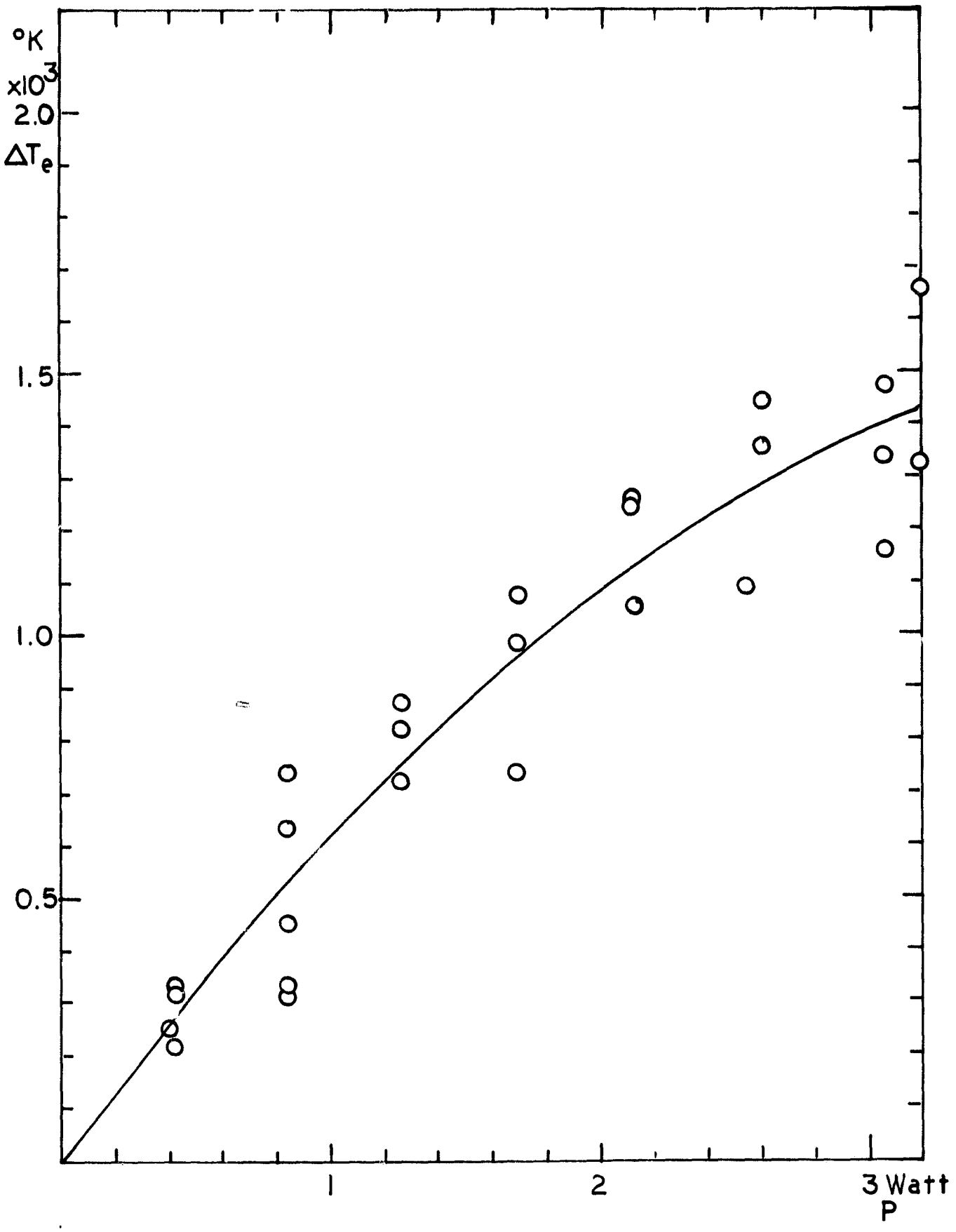

Figure 7. Electron temperature elevation in a pure nitrogen plasma ($H_o \approx 650$ BTU/lb) as a function of applied microwave power

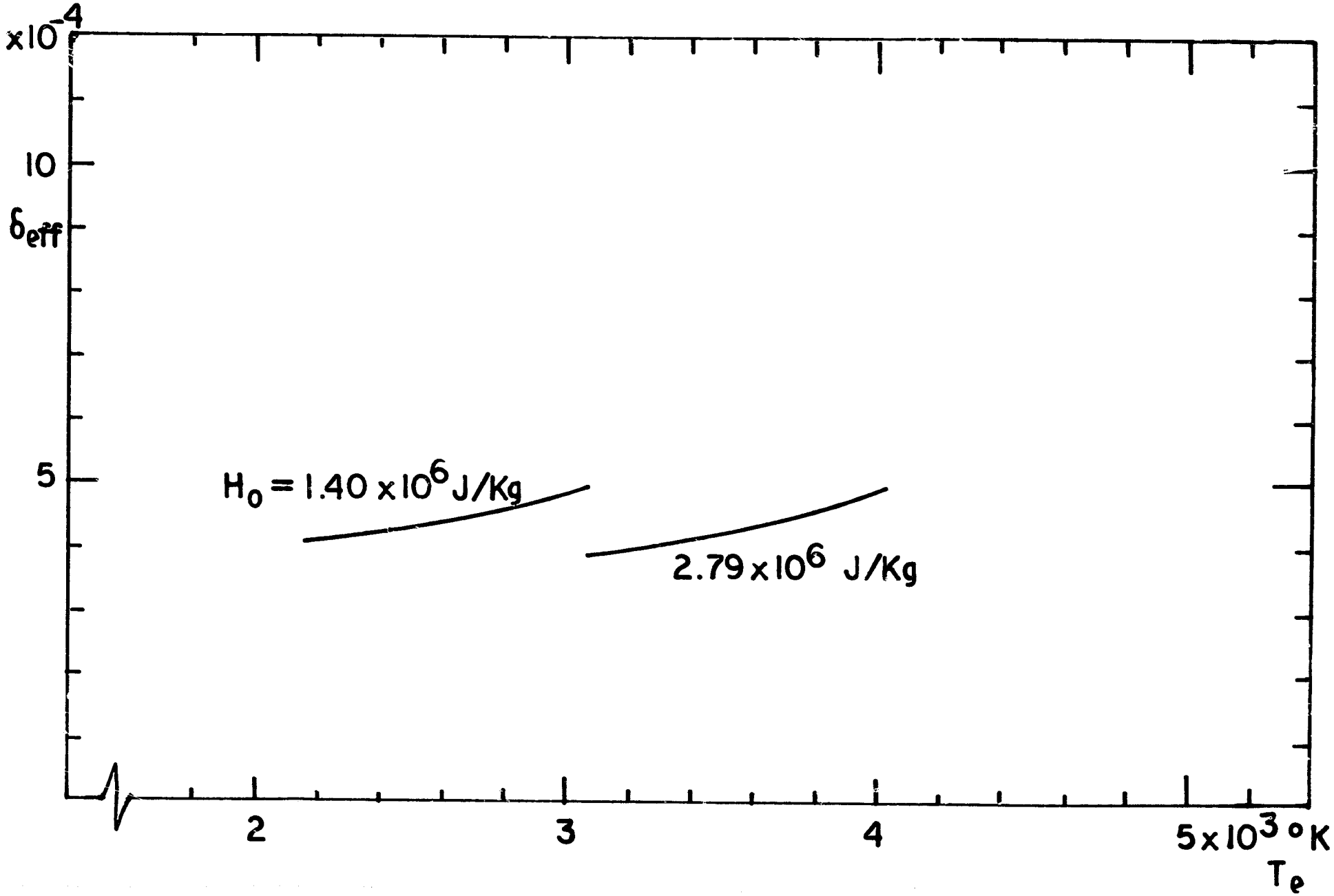

Figure 8. Electron energy-loss factor for pure nitrogen as a function of electron temperature. Data at two enthalpies, 650 and 1200 BTU/lb, are shown.

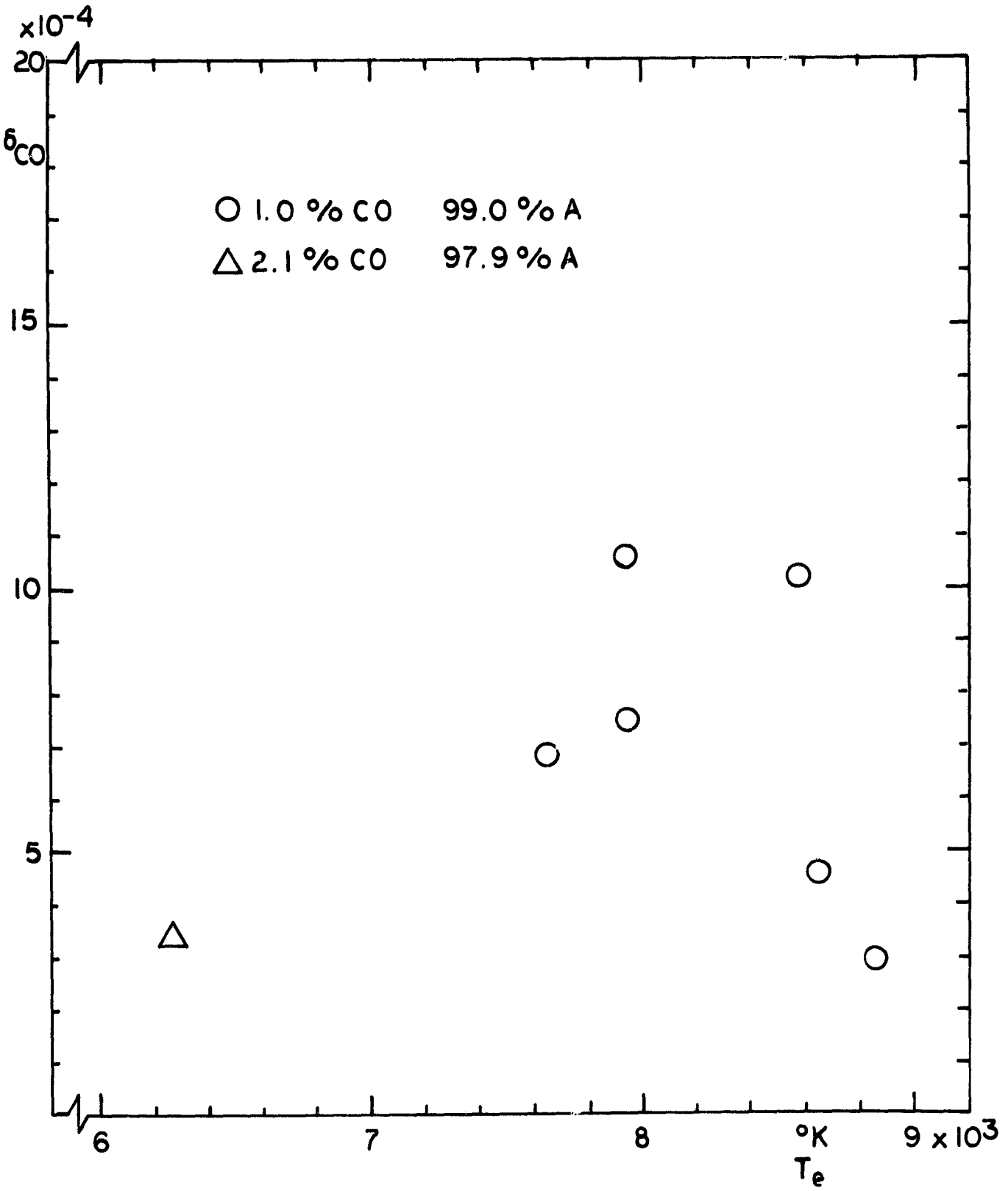

Figure 9. Electron energy-loss factor for carbon monoxide as a function of electron temperature. Data shown result from the solution of the mixture rule equation with two molecular concentrations of CO in argon at a stagnation enthalpy of 534 BTU/lb

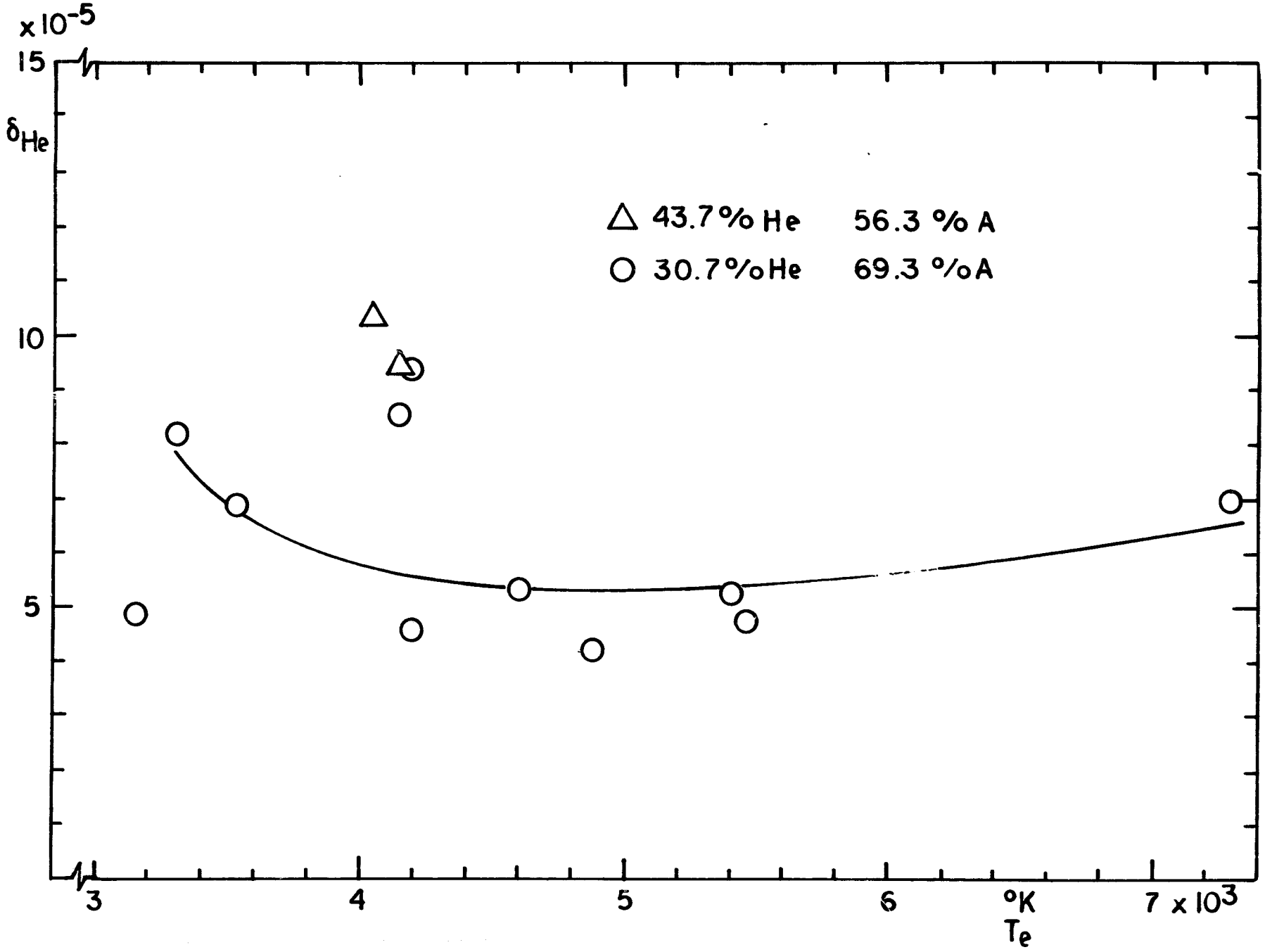

Figure 10. Electron energy-loss factor for helium as a function of electron temperature. Data shown are derived from the mixture rule equation with two molecular concentrations of helium in argon at a stagnation enthalpy of 420 BTU/lb.

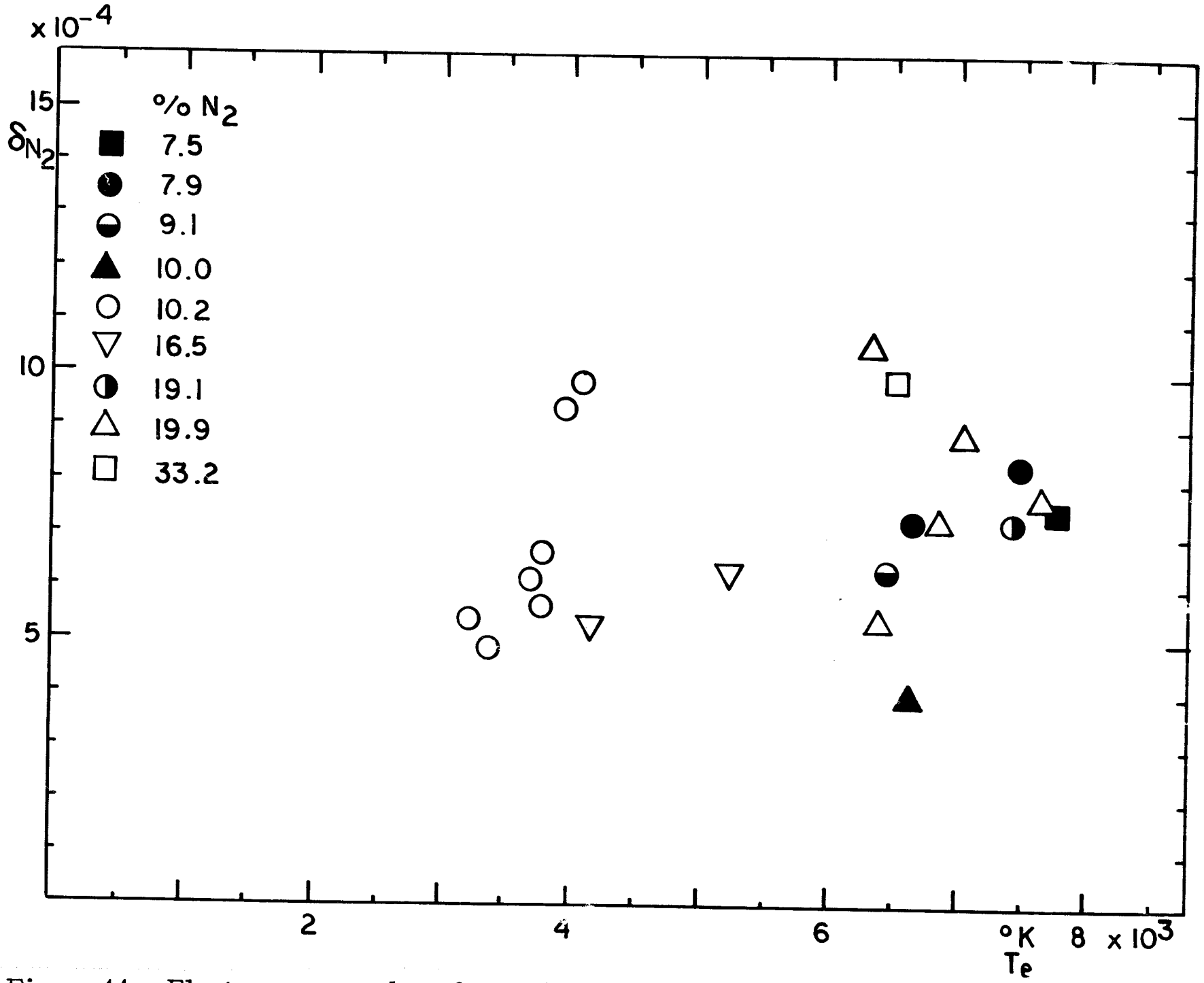

Figure 11. Electron energy-loss factor for nitrogen as a function of electron temperature. Data shown result from solution of mixture rule equation with various molecular concentrations of nitrogen in argon.

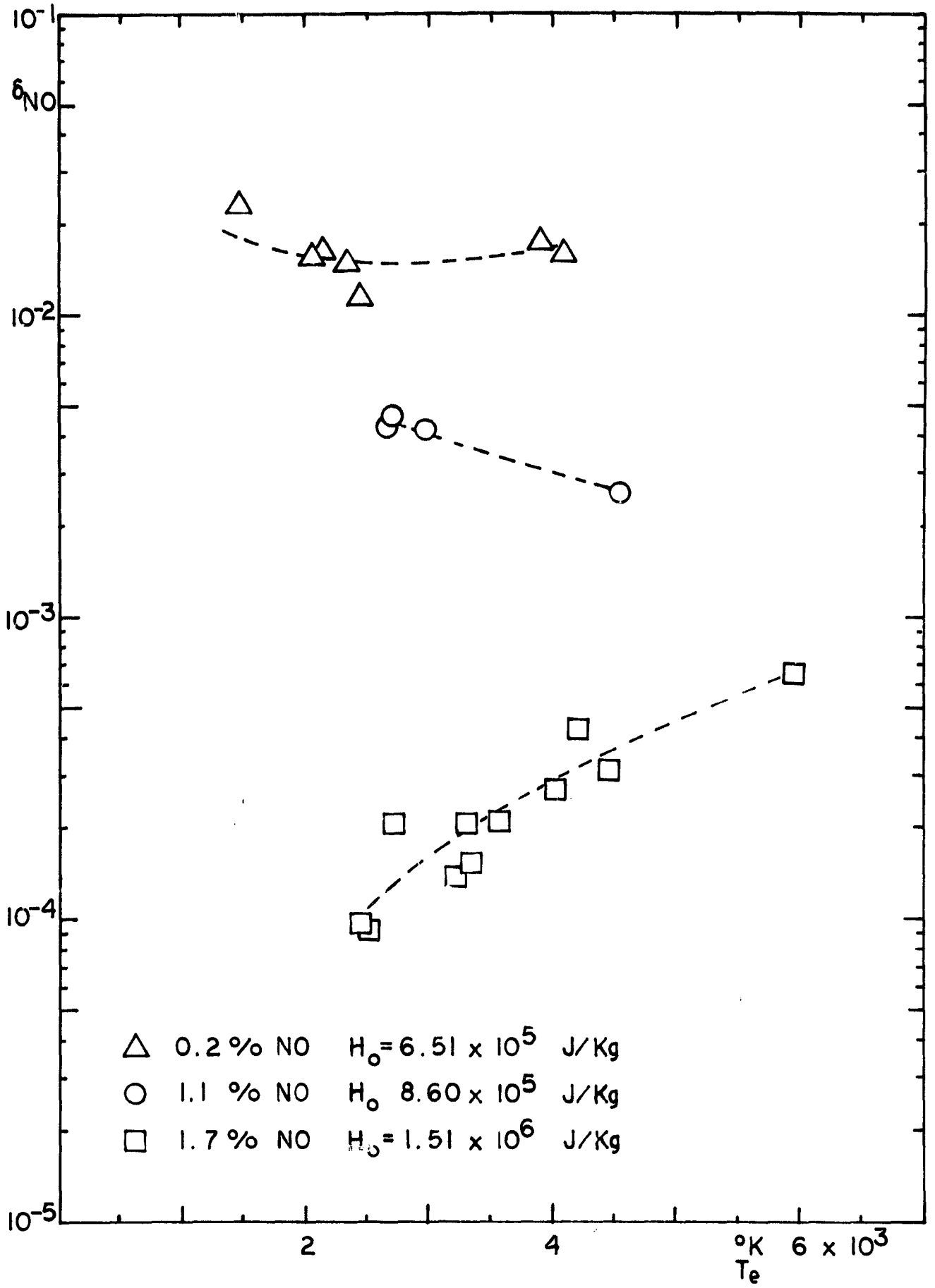

Figure 12. Electron energy-loss factor for nitric oxide as a function of electron temperature, computed from the mixture rule for three molecular concentrations of NO in argon and plasma stagnation enthalpy conditions

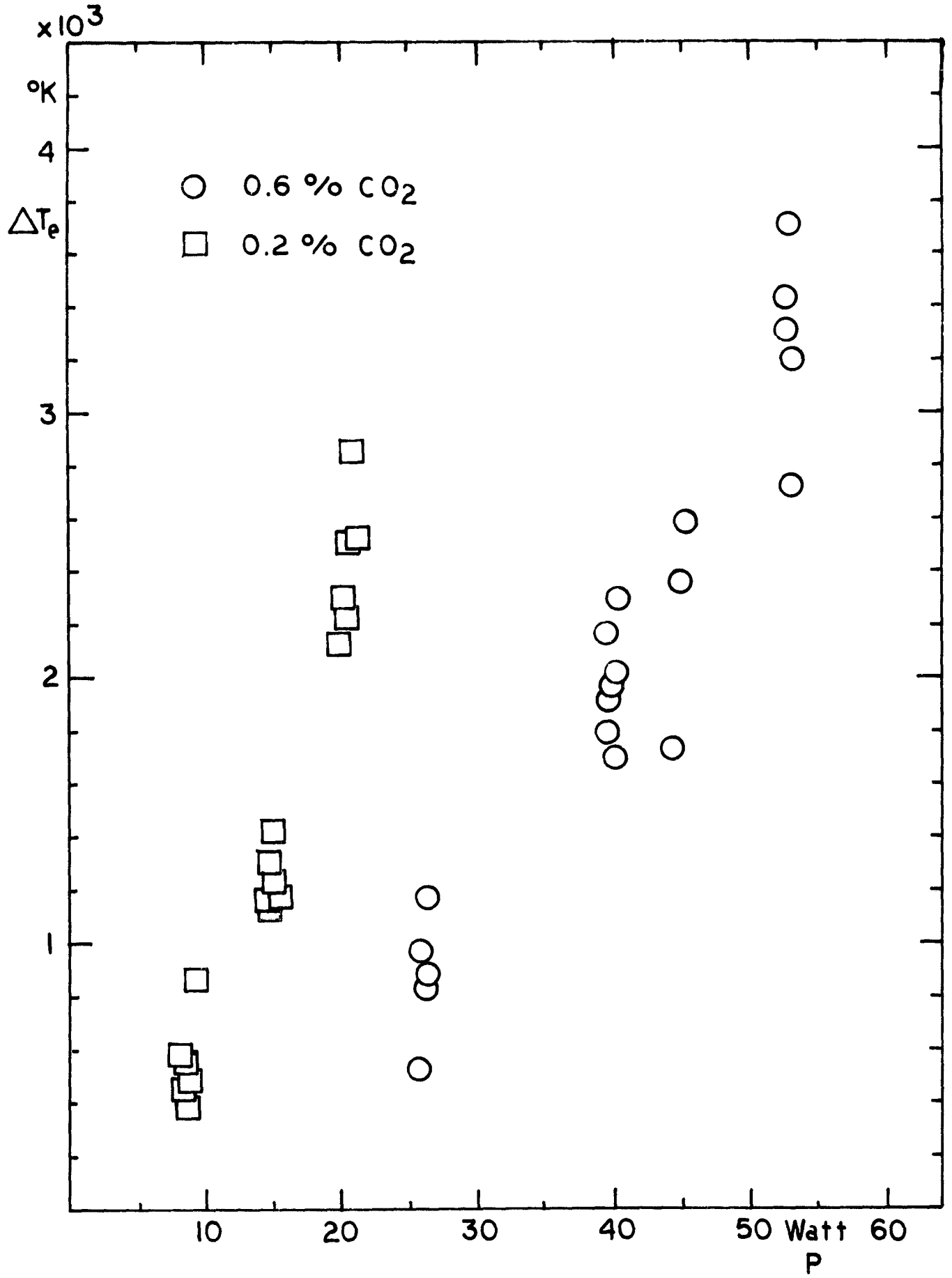

Figure 13. Electron temperature elevation as a function of rf power for two molecular concentrations of CO_2 in argon

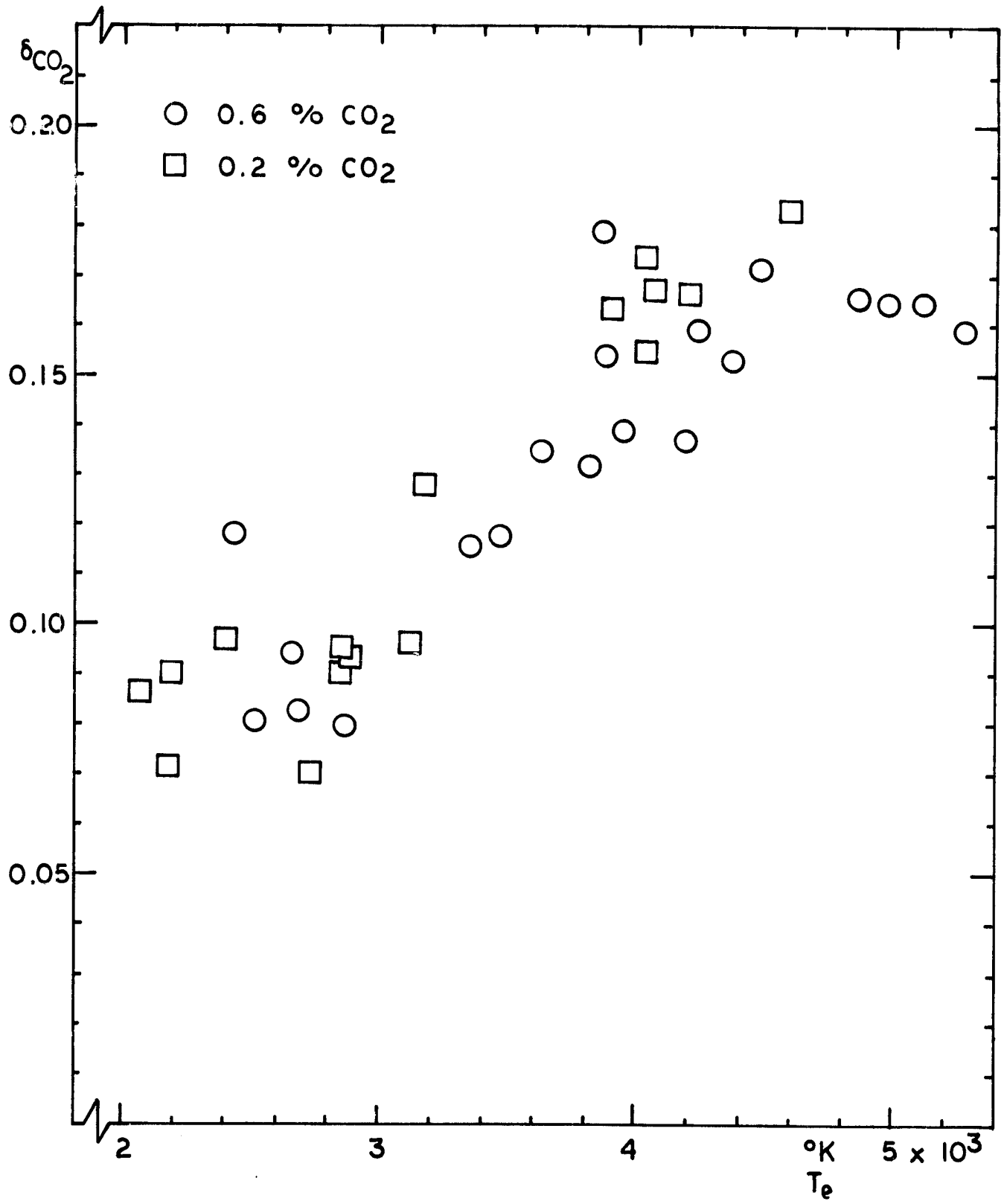

Figure 14. Electron energy-loss factor for carbon dioxide as a function of electron temperature. The symbols identify the molecular concentration of CO_2 in argon from which δ_{CO_2} was determined

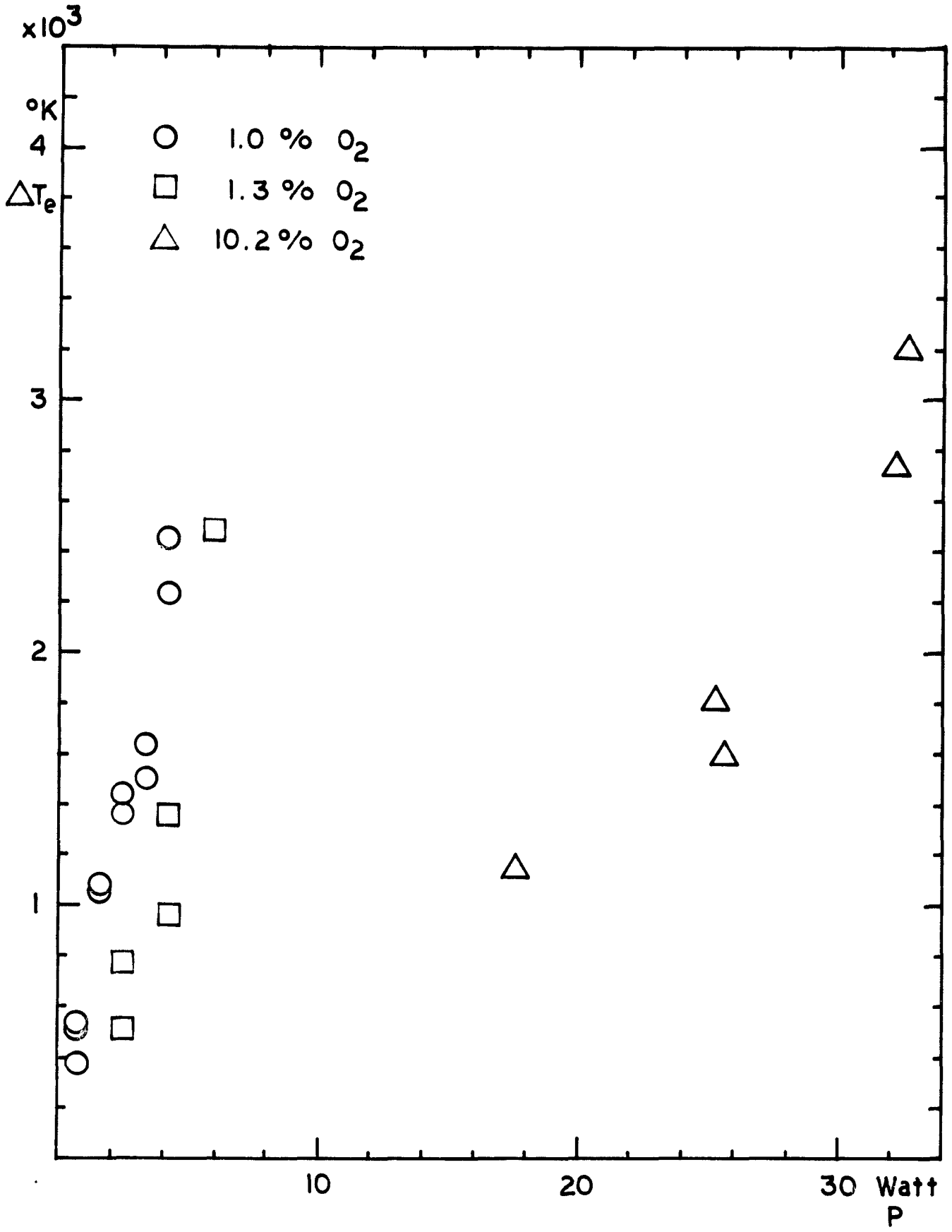

Figure 15. Electron temperature elevation as a function of rf power for three molecular concentrations of O_2 in argon

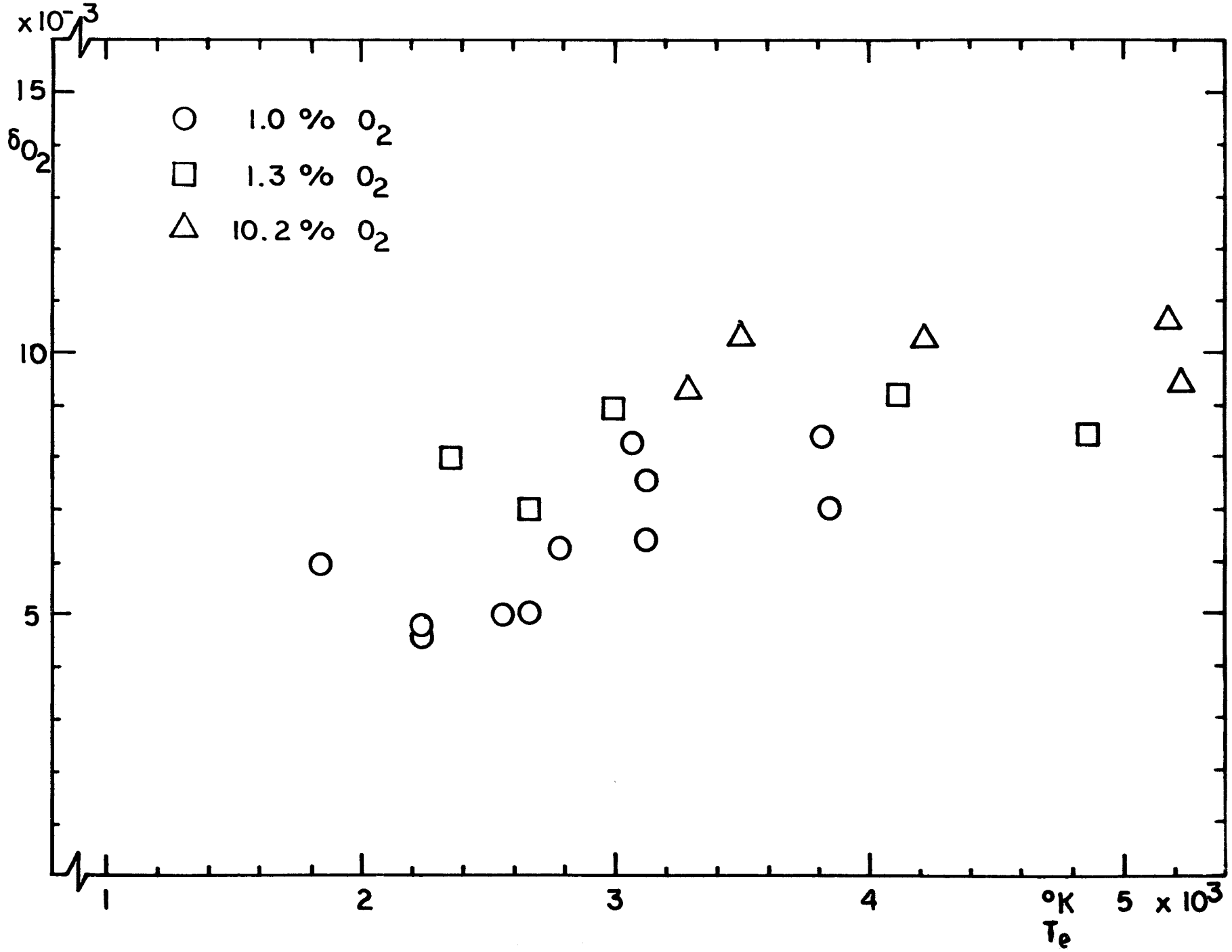

Figure 16. Electron energy-loss factor for oxygen as a function of electron temperature. The symbols identify the molecular concentration of O_2 in argon from which δ_{O_2} was determined

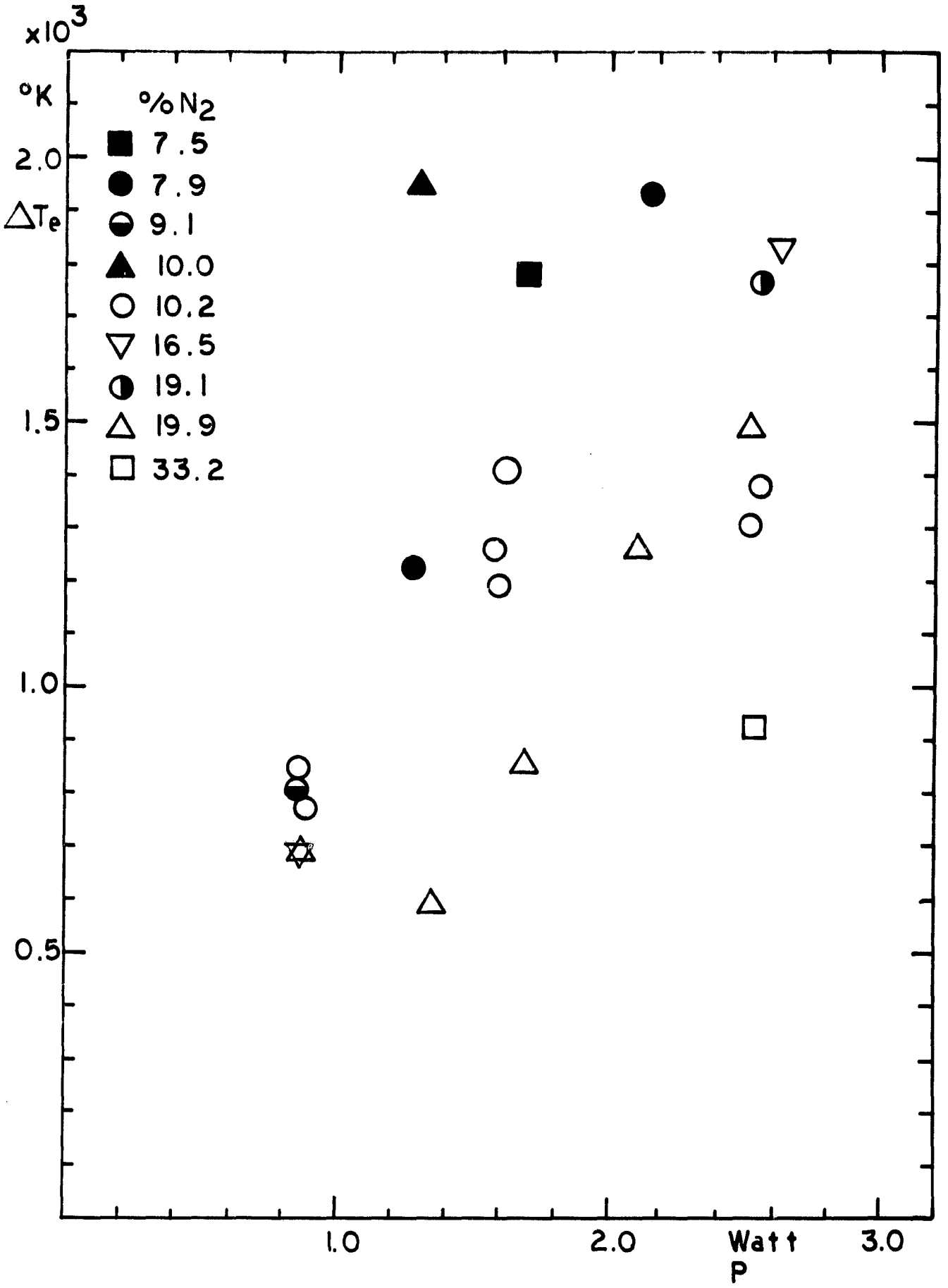

Figure 17. Electron temperature elevation as a function of applied microwave power for various molecular concentrations of nitrogen in argon

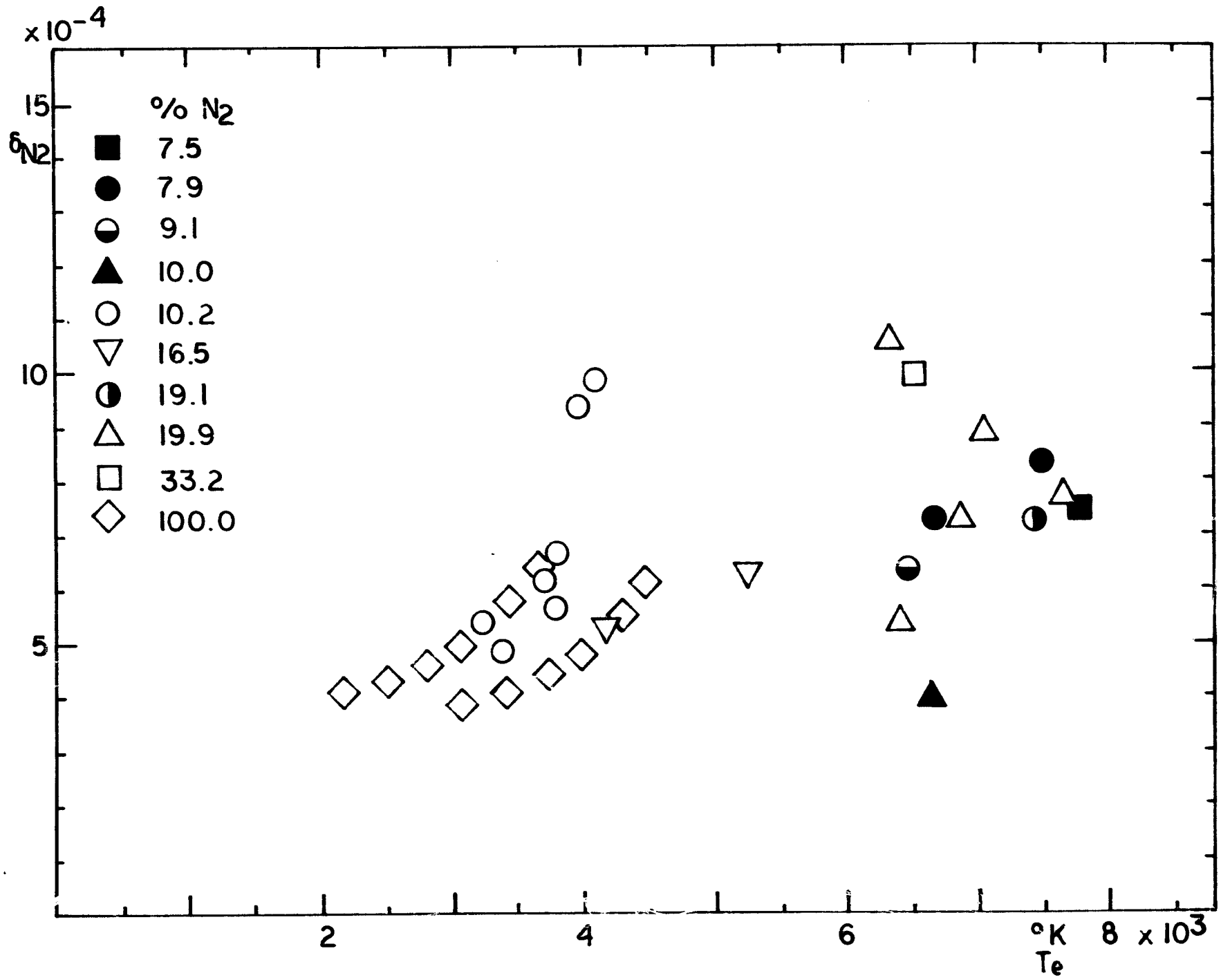

Figure 18. Electron energy-loss factor for nitrogen as a function of electron temperature. Data for both pure nitrogen and for various molecular concentrations of nitrogen in argon are shown

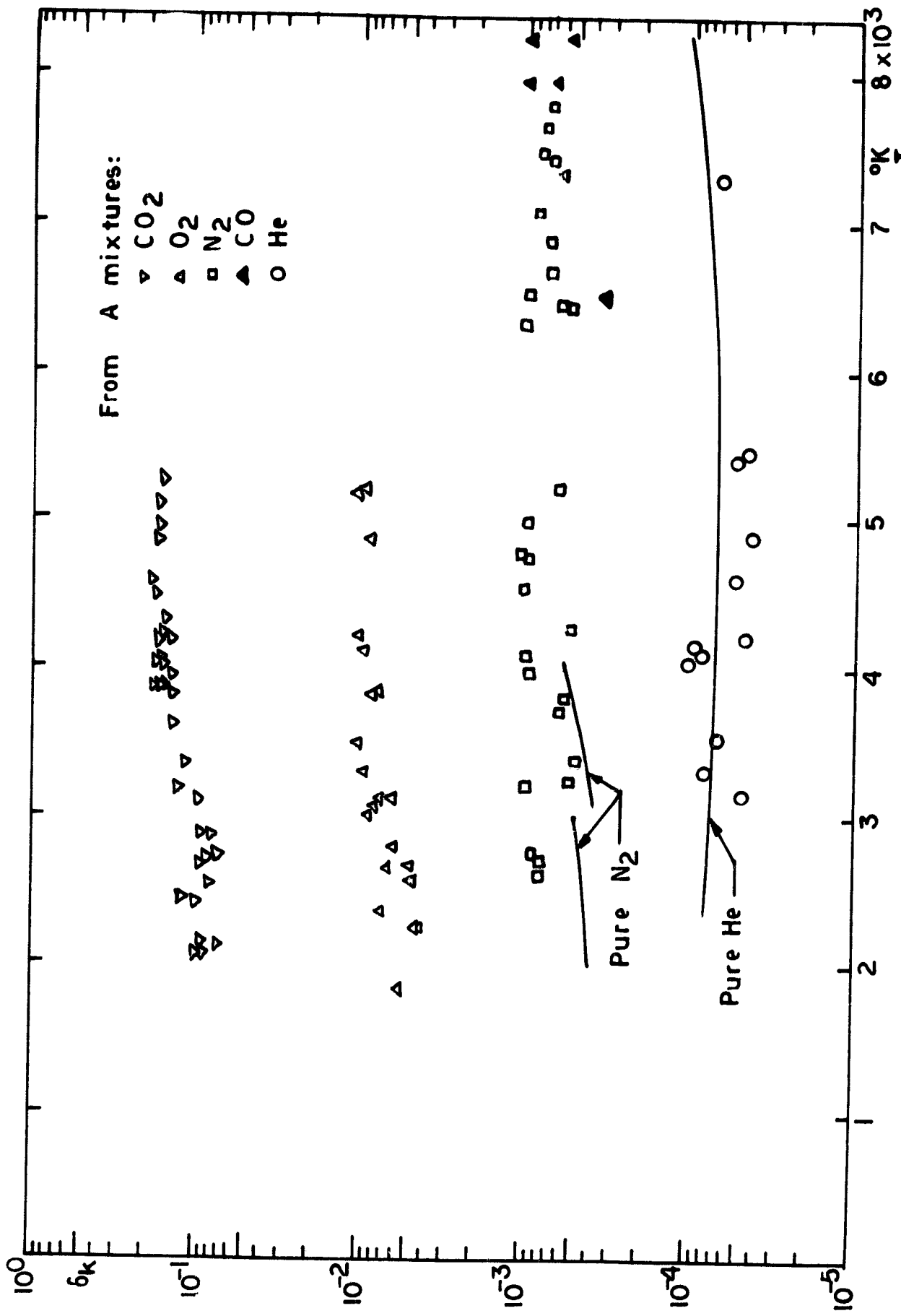

Figure 19. Measured energy-loss factor for CO_2, O_2, N_2, CO and He. Points represent results derived from mixture rule equation, while the solid lines represent data taken with pure gases.

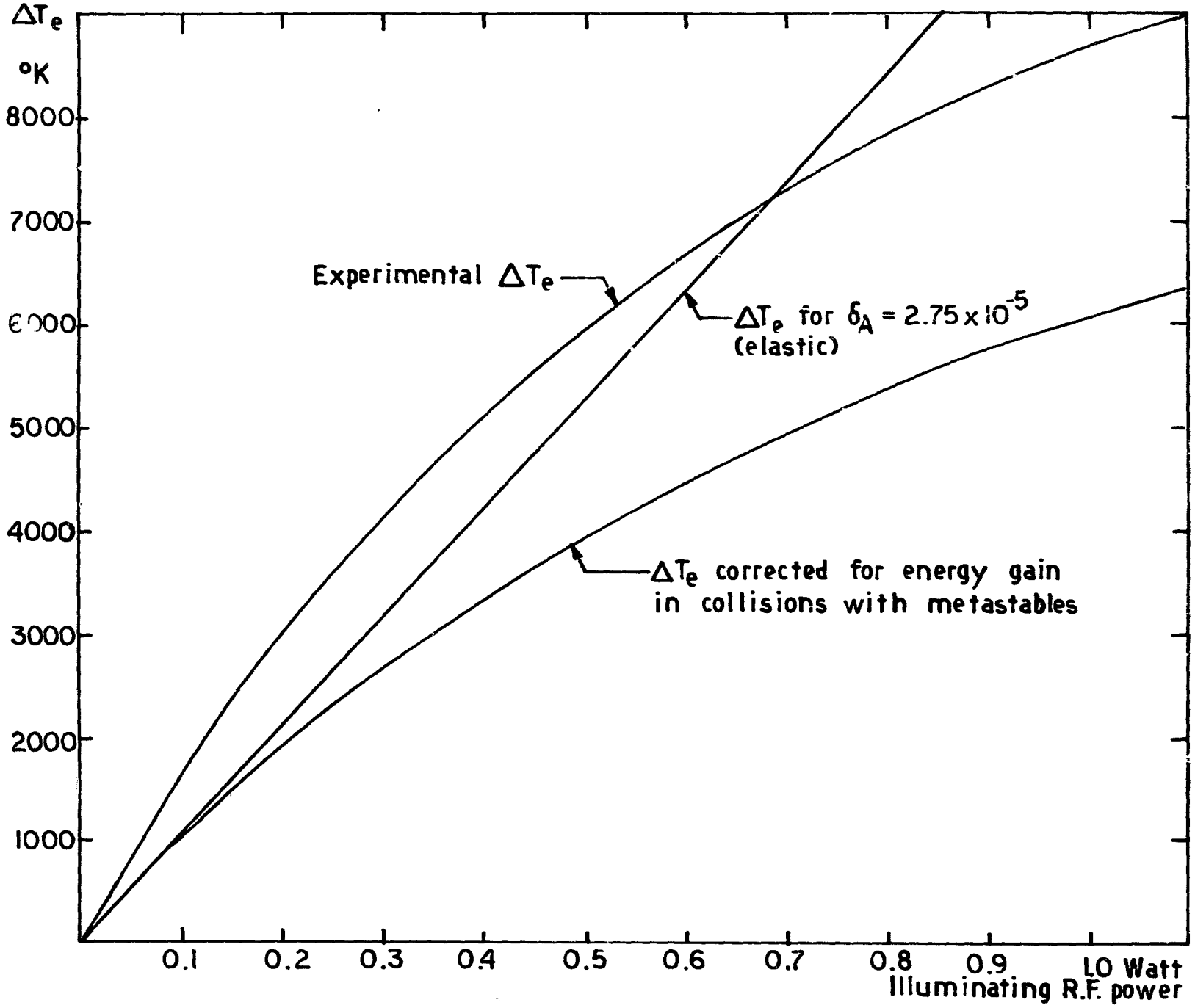

Figure 20. Increase of electron temperature by microwave energy in argon.

APPENDIX A

USE OF THE MIXTURE RULE

Measurement of the energy loss factor in certain gases is complicated because they are difficult to handle or work with, under the conditions of the experiment, when they are pure. The loss factor of these gases can be obtained by carrying out measurements of ΔT_e vs. P for mixtures of these gases with some inert gas of known properties, e.g. argon. Argon may be considered an ideal primary gas; its advantages are obvious: (1) it has a low energy loss factor (ca 2.7×10^{-5}) that should be nearly constant over a wide temperature range and therefore it is easier in argon both (a) to establish Maxwellian distributions and (b) to apply the mixture rule with accuracy, (2) it is a good source of electrons (has relatively low ionization potential), (3) it is monatomic and therefore susceptible to some theoretical treatment, (4) it has a low cross section for momentum transfer and (5) it is chemically inert.

To illustrate the (theoretical) promise of argon as a primary gas consider the determination of the energy-loss factor for oxygen by use of the mixture rule. Application of the mixture rule yields, for the energy-loss factor of the mixture δ_{eff}, the expression

$$\delta_{eff} = \frac{4 v_{ea}}{3 \nu_t} (\delta_A n_A Q_{eA} + \delta_{O_2} n_{O_2} Q_{eO_2}) \qquad (A1)$$

in our usual notation.

Now in the range of the experiments $\delta_A \approx 3 \times 10^{-5}$, $\delta_{O_2} \approx 6 \times 10^{-3}$, $Q_{e,A} \approx 10^{-20}$ m^2, $Q_{e,O_2} \approx 5 \times 10^{-20}$ m^2, accepting values for these parameters that will minimize the effect of the oxygen contribution and maximize the effect of the argon contribution. Even then we see that operation with a 1% O_2 - 99% A mixture yields for the argon contribution $\delta_A n_A Q_{e,A} \approx 0.99 \times 3 \times 10^{-5} \times 10^{-20} \approx 3 \times 10^{-25}$ and for the oxygen contribution $\delta_{O_2} n_{O_2} Q_{e,O_2} \approx 10^{-3} \times 6 \times 10^{-3} \times 5 \times 10^{-20} \approx 3 \times 10^{-24}$ and thus the energy loss factor for the mixture is substantially (i.e., within 100%) the energy-loss factor for oxygen since the oxygen contribution is about ten

times bigger than the argon contribution even at 1% oxygen content!

Thus equation (A1) can be rewritten

$$\delta_{eff} = \frac{4 v_{ea} \delta_{O_2} n_{O_2} Q_{eO_2}}{3 \nu_t} \left(1 + \frac{\delta_A n_A Q_{eA}}{\delta_{O_2} n_{O_2} Q_{eO_2}}\right) \tag{A2}$$

and since $\nu_t = \frac{4}{3} v_{ea} (n_A Q_{eA} + n_{O_2} Q_{eO_2})$, we can simplify equation (A2) to obtain:

$$\delta_{eff} = \frac{\delta_{O_2} n_{O_2} Q_{eO_2}}{n_A Q_{eA} + n_{O_2} Q_{eO_2}} \cdot \left(1 + \frac{\delta_A n_A Q_{eA}}{\delta_{O_2} n_{O_2} Q_{eO_2}}\right) \tag{A3}$$

Equation (A3) gives

$$\delta_{eff} = \delta_{O_2} \tag{A4}$$

when $n_{O_2} Q_{eO_2} >> n_A Q_{eA}$, a condition that can be achieved by operating at, say, 10% A and 90% O_2. Operation under these conditions would obviate the need to know the collision cross sections for momentum transfer (and also the measurement of δ_A) and would yield values of δ_{O_2} with an error, ideally speaking, of less than 5% even if Q_{eA} was assumed unknown. Assuming that Q_{eA} and Q_{eO_2} are known within a factor of 2 then operation even at 50% A - 50% O_2 would yield values of δ_{O_2} accurate within 10%.

Another way to remove considerations of the collision cross sections for momentum transfer from the experiment is to measure δ_{eff} at different ratios of the particle concentrations n_A/n_{O_2} and plot $1/\delta_{eff}$ as a function of n_A/n_{O_2}. Then the slope of this curve is $(Q_{eA}/Q_{eO_2})/\delta_{O_2}$. For $n_{O_2} > 0.1\, n_A$, since $\delta_{O_2} >> \delta_A$, we can rearrange equation (A3) to read

$$1/\delta_{O_2} + \eta X/\delta_{O_2} = 1/\delta_{eff} \tag{A5}$$

where $X = Q_{eA}/Q_{eO_2}$ and $\eta = n_A/n_{O_2}$. Then, since Q_{eA}/Q_{eO_2} and δ_{O_2} do not vary with η, we obtain

$$X/\delta_{O_2} = \frac{d(1/\delta_{eff})}{d\eta} \tag{A6}$$

This slope is constant and the curve is a straight line. The quantity $1/\delta_{O_2}$ can be obtained as the intersection between this straight line and the ordinate ($n_A/n_{O_2} = 0$). Care must be taken, of course, that T_e and T_a remain constant as we vary n_A/n_{O_2}).

This procedure is actually a self-testing method: If the curve is not a straight line, something is wrong! Once the straightness of this line is established, we can obtain accurate values of δ_{O_2} simply by solving any two of a set of equations obtained by measuring δ_{eff} at any two values of n_A/n_{O_2} in the region of linearity.

For example, at $n_{O_2} > 0.1\, n_A$, we can write, with good approximation,

$$\delta_{eff} = \frac{\delta_{O_2}}{1 + \frac{n_A Q_{eA}}{n_{O_2} Q_{eO_2}}} \tag{A7}$$

If we measure δ_{eff} at 50% A and 50% O_2 we obtain

$$\delta_{eff,\,50\text{-}50} = \frac{\delta_{O_2}}{1 + \frac{Q_{eA}}{Q_{eO_2}}} \tag{A8}$$

If we measure δ_{eff} at, say, 25% A and 75% O_2, we obtain

$$\delta_{eff,\,25\text{-}75} = \frac{\delta_{O_2}}{1 + \frac{1}{3}\frac{Q_{eA}}{Q_{eO_2}}} \tag{A9}$$

Equations (A8) and (A9) can be solved simultaneously to give the desired results. Note that this approach would also be a valid method for determining $Q_{e\kappa}$'s.

In general, of course, the mixture rule is

$$\delta_{eff} = \frac{\sum_{\kappa} \delta_\kappa n_\kappa Q_{e\kappa}}{\sum_{\kappa} n_\kappa Q_{e\kappa}} \tag{A10}$$

which indicates that the effective energy-loss factor is the average of the δ's of the components, weighted by their number densities and their total (integrated) electron collision cross sections for momentum transfer. In the case of two-gas mixtures, say argon and a seed gas κ, equation (A10) becomes

$$\delta_{eff} = \frac{\delta_A n_A Q_{eA} + \delta_\kappa n_\kappa Q_{e\kappa}}{n_A Q_{eA} + \delta_\kappa Q_{e\kappa}} \tag{A11}$$

If we let $\eta = n_A/n_\kappa$ and $X = Q_{eA}/Q_{e\kappa}$, equation (A11) easily simplifies to the form

$$\delta_\kappa = \delta_{eff} + \eta X \cdot (\delta_{eff} - \delta_A) \tag{A12}$$

We take the value of δ_A to be fairly well known. ($\delta_A = 2.72 \times 10^{-5}$ was used in the reduction of the present data. Note that in most conditions encountered in these measurements, $\delta_{eff} >> \delta_A$, so that the exact value of δ_A was not critical). In practice, the method worked extremely well. The value of η is determined from the flow meter readings on the assumption that the presence of other species is negligible. The value of X is found from our calculations of integrated velocity-dependent collision cross sections for momentum transfer as functions of electron temperature (ref. A1). Finally, δ_{eff} was obtained in the usual way ($\delta_{eff} = 0.287 \frac{P_{av}}{\Delta T_e}$) from the Langmuir probe data. A short program was written to find δ_{eff} and X, and to solve equation (A12).

It was noted that the results of nitrogen in the mixture were sensitive to small amounts of contamination. This problem was minimized if (1) for low nitrogen flow rates, long periods of bleeding the nitrogen lines were observed, or, (2) high flow rates of nitrogen were used. Note that (2) has the additional advantage of decreasing η, thereby making knowledge of the exact value of δ_A (as a function of T_e) less important. Precautions to avoid contamination, of course, were always carefully taken.

The carbon dioxide and oxygen data are much less subject to contamination. The oxygen mixture runs were all performed before carbon dioxide was introduced into the system. Thus, since δ_{O_2} is about an

order of magnitude higher than that for any other gas except CO_2, the effects of contamination are negligible. Similarly, little if any effect of contamination from other gases used in the experiment is expected for carbon dioxide, due to its very high energy-loss factor (an order of magnitude higher than δ_{O_2}).

Effects of dissociation of the seed gases are also estimated to be small under the conditions of the experiments. If we use the measured values of electron temperature without electric field for the tas temperature[†], we can calculate an upper limit on the error caused by dissociation. For CO_2 the average electron temperature without rf was less than 1800 ^{o}K, and the tank pressure was 290 μ Hg. Using Reynolds' values for the equilibrium constant of the reaction $CO_2 \rightleftharpoons + \frac{1}{2} O_2$ at this temperature (ref. A2) we estimate that less than 9% of the carbon dioxide is dissociated. This leads to a correction of δ_{CO_2} of less than + 1% (using $\delta_{O_2} = 6 \times 10^{-3}$ and $\delta_{CO} = \delta_{CO, el} = 4 \times 10^{-5}$). A similar calculation for the O_2 data yields a correction of less than + 3% (using $\delta_{O} = \delta_{O, el} = 7 \times 10^{-5}$). As the experimental spread of the data is greater than either of these corrections, dissociation can be ignored.

An excellent check on the validity of the methods used in these measurements is provided by the fact that the values we obtain for the δ's of the pure gases intermingle, regardless of the particular mixture ratio used. For example, all of the carbon dioxide data plotted together as a function of electron temperature can be fitted with a cubic having a standard error of only 1.7×10^{-2} (about 10-15%). For the oxygen data, the standard error to a quadratic fit is just 1.2×10^{-3}, or about 15-20%. Such close agreement among data at differing mixture ratios must be attributed to a) accuracy of the cross section values, b) accuracy in the measurement of mixture ratios, and c) the correctness of neglecting the presence of other species.

[†] This assumes that there exists a coupling and equivalence between free electron temperatures and temperatures of the heavy components of the plasma. It has been established previously that there is coupling between vibrational and electron temperatures in a nitrogen plasma.

REFERENCES OF APPENDIX A

A1. Demetriades, S. T.; Argyropoulos, G. S.; and Fonda-Bonardi, G.: Experimental Determination of Collision Cross Sections for Momentum Transfer, Final Technical Report, Contract No. AF 49(638)-1594.

A2. Reynolds, W. D. Thermodynamics, McGraw Hill Publishing Co., New York (1965), p. 444.

APPENDIX B

MICROWAVE DIAGNOSTICS

Early in the experimental program some concern was caused by unduly large scatter of the measured data points for the temperature elevation of electrons, and suspicion was directed towards the performance of the microwave system. Accordingly, a complete investigation of its performance was made.

The microwave system used for the measurements is schematically shown in figure B1. The signal source is a RK 5609 magnetron packaged in a cabinet with its power supply by the manufacturer. The frequency is fixed (nominally 2450 Mhz) and the power is variable by means of a control knob on the front panel. A panel meter indicates the approximate percentage of the maximum nominal power output selected by the control knob. A long coaxial cable provides several decibels of fixed attenuation to reduce the power available at the terminal to a value in the range of interest (0 to 5 watt); a variable attenuator provides a fine control. In the original configuration the variable attenuator was followed by a forward-reading directional coupler, a double-stub tuner, a backward-reading directional coupler, a double-stub tuner, a backward-reading directional coupler, some transitional connections, the test cell, more connections, another directional coupler, and a termination.

Measurements of plasma properties with the system in this configuration revealed some puzzling variations of indicated electron temperature which did not correlate properly with the microwave power indicated by bolometers attached to the directional couplers. Accordingly, an investigation was undertaken to identify the sources of the suspected discrepancies. The investigation addressed itself to three aspects of the operation of the system, namely

1. Possibility of resonances in the test cell which may create localized microwave fields appreciably different from those computed on the basis of cell geometry and input power.
2. Refinements of the tuning procedure to insure that the fields in

the cavity would correspond closely to the computed ones.

3. Stability and performance of the primary power source.

I. Waveguide Resonances

The test cell consists of a rectangular waveguide having cross-sectional dimensions (approximately 0.152 m wide by 0.101 m high) large enough to permit propagation of more than one mode. In particular, the TE_{10}, TE_{20}, TE_{01}, TE_{11} and TM_{11} modes are above cutoff at the operating frequency. The field geometries pertaining to these modes are shown in figures B2 through B6. The test cell proper is joined to two sections of standard waveguide (which can only sustain the TE_{10} mode) by means of tapered transitions; the standard waveguide comprises a transition to a coaxial line designed to predominantly launch the TE_{10} mode in the waveguide. The very tight coupling to this mode, and the good match of the transitions, insures that the energy associated with the TE_{10} mode is smoothly propagated from the input end of the cell to the output end, with minimal reflections, and with losses due only to the finite wall conductivity and, possibly, absorption by the plasma, which is contained in a transversal, thin-walled, quartz tube.

The other modes cannot propagate into the tapered ends of the test cell because there the transverse dimensions decrease to below cutoff at the operating frequency, and therefore the energy associated with these modes is totally reflected at each end of the test cell, and a resonance can occur. If the operating frequency is close to one of the resonant frequencies of the test cell, two effects can occur:

a. The locations of the modes and antimodes of the resonant field pattern with respect to the plasma column will cause the plasma to see a local field strength different from that computed on the basis of the TE_{10} mode alone.

b. The contribution of the resonant field will vary by a large and unpredictable factor in response to small drifts of the operating frequency.

Of all the modes which can resonate in the test cell, the TM_{11} is the one

most likely to be strongly excited because longitudinal current components are set up in the walls of the guide by the hole through which the plasma tube is inserted, and by the junction discontinuity of the tapered ends (see figure B7). An even stronger coupling mechanism to the TM_{11} mode is provided by the coaxial transition (see figure B8), which also couples to the TE_{11} mode. The short length of below-cutoff guide between the coaxial transition and the large guide provides some attenuation having simply the effect of increasing the Q_L of the resonant cavity (loaded Q) by increasing the coupling Q_c:

$$1/Q_L = 1/Q_o + 1/Q_c \tag{B1}$$

An estimate of the loaded Q_L for this cavity can be made on the basis of the known wall losses and the estimated coupling coefficient at the ends; the result is of the order of 10^3. Therefore the half-power width of the resonance will be of the order of

$$B = f/Q_L \simeq 2 \text{ Mhz} \tag{B2}$$

The spacing between the resonances in the frequency domain can be estimated on the basis of the length of the cavity and the guide wave length. Although the TE_{11} and TM_{11} are degenerate because they have the same eigenvalues and therefore the same guide wave length, the degeneracy of the resonance is resolved by the different mechanism of total reflection in the tapered ends as well as by the different effect of the perturbations due to the holes in the sidewalls and the presence of the quartz tube. Therefore each mode is expected to have a distinct spectrum of resonances; and two resonances may happen to be near the operating frequency. If we assume that the effective plane of total reflection is about 5 cm into the tapered sections, we find that resonances with $p = 3$ could occur quite near the nominal operating frequency ($p\lambda_g/2 = 0.393$ m).

It was therefore of some importance to ascertain whether the operating frequency did or did not coincide with a resonance. This was done by means of a swept frequency oscillator (EH Model 560) used in place of the normal power source. A crystal detector was connected to the backward-reading directional coupler and the reflection coefficient of the test cell so

detected was displayed on an oscilloscope. This arrangement revealed two resonances quite close to the operating frequency (which was displayed by generating a marker in the form of the beat note between the swept oscillator and the magnetron signal, injected through another directional coupler). It was determined, however, that the operating frequency was sufficiently different from either resonance as to insure no interaction under all foreseeable circumstances. Figure B9 is a tracing of the graph generated by an x-y plotter used to produce a permanent record in place of the oscilloscope. The horizontal axis is calibrated in frequency using the built-in calibration features of the swept oscillator. The location of the magnetron frequency is identified to 2469 Mhz; the resonances are indicated by arrows at 2455 and 2485 Mhz. The emitted frequency was obtained for this particular magnetron by feeding the magnetron signal through a forward directional coupler, in the same direction as the swept frequency signal, and reading on the oscilloscope the beat note out of another forward facing coupler. It was found also that both resonances were strongly affected by the presence or absence of the quartz tube (as could be expected for TE_{11} and TM_{11} modes), and to some extent by the position of the Langmuir probe of the plasma diagnostic system, but in no case did they approach the operating frequency to any detrimental degree. The match of the line at the operating frequency was slightly detuned to make the beat note marker visible; in normal operation the line is tuned for zero reflected power at the operating frequency. It should be noted that the width of the 2455 and 2485 resonances is slightly more than 1 Mhz, in good agreement with the estimates.

II. Tuning Procedure

The electric field strength, or power density, seen by the plasma in a particular location in the test cell can be calculated exactly from a measurement of the power flow if no reflections are present in the guide. If some component downstream of the test cell is imperfectly matched, the reflected energy propagates through the test cell in the opposite direction with the formation of standing waves. The presence of standing waves creates alternating maxima and minima of field strength and power density, so that the

power coupled into the plasma depends on the relative position of the standing wave pattern with respect to the plasma tube. The power coupled to the plasma will be higher than that computed for a reflectionless wave if the plasma is at or near a field maximum, and vice versa. The maxima and minima present in the waveguide are related to those present in a case of resonance as discussed above: the localized fields represent another form of trapped energy between obstacles in an otherwise uniform waveguide. Except for the magnitude of the quantities involved, the mechanism is identical to that of resonance: the only difference is that the coupling to the input and output lines is close to one rather than close to zero, and therefore the amount of energy trapped is more easily measured in terms of reflection coefficient R or standing wave ratio S rather than quality coefficient Q. figure B10 illustrates this point.

The upper line shows a transmission line ending in a termination, and provided with an obstacle (connector, corner, etc.) upstream of the termination, such that power P_2 is reflected when power P_1 is supplied to the input terminal of the system. A tuner T_1 cancels the reflection so that a perfect match is seen at the input.

The second line shows the local power density P_1 associated with the forward propagating wave. It suffers two discontinuities, one at the tuner and another at the obstacle. The third line shows the power associated with the backward propagating wave P_2, which exists only between the obstacle and the tuner. Both show the effects of attenuation.

The local power density W associated with the system of both superimposed waves is shown in the next line, and exhibits large local fluctuations. In particular, the ratio of maximum to minimum power density is equal to the square of the ratio of the maximum to minimum field strength:

$$\frac{W_{max}}{W_{min}} = S^2 = \left(\frac{1 + R}{1 - R}\right)^2 \qquad \text{(B3)}$$

where R, the reflected coefficient, is the ratio of the reflected field to the forward field:

$$R = (P_2/P_1)^{1/2} \qquad \text{(B4)}$$

The measurement of the ratio S is easy if the region of interest is accessible to suitable diagnostic instrumentation, but presents serious problems if only remote terminals are accessible, since these terminals have unknown discontinuities between them. A reasonably low standing wave ratio S in the test cell can be obtained with reasonably good confidence by adding another directional coupler D_2 downstream of the tuner but upstream of the test cell, and a second double-stub tuner T_2 downstream of the test cell. If the power detected at D_2 is minimized by tuning T_2, there is a good probability that the standing wave ratio S will be minimized everywhere between the two. This test will fail if there are other unidentified sources of reflections between T_2 and D_2; but separate measurements on the test cell (with and without quartz tube) showed that $R \leq 0.03$ at the specified operating frequency, yielding a maximum variation of S^2 of the order of $\pm 6\%$. This much uncertainty is probably acceptable if pains are taken to insure good tuning of T_2 before the test.

III. Magnetron Stability

Magnetrons are known to exhibit instabilities when connected to a long transmission line terminated in an imperfectly matched load, particularly when operated at less than maximum power.

The desired power level in the test cell was generally set by adjusting the magnetron power supply to a (less than maximum) power output level slightly in excess of the desired value, and then trimming it with a variable attenuator; tuner T_1 was then adjusted for maximum power into the load. But since a magnetron generally puts out more power when working into an appropriate mismatch, there is a strong possibility that a power maximization procedure could also lead towards an unstable operation.

This was checked by attaching a crystal detector as a monitor to one of the directional couplers, and displaying its output on an oscilloscope. The bolometers normally used for measuring the power output and/or reflections were unsuitable because of their relatively long time constant which made them unable to follow rapid power variations. The crystal did

show that the power output of the magnetron was subject to wide fluctuations when the power control knob, the attenuator and the tuner had particular settings. The relationship between them was mapped out and regions of unstable operation, conditionally stable and unconditionally stable operation were identified. The conditionally stable region is characterized by magnetron stability only if the tuner is set to some preferred position; otherwise instability results. The three regions are presented in figures B11 and B12. It should be noted that the label "0 Att. dial" in figure B12 refers also to the entire boundary of the unstable region, in which no reproducible readings could be obtained. The boundary of the unconditionally stable region of figure B12 was obtained for those readings of the attenuator dial which form the boundary of the stable region in figure B11.

It is clear that a power output of 5 watt, as normally used in the tests, falls outside of the unconditionally stable region and therefore requires careful setting of tuner T_1 to avoid instabilities: a crystal detector monitor is essential for proper tuning in this power range, and so it was made a permanent part of the apparatus.

Also noteworthy is the very large and sudden change of characteristics around a setting of 30 (meter reading). The posibility of easily crossing into an unstable mode of operation around a power output of 3 watts (where the time-averaging of the bolometer power meter may differ from the time-averaging properties of the electrons-to-probe-to-recorder system) may account for some of the scatter of the data collected during the early measurements of plasma electron temperatures, particularly around a power level of 3 watt.

The frequency stability of the magnetron was also checked by using the built-in calibration of the swept frequency oscillator. It was found that the frequency did shift with changes of power level setting, as shown in figure B13. The shift was, however, too small to cause measureable changes in tuning of the system, and in particular it was too small to bring the operating frequency close to one of the resonances of the test cell. For this reason frequency stability can be considered adequate and can be safely ignored as a factor in the variations of performance of the system.

IV. Conclusions

In conclusion, the system proved to be capable of satisfactory operation provided the stability of the magnetron was monitored by a crystal detector connected to a directional coupler, and provided the double-stub tuner was set so as to maintain the magnetron in a stable operating region: this condition requiring verification at each setting of the power level. Under these conditions the power present in the waveguide would correspond within better than ± 6% to the power computed for the TE_{10} mode from the indications of the bolometers. Stable operation of the power supply at any desirable rf power setting up to about 100 watts could be attained by removing more and more of the coaxial cable serving as attenuator and dispensing with the variable trimming attenuator.

The tuning procedure here outlined was then carefully observed in all subsequent measurements and the scatter of the data points was substantially reduced.

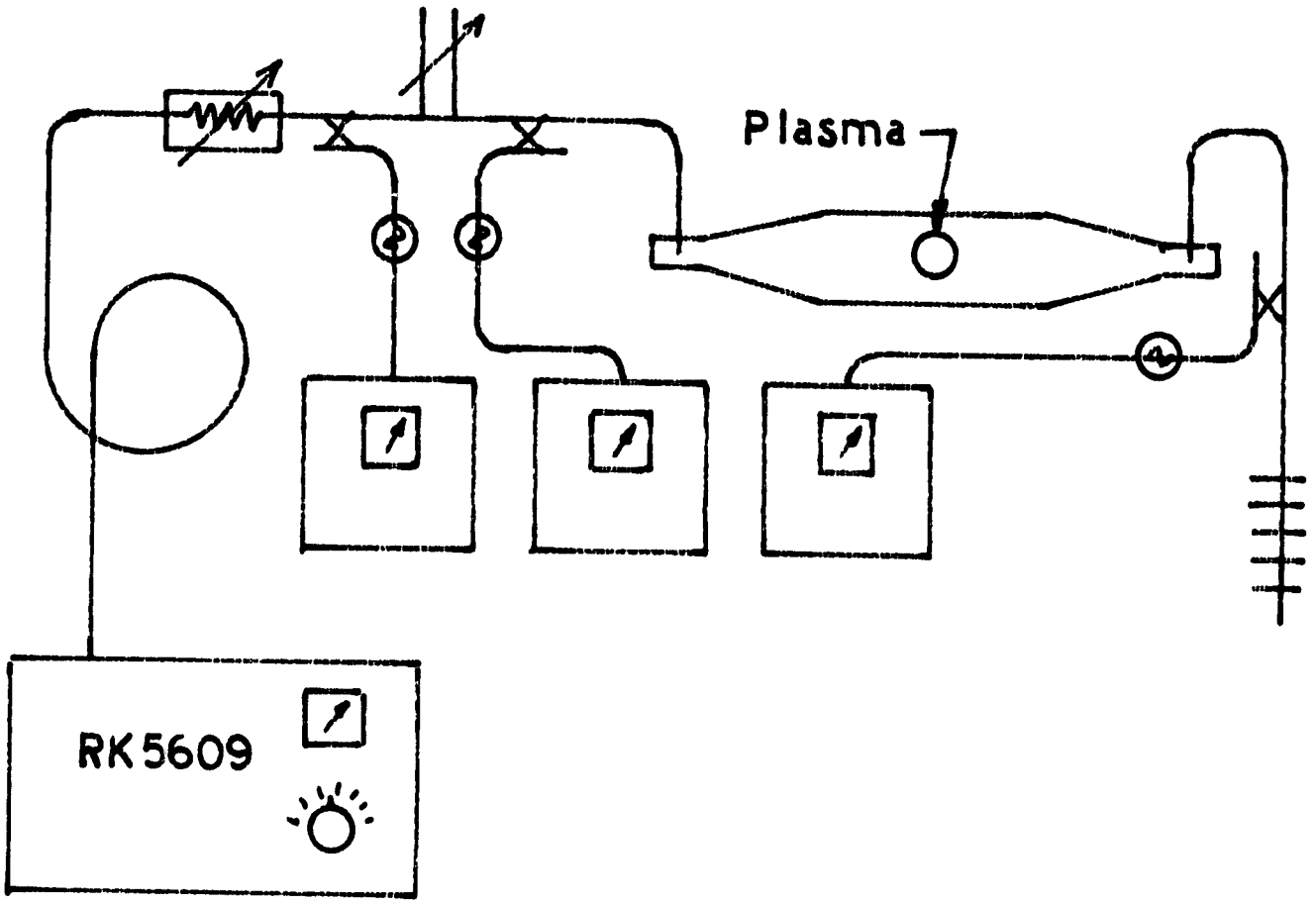

Figure B1. Block diagram of microwave system

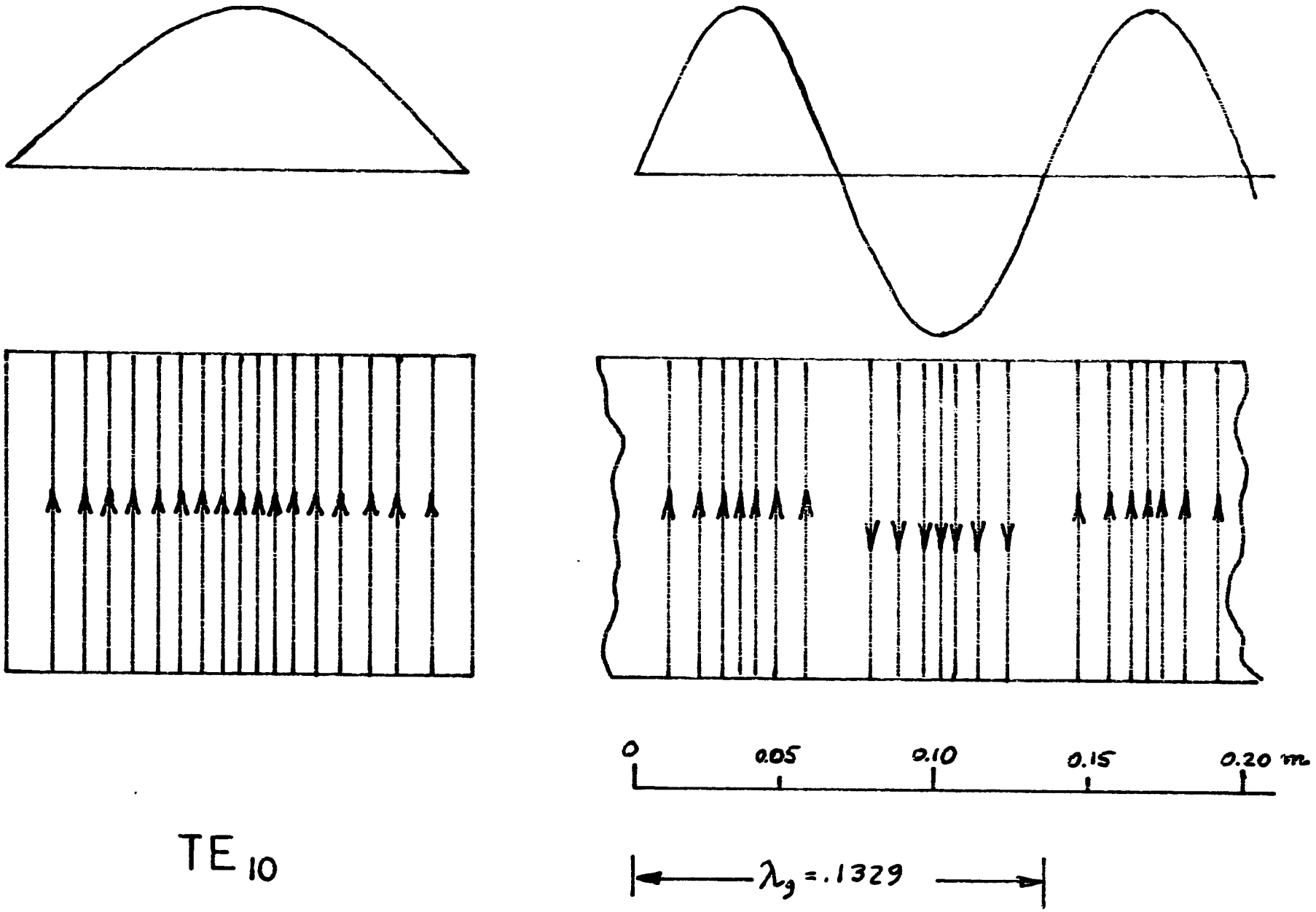

Figure B2. E field geometry of TE_{10} mode

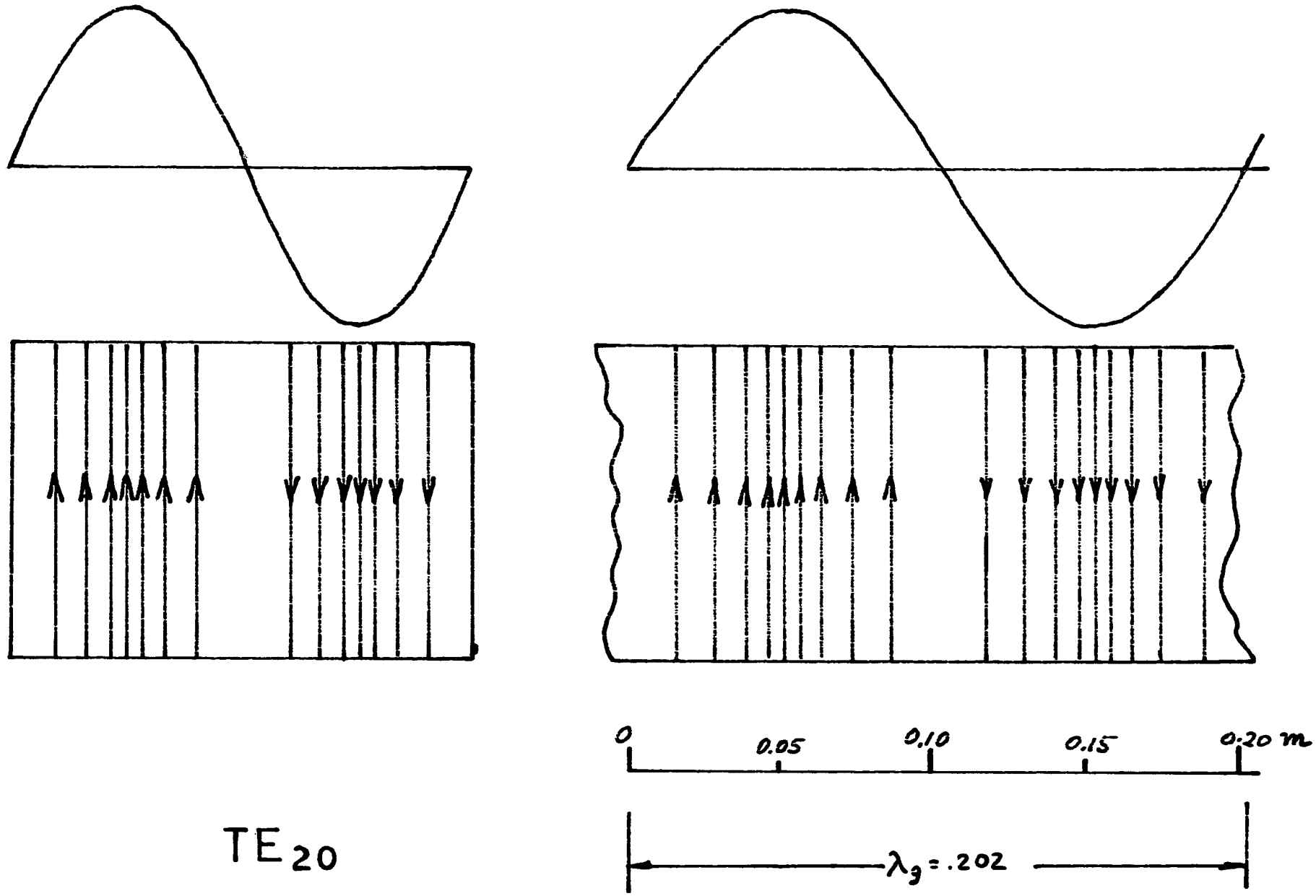

Figure B3. E field geometry of TE_{20} mode

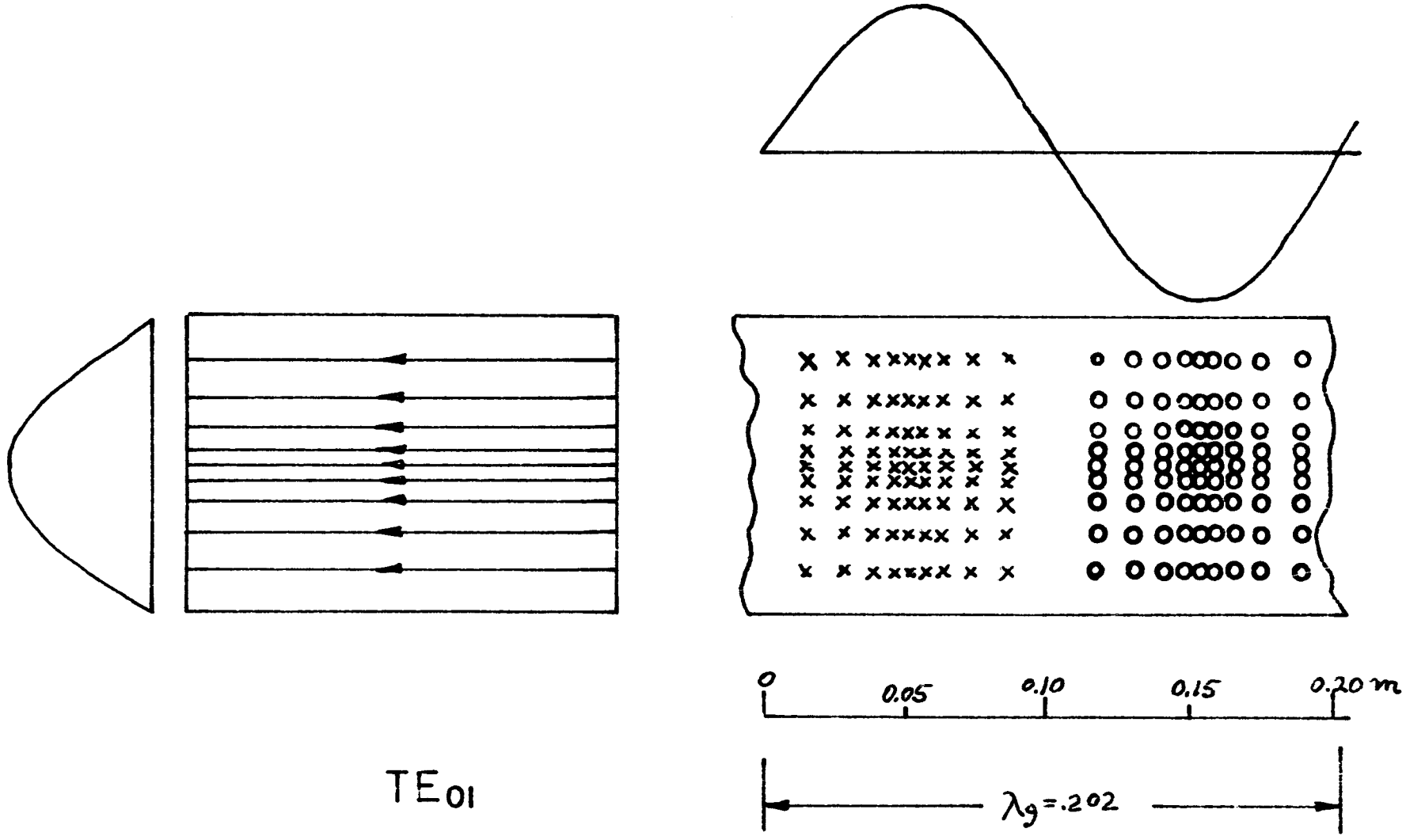

Figure B4. E field geometry of TE_{01} mode

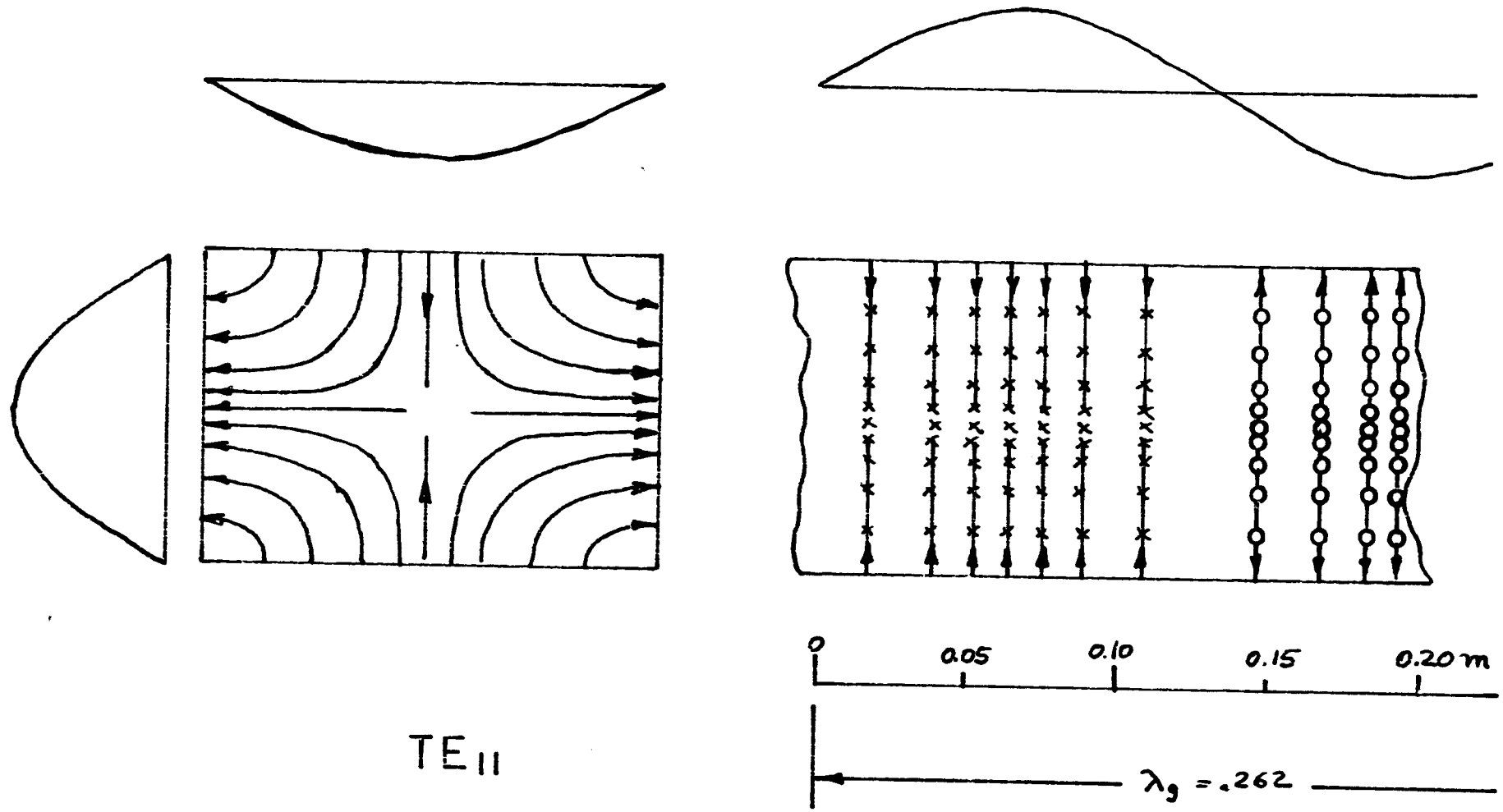

Figure B5. E field geometry of TE_{11} mode

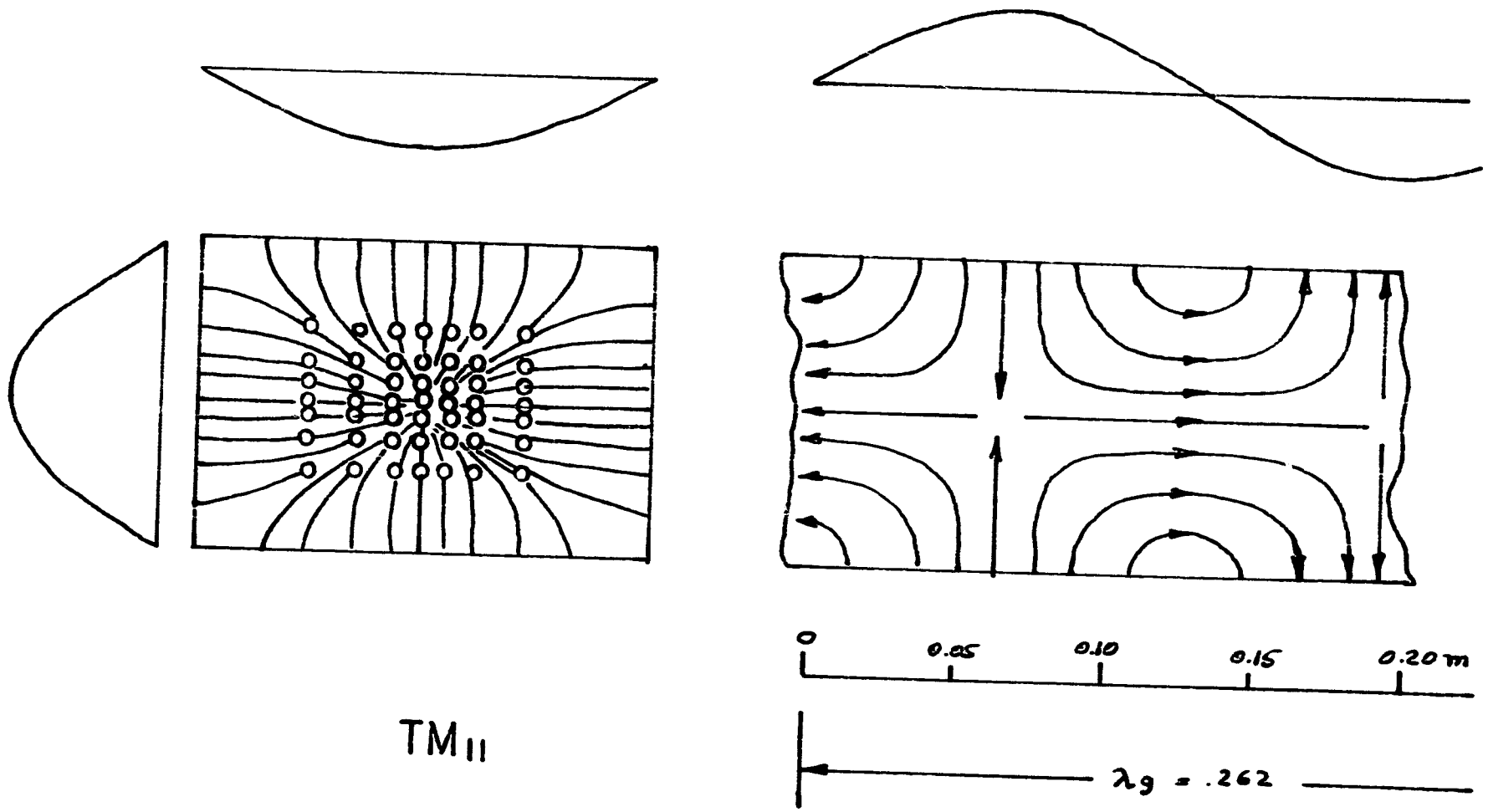

Figure B6. E field geometry of TM_{11} mode

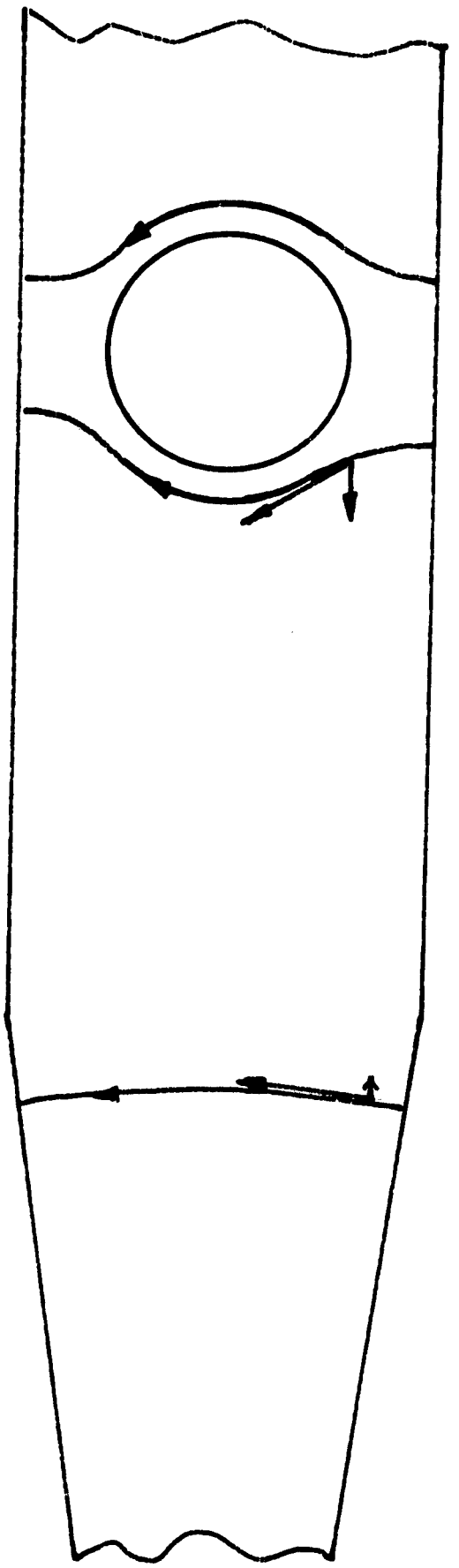

Figure B7. Excitation of TM_{11} mode due to discontinuities

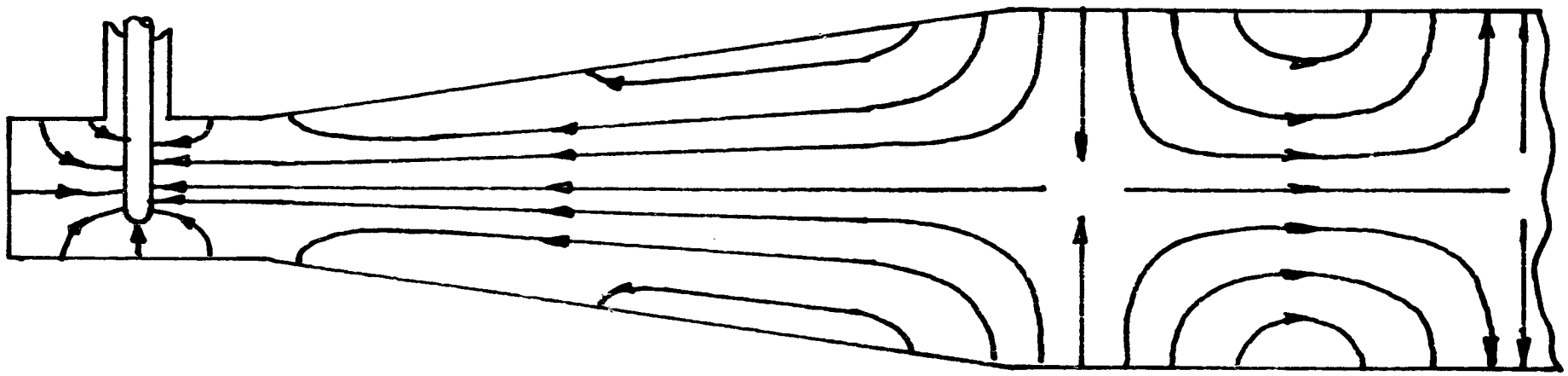

Figure B8. Excitation of TM_{11} mode due to coaxial transition

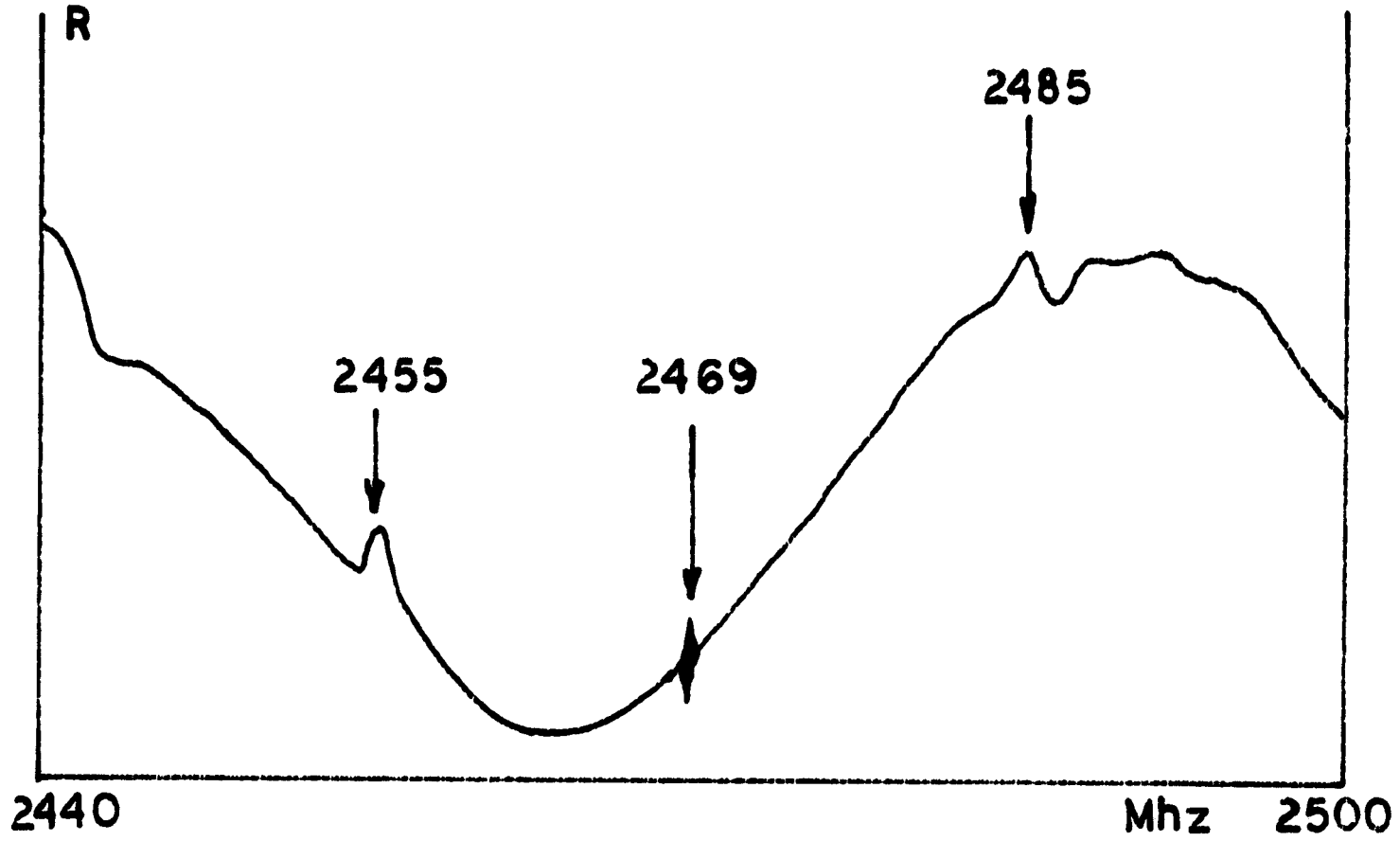

Figure B9. Test cell resonances in frequency domain

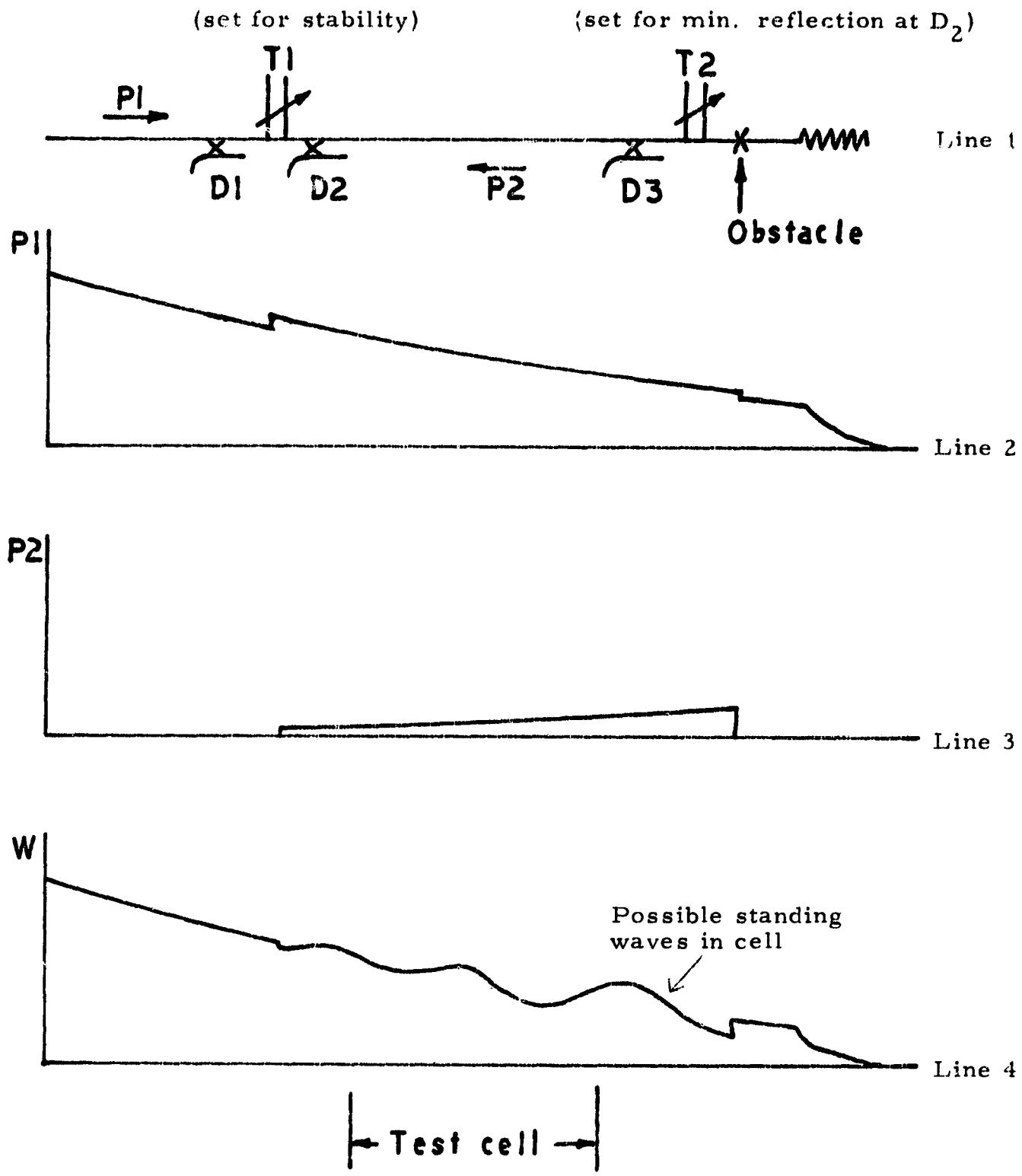

Figure B10. Direct and reflected power in mismatched line

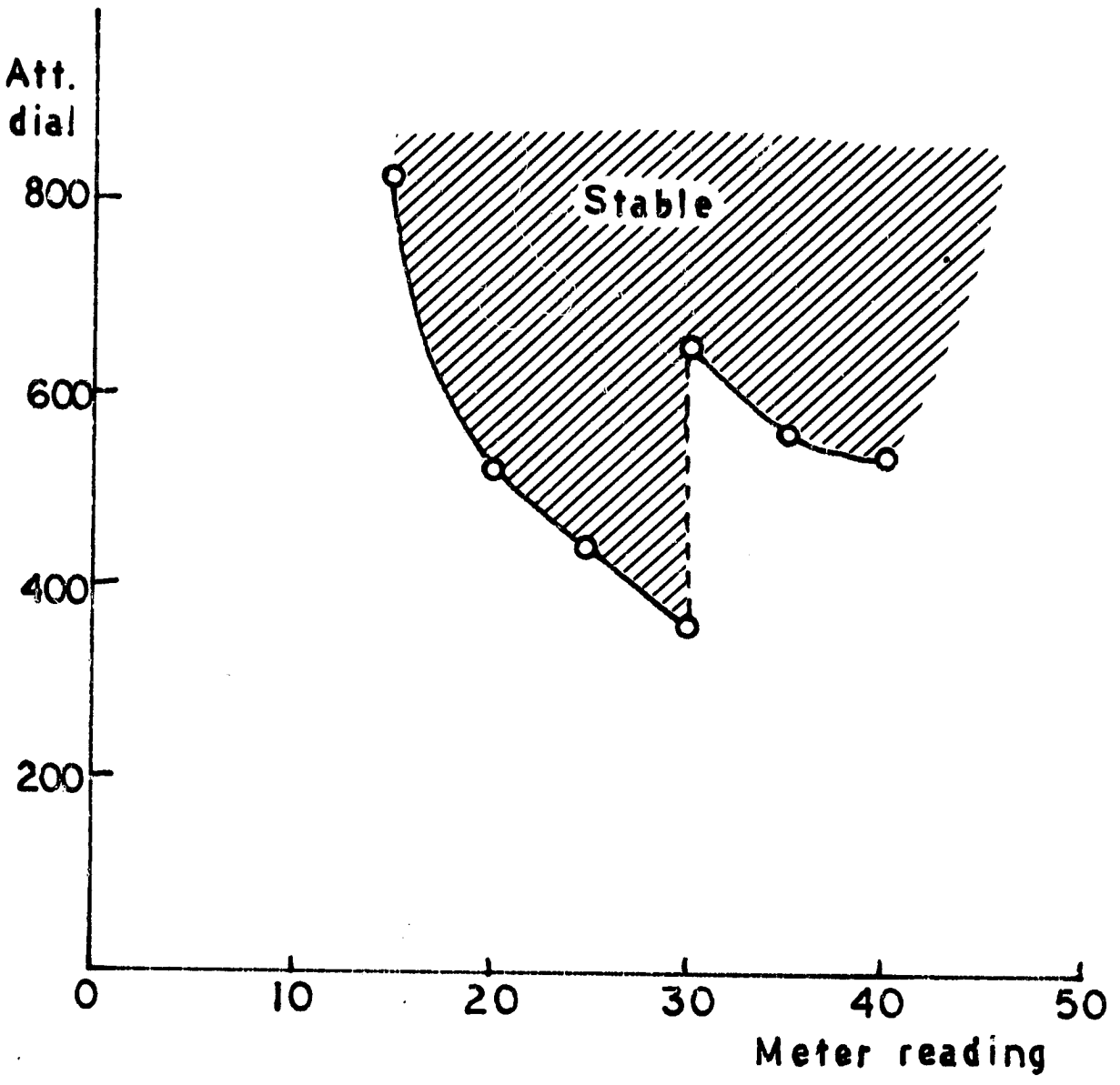

Figure B11. Attenuator settings for stable magnetron operation

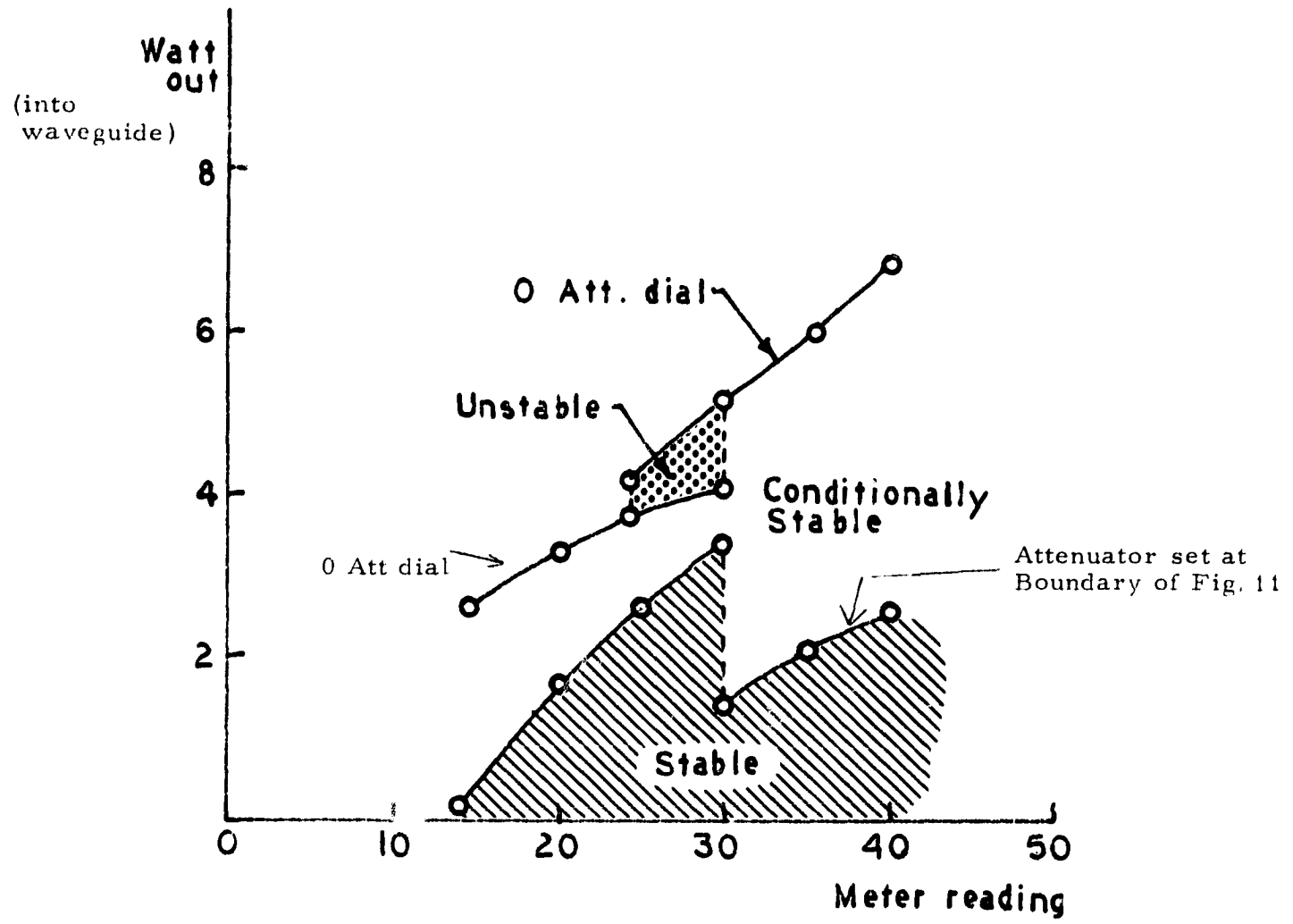

Figure B12. Power output for stable magnetron operation

Example: When meter reading is set at 40%
Attenuator set above ~ 600: circuit is stable
Attenuator set below ~ 600: circuit must be tuned with T1

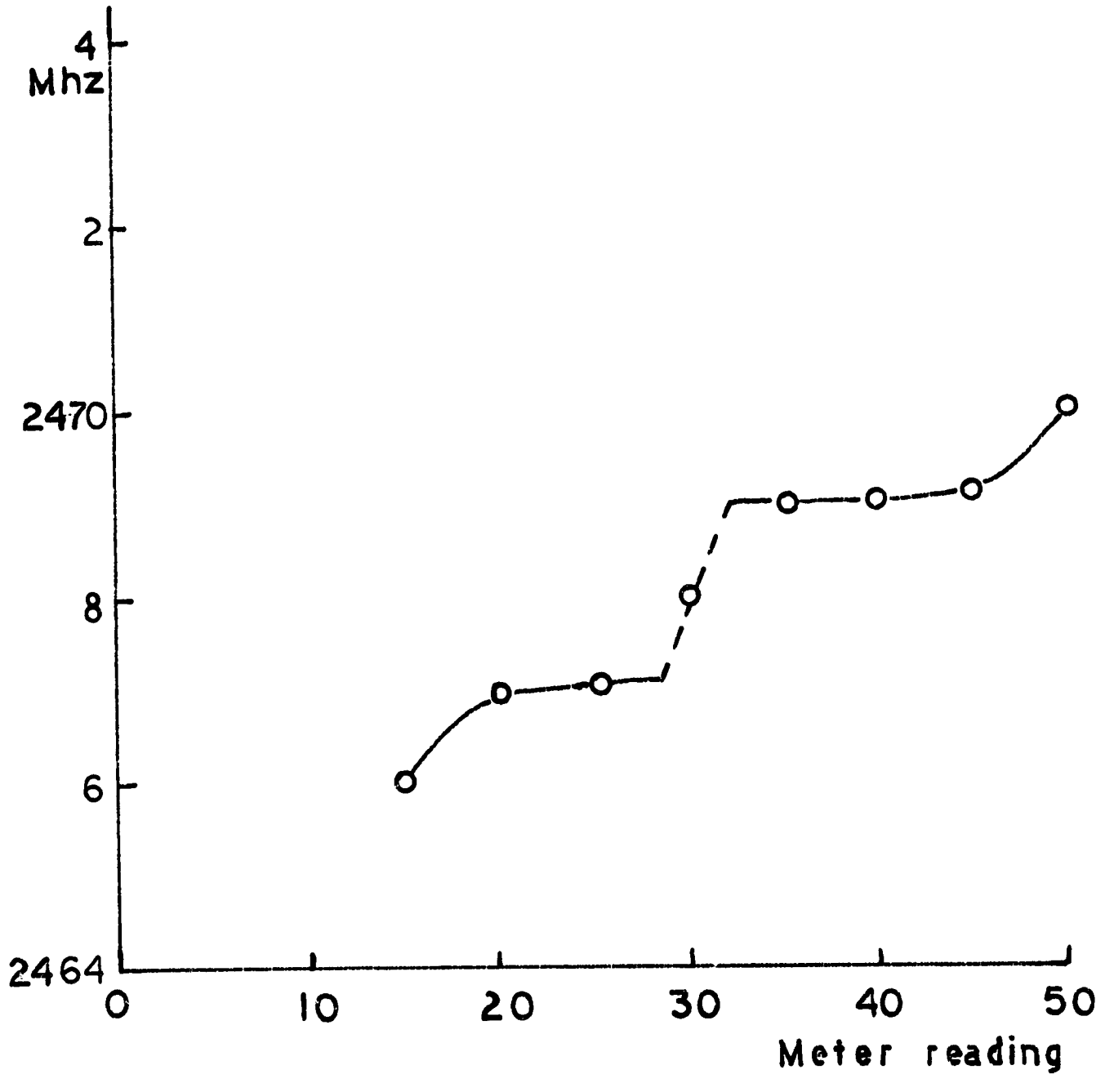

Figure B13. Frequency stability of magnetron

APPENDIX C
DETERMINATION OF SPECIES CONCENTRATION

The determination of the species concentrations is particularly important for the correct interpretation of the experimental results in cases where some species have very large cross sections for processes which can affect the measurements. The case of greatest practical interest involves the presence of oxygen (even in very small amounts) in nitrogen plasma or other mixtures, as well as the presence of disassociated or ionized atoms. Consequently several techniques were employed to determine the species concentrations. These are discussed below.

I. Heavy Particle Concentration

The departure from local thermodynamic equilibrium in the flows encountered in this investigation makes it difficult to use conventional spectroscopic techniques to determine the composition of the heated gases. After a careful survey of alternative techniques for determining the composition of the heated gases under investigation, it was decided to assign the highest priority to techniques involving chemical titration of the non-equilibrium flows since they appear to offer the optimum method for determining gas flow composition under the conditions of the experiment. However, since the equipment was available, conventional spectroscopic techniques have also been used where possible.

Under the conditions of the experiment, species concentration determination by chemical titration appeared to be particularly convenient and economical, and for these reasons it was considered particularly promising. Some simple preliminary experiments were devised to check its feasibility, and since they were met with qualitative success (in the sense that the predicted chemiluminescent behavior was observed), their outcome encouraged our inclination to concentrate on this method. The quantitative results of the systematic experiments reported here are sufficiently precise to justify our initial optimism.

The titration technique for determination of compositions has been the subject of considerable attention in recent years (refs. C1-C8). A

description of this technique, which is particularly useful in the determination of oxygen and oxygen atoms in dissociated flows of oxygen and nitrogen molecules, is appropriate.

Let us consider a mixture of N_2 and N and let us introduce a metered flow of nitric oxide, NO, in the titration inlet. The NO reacts with the N atoms to form electronically excited NO^* and N_2.

These reactions follow the steps (ref. C3)

$$N + NO \rightarrow N_2 + O \qquad (C1)$$

$$N + O + M \rightarrow NO^* + M \qquad (C2)$$

where (C2) is very slow compared to (C1), and

$$NO^* \rightarrow NO + h\nu \qquad (C3)$$

This nitrogen afterglow can be summarized as

$$2N \rightarrow N_2 + h\nu \qquad (C4)$$

The intensity of this nitrogen afterglow is given by

$$I_2 = 0.6 \times 10^{-11} (T/300)^{-0.90} [N]^2 \text{ photons/cm}^3\text{-sec} \qquad (C5)$$

where the brackets indicate the particle density for the species in question.

If one increases the NO flow rate slowly, the intensity of the nitrogen afterglow (due to de-excitation of NO^*) eventually decreases as more and more N atoms are being removed. At the point where all N has been converted into O and N_2, the afterglow due to NO^* ceases. This is the titration equivalence point at which the injected NO flow rate is equal to the original N flow rate in the jet (or streamtube), and the concentration of NO (that would have existed if it were not decomposed by N) is exactly equal to and cancels the original concentration of N with (C2) is negligible.

Upon further addition of NO, the excess NO reacts with the oxygen atoms forming excited NO_2^*:

$$NO + O \rightarrow NO_2^* \rightarrow NO_2 + h\nu \qquad (C6)$$

The intensity of the radiation produced by this <u>air</u> afterglow reaction is given by

$$I_4 = k_{NO_2}[NO][O] \qquad (C7)$$

The NO_2 afterglow consists of a continuum extending from 400 mm to the infrared. The N_2 and NO_2 afterglows, equations (C4) and (C6) respectively, overlap spectrally (see figures C1 and C2) and therefore we can use the known NO_2 continuum as a calibration standard. (However, this is not necessary since I_2 and I_4 have been measured.) Note that at equivalence the oxygen atom concentration $[O]$ is equal to the original nitrogen atom concentration $[N]_o$. The NO concentration beyond the equivalence point is proportional to the excess NO flow rate, i.e., $[NO] \propto (NO) - (NO)_o$ where $(NO)_o$ is the flow rate of NO at equivalence, i.e., when it is equal to the original N flow rate. Thus we can obtain the concentration of N by increasing the flow rate of NO to the point (titration null point or equivalence point) where the intensity of some excited NO^* band drops to zero and measuring the flow rate of NO at the point when that happens. As a check we can obtain the intensity of the NO_2^* continuum – it should also be zero at the same point. This is indeed found to be the case, and a very sharp null is obtained at the titration equivalent flow of NO.

The determination of atomic oxygen concentration can proceed in several ways. For example, we can observe the intensity of the NO_2^* continuum as a function of increasing NO flow rate. At the point where this intensity stops to increase with increasing NO, we have reached the situation where all the atomic oxygen has been consumed by the reactions summarized by equation (C6). More precise results could be obtained by the NO_2-titration technique developed by Kaufman (ref. C7) for determination of oxygen atom concentration or the optical-absorption technique of Jacobs <u>et al.</u> (ref. C8). Kaufman's NO_2-titration yields absolute values of $[O]$.

Similarly, when we start with mixtures of N_2, O, N and O, nitric oxide titration can be used to obtain the concentrations of both N and O by

a combination of the techniques described above. However, since a leveling-off of intensity is more difficult to measure accurately (because of a asymptotic behavior) than an extinction of intensity, the alternate scheme of nitrogen dioxide (NO_2) titration can be used to determine oxygen atom concentration. The basic reactions involved in [O] determination are:

$$NO_2 + O \rightarrow NO \text{ (ground state)} + O_2 \tag{C8}$$

$$NO + O \rightarrow NO_2^* \rightarrow NO_2 + h\nu \tag{C9}$$

The titration equivalence point where the NO_2^* glow (air or oxygen afterglow) disappears is reached when the injected NO_2 flow rate is just equal to the original O flow rate in the streamtube. Titration with a combination of NO and NO_2 injection yields the two equivalence points required for simultaneous determination of [O] and [N]. The glow is most intense when the flow of added NO_2 is one half of the flow of atomic oxygen (ref. C7).

Results for N_2

Some doubts existed concerning the feasibility of these techniques when applied to our experiment since the heated gas stream we use is very fast, the pressure is low and the mixing and reaction lengths could be very long. However, when we tried to resolve this doubt by injecting NO into a heated nitrogen gas stream both the excited NO^* and excited NO_2^* glows were observed succesively and the NO^* glow (nitrogen afterglow) could be made to disappear by increasing the nitric oxide flow rate.

In these experiments a stainless capillary tube with an outside diameter of 0.028 inches and an ID of 0.020 inches was used for NO injection. The injector tube pointed upstream (i.e., injected the gas against the plasma-jet flow) and was parallel to the axis of the free jet. The injector tube was projected by a quartz jacket that was mounted coaxially on the heat exchanger which, in turn, was mounted on the 3-degree-of-freedom traversing system.

The injected gas formed a bow shock wave ahead of the injector tube whose strength (as judged by its luminosity) and stand-off distance increased with the flow rate of NO. Within this luminous bow shock wave a second,

hemispherical luminous wave front appears. Since this hemispherical luminous front disappears when an equal amount of pure N_2 is injected from the tube, we have dubbed it the "reaction front." Figure C3 is a schematic of the appearance of the interaction of the jet and the injected NO flow.

It should be noted that these experiments also established that the NO flow through the capillary was sufficient to keep its wall cool at high enthalpies.

The experimental results indicate that titration techniques offer considerable promise for obtaining a spatially resolved estimate of the atomic species concentrations of our jet of plasma.

In the present experiments there is, at equivalence, a startling, sharp and well-defined extinction of the nitrogen afterglow in the entire tank and also in the jet downstream of the point of injection. It is actually as if someone turned off the lights. Consideration of the reaction rates involved shows that at extinction and relatively long-lived nitrogen atoms injected into the tank by the arcjet are exactly and completely recombined by an equal number of nitric oxide molecules injected into the stream through the capillary tube. A schematic of the salient points of the observable luminosity structure appears in figure C3. At equivalence, all luminosity downstream of the dotted line of figure C3 disappears. The shock front shown in figure C3 is a true bow-shock similar to one that would have been caused by a blunt body under the same conditions. This shock starts off almost spherical near the jet axis and then changes its shape to a front that stands more perpendicular to the flow when it reaches the jet boundaries where the Mach number is lower. Immediately behind this shock and tangent to it at the jet or injector axis is a practically spherical luminous wave. Only the front half of this is visible at equivalent. This second, spherical luminous wave appears to be centered at the injector tip and its diameter is a function of the NO flow rate just as the stand-off distance of the bow shock (which is tangent to the second luminous wave at the jet axis) is also a function of the NO flow rate. However, its luminousity has a minimum at equivalence.

Since the second luminous wave does not exist when an equal volumetric flow rate of N_2 is injected, we have decided to call it the reaction front.

Figures C4, C5 and C6 present the results obtained, showing the concentrations of N_2, N, and the ratio $[NO]/[N_2]$ respectively.

It is now possible to compute, using the AEDC-NBS Tables of thermodynamic properties and composition (ref. C9), the effective temperatures for ionization and dissociation (that is, the temperatures corresponding to the observed levels of ionization and dissociation) as a function of arcjet stagnation temperature and/or enthalpy as measured in the system. The results are presented in figure C7 and table C-I.

The important result of figure C7 is that the effective ionization and dissociation temperatures coincide within 10 % or less and both are considerably above the stagnation temperature derived from an arcjet energy balance. The implication of figure C7 is that equilibrium does not prevail in the arc we are using and in the mode of operation we have established, at least not in the lower arc pressures. Note that as the enthalpy (or pressure in the plenum chamber since the flow rate is constant) increases the results approach closer and closer to equilibrium and $T_{eff,\,ion} \rightarrow T_{eff,\,rec} \rightarrow T_o$. Note that at $T_o \approx 5000\ ^oK$ we have $p_{plenum} \approx 0.8$ atmos.

Results for N_2-O_2 mixtures

The titration of N_2 - O_2 mixtures was performed with the method of maximum glow discussed on page 99, and the results are presented in table C-II.

An interesting point is that extinction is harder to ascertain in N_2-O_2 mixtures (because of the presence of NO) and that is why we worked with the maximum glow technique. Another interesting point is that the literature is sufficiently vague concerning the effect of initial amounts of NO on this titration. In fact there is some reason to believe that the NO_2 titration in the presence of NO yields the quantity $[NO] + [O]$ and not just $[O]$.

After many vain attempts to obtain equilibrium composition and thermodynamic tables for arbitrary mixtures of $N_2 + O_2$, including NO, from the literature we perfected a computer program that yields the required information, i.e., given any two of the following parameters - pressure, temperature, enthalpy, density or entropy, it computes all the

other parameters plus the speed of sound, specific heats and compositions for any arbitrary N_2+O_2+Argon mixture under equilibrium conditions. We are indebted to Dr. W. Norman of USAF/AEDC/ARO (who also made available to us the NBS thermodynamic and thermochemical constants) for part of this computer program. Some typical results are presented in figures C8 through C11. It is interesting to note that the measured production at oxygen atoms in the arc is considerably higher than the equilibrium values of low enthalpy, but yet closer and closer to the equilibrium values as the enthalpy increases. This is in agreement with the results obtained for nitrogen dissociation.

II. Charged Particle Concentration

The measurement of electron and ion densities is accomplished with the Langmuir probe. If we assume an essentially Maxwellian distribution for the components of the plasma (and care is always taken to insure that this is the case), we can use the standard expression for current density through a thin sheath (ref. C10), and solve for the charged particle density: for electrons,

$$n_e = \frac{1}{2} (j_{esat}/e)(\pi m_e/2kT_e)^{1/2} \qquad (C10)$$

and for ions

$$n_i = \frac{1}{2} (j_{isat}/e)(\pi m_i/2kT_i)^{1/2} \qquad (C11)$$

Here the current densities j_{esat} and j_{isat} are measured at the electron saturation bias voltage V_s, i.e., where the bias voltage is equal to the plasma potential.

In practice, the information necessary to solve equations (C10) and C(11) is determined entirely from the current-voltage traces we obtain with the Langmuir probe. The electron temperature is determined in the usual way (i.e., by measuring the slope of a log I vs. V plot in the region of transition from ion to electron current), and, to solve (C11), the ion temperature by locating the "knee" at which the electron temperature determining line and the line through the electron-saturated portion of the trace

intersect. The values of j_{esat} and j_{isat} are found by extrapolating lines through the electron- and ion-saturated regions to V_s and reading the currents I_{esat} and I_{isat} which are divided by the area of the probe to give the current densities. The values of n_e and n_i are obtained by these methods agree in nearly all measured cases to within a factor of two. Figures C12 and C13 show measured electron density and temperature, respectively, in a pure nitrogen plasma as a function of stagnation enthalpy.

REFERENCES OF APPENDIX C

C1. Young, R. A.; and Sharpless, R. L.: J. Chem. Phys., vol. 39, no. 4, 1963, p. 1071.

C2. Hartunian, R. A.; Thompson, W. P.; and Hewitt, E.: J. Chem. Phys., vol. 44, 1966, p. 1765.

C3. Gross, R. W. F.: "Temperature Dependence of Chemiluminescent Reactions, Vol. I, the Nitrogen Afterglow," Aerospace Corp. Report No. TR-1001 (2240-20)-6, vol. I, June 1967.

C4. Gross, R. W. F.: "Temperature Dependence of Chemiluminescent Reactions, Vol. II, the Nitric Oxide Afterglow," J. Chem. Phys., vol. 48, March 1968, p. 2582.

C5. Kaufman, F.: Progr. Reaction Kinetics, vol. 1, 1961, p. 1.

C6. Jacobs, T. A.; Carson, B. H.; and Giedt, R. R.: Appl. Opt., vol. 6, 1965, p. 754.

C7. Hartunian, R. A.; Thompson, W. P.; and Hewitt, E. W.: J. Chem. Phys., vol. 44, no. 5, 1966, p. 1765.

C8. Fontijn, A.; Meyer, C. B.; and Schiff, H. I.: J. Chem. Phys., vol. 40, 1964, p. 64.

C9. Hilsenrath, J.; and Klein, M.: "Table of Thermodynamic Properties and Chemical Composition of Nitrogen in Chemical Equilibrium Including Second Virial Corrections from 1600 ^{o}K to 15,000 ^{o}K," National Bureau of Standards, AEDC-TR-66-65, April 1966.

C10. Chen, F. C.: "Electric Probes," Plasma Diagnostic Techniques, R. H. Huddlestone and S. L. Leonard, eds., New York, Academic Press, 1965, p. 126.

TABLE C-Ia

Effective Temperature for Dissociation of Nitrogen Computed from Measured Dissociation Fraction as a Function of Enthalpy for Thermal Dynamics 50-N arcje

Run No.	Stagnation Enthalpy H_o (BTU/lb)	Arc Chamber Pressure (atm)	Stagnation Temperature (^oK)	Density Ratio ρ/ρ_o (ρ_o at STP)	$\log_{10} \rho/\rho_o$	Nitrogen Atom Mole Fraction $n_N/(n_{N_2}+n_N)$	Effective Temp. for Dissociation (^oK)
148A	895	0.508	1830	0.075	-1.125	0 0132	4684
149A	1245	0.556	2450	0.061	-1.215	0.0328	5030
150A	1640	0.623	3170	0.054	-1.268	0.0532	5235
151A	2140	0.710	4040	0.048	-1.319	0.0823	5438
152A	3120	0.783	5110	0.041	-1.387	0.1220	5626

TABLE C-Ib

Effective Temperature of Ionization of Nitrogen Computed from Measured Ionization Fraction as a Function of Enthalpy for Thermal Dynamics 50-N arcjet

Run No.	Stagnation Enthalpy H_o (BTU/lb)	Arc Chamber Pressure (atm)	Stagnation Temp. (^oK)	Density Ratio ρ/ρ_o (ρ_o at STP)	Electron Number Density $n_e \times 10^{15}$ (elec/m^3)	Nitrogen Molecule Number density $n_{N_2} \times 10^{20}$ (molec/m^3)	Nitrogen Atom Number density $n_N \times 10^{20}$ (atom/m^3)	Effective Temp. for Ionization T_{eff} (^oK)
158A-C	909	0.498	1850	0.074	0.958	161.5	2.38	4419
158F	1325	0.582	2600	0.061	2.30	127.0	4.95	4629
158D-E	1736	0.632	3340	0.059	4.00	98.0	6.27	4809
158G	1995	0.698	3800	0.050	7.97	81.5	6.53	4995
158H-I	3197	0.832	5170	0.043	40.3	33.0	4.35	5669
158K-L	4030	0.932	5640	0.045	143			

TABLE C-II

Results of atomic oxygen determination by NO_2 - titration of an approximately 11% O_2 - 89% N_2 mixture (by volume) at various enthalpies.

Oxygen flow rate, $[O_2]_0$ molecules/sec	Enthalpy BTU/lb	NO_2 flow rate at maximum glow intensity molecules/sec	Atomic oxygen flow rate molecules/sec	Measured. Ratio $\frac{[O]}{[O_2]_0 - \frac{1}{2}[O]}$	Equilibrium Theoretical $\frac{[O]}{[O_2]}$	Equilibrium Theoretical $\frac{[O] + [NO]}{[O_2]}$
13.65×10^{20}	1245	2.6×10^{20}	5.2×10^{20}	0.47	0.033	0.21
13.65×10^{20}	1540	4.5×10^{20}	9.0×10^{20}	0.98	0.19	0.54
13.65×10^{20}	1715	5.4×10^{20}	10.8×10^{20}	1.31	0.44	0.91
13.65×10^{20}	1910	6.0×10^{20}	12.0×10^{20}	1.57	0.91	1.56

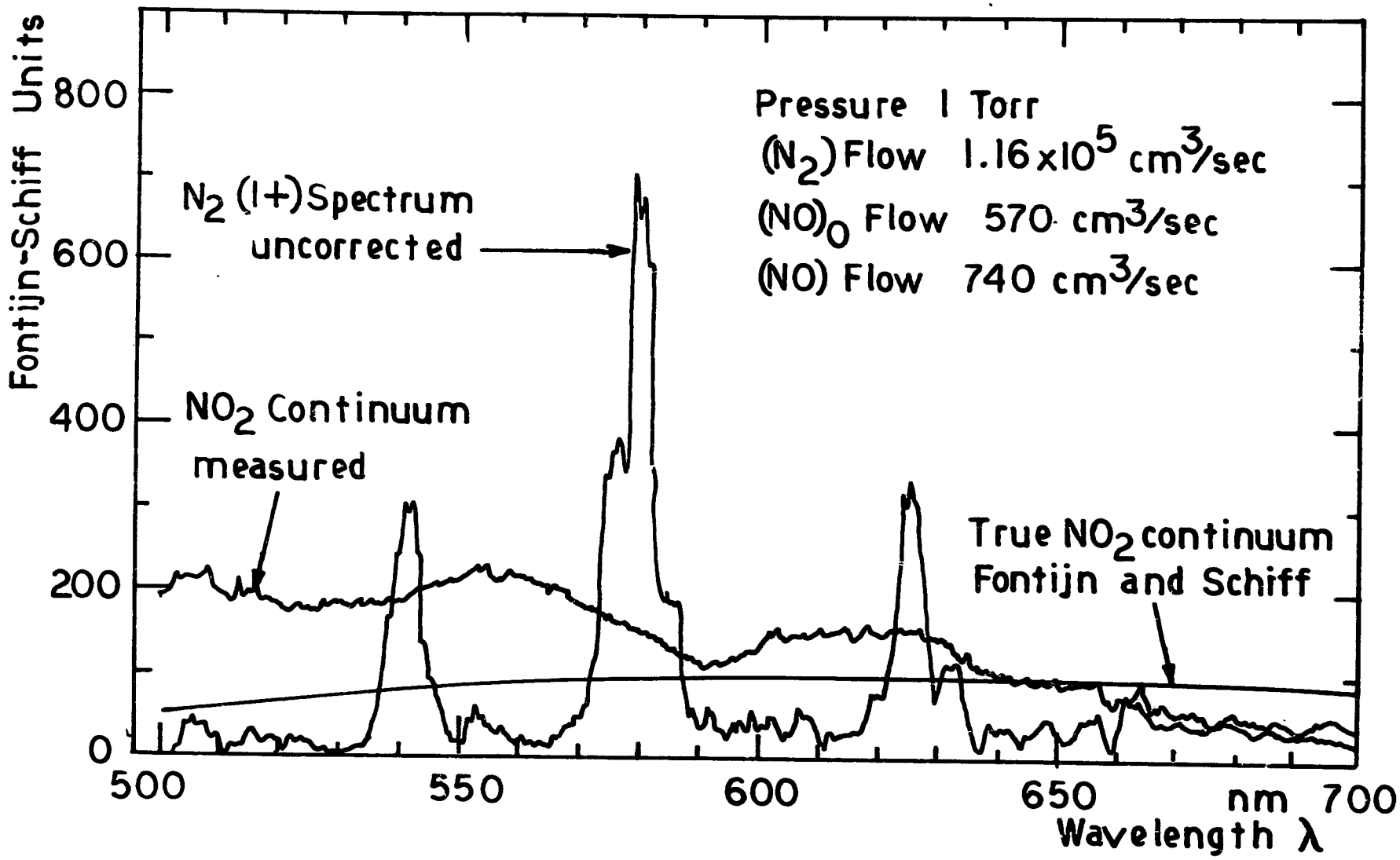

Figure C1. $N_2(1+)$ bands of nitrogen afterglow

Adapted from, and
by permission of
R. W. F. Gross
Aerospace Corp.

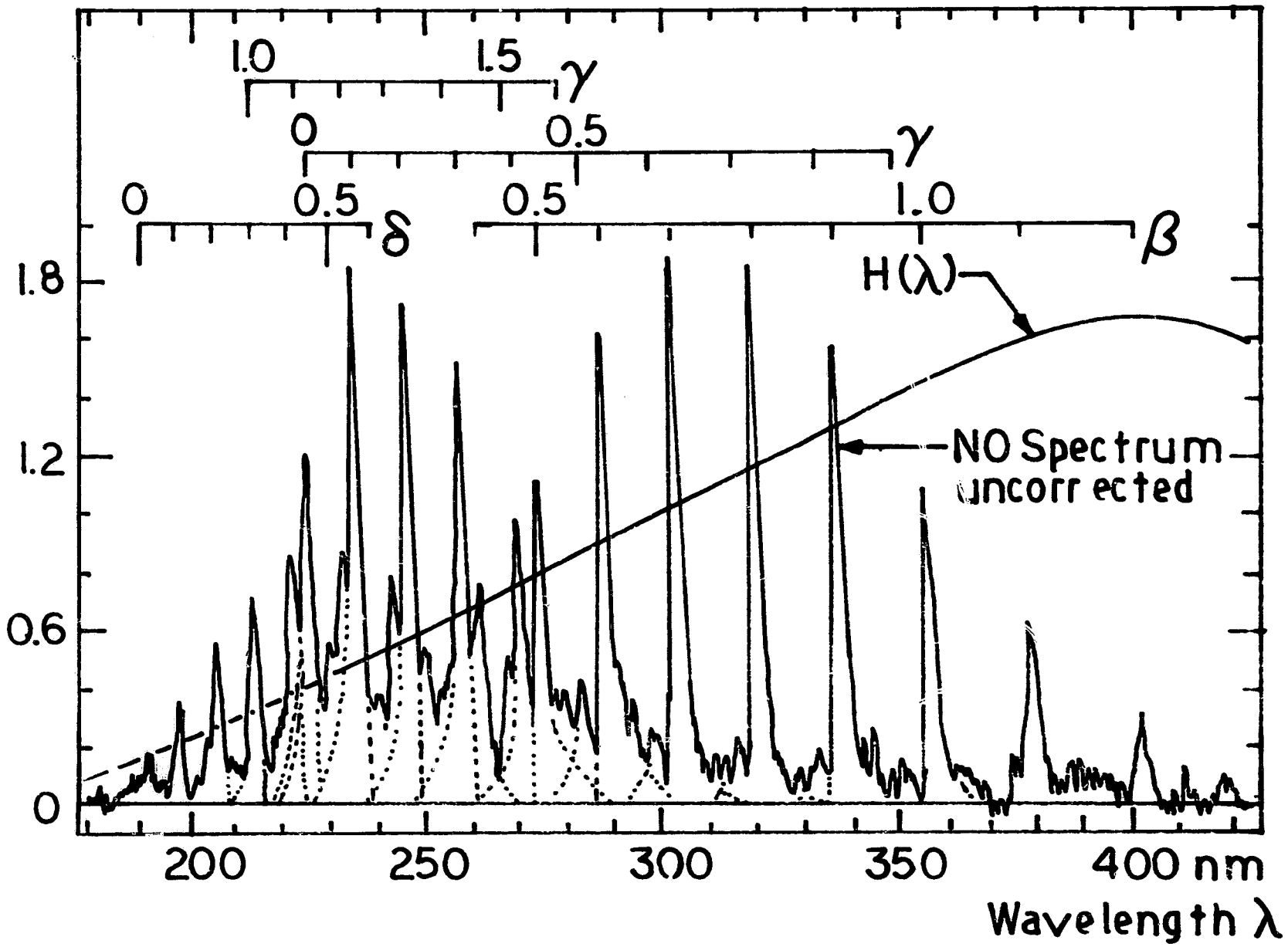

Figure C2. Nitric oxide spectrum

Adapted from, and
by permission of
R. W. F. Gross
Aerospace Corp.

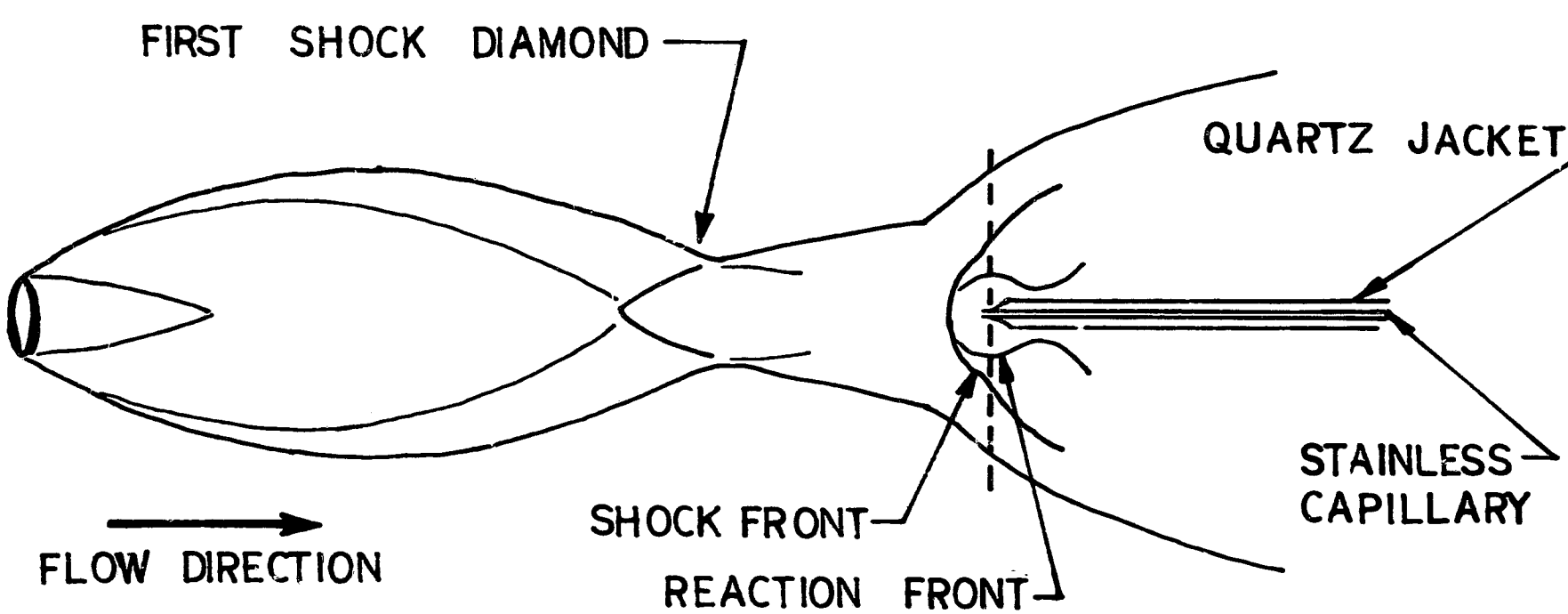

Figure C3. Schematic of nitric oxide titration of N_2 plasmajet, tracing observed luminosity structure when a slight excess of NO beyond the equivalence point is injected. All luminosity beyond the dotted line disappears at equivalence

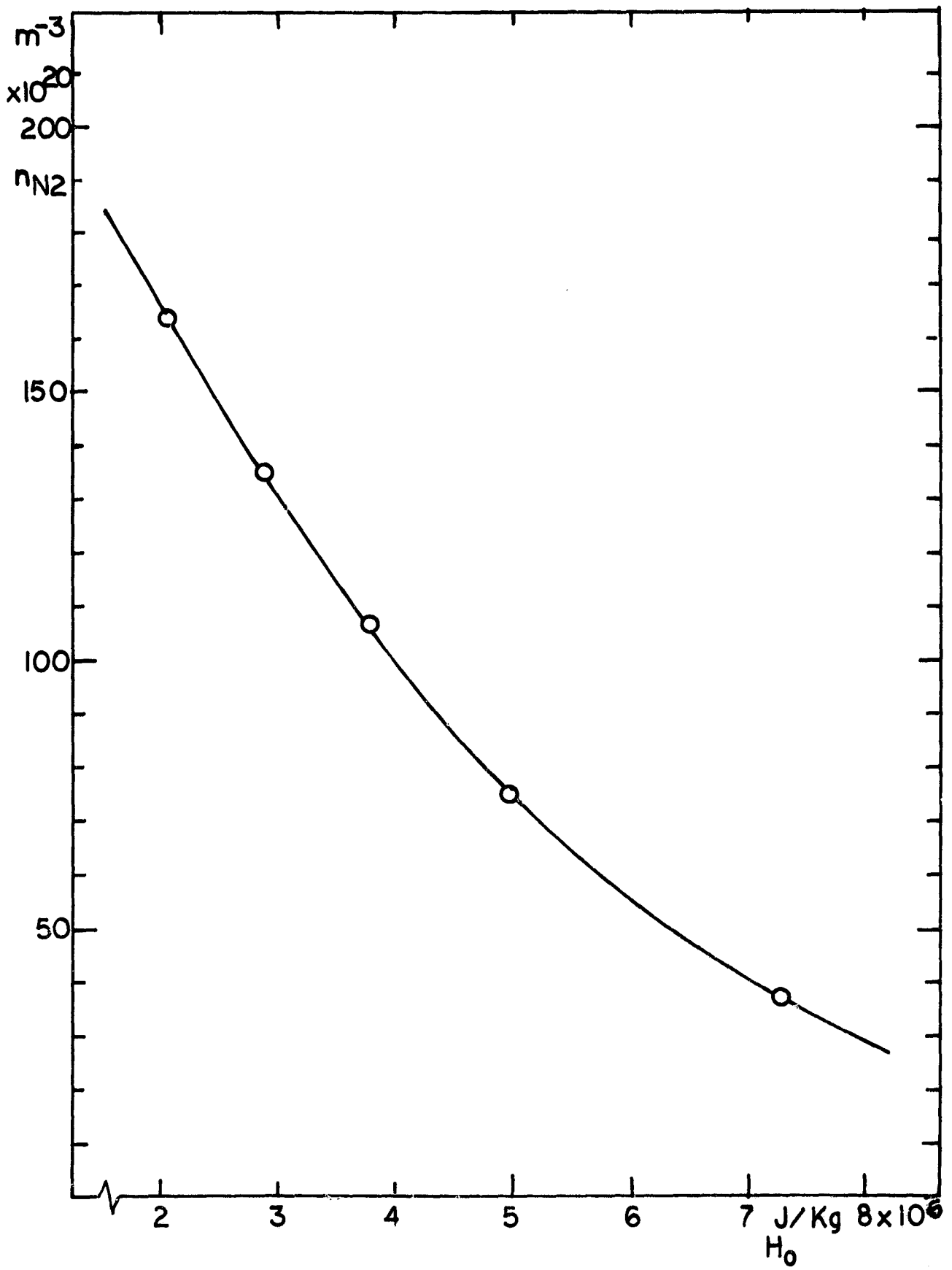

Figure C4. Number density of nitrogen molecules in plasma-jet, based on measured stagnation temperatures at 0.6 Torr, as a function of stagnation enthalpy

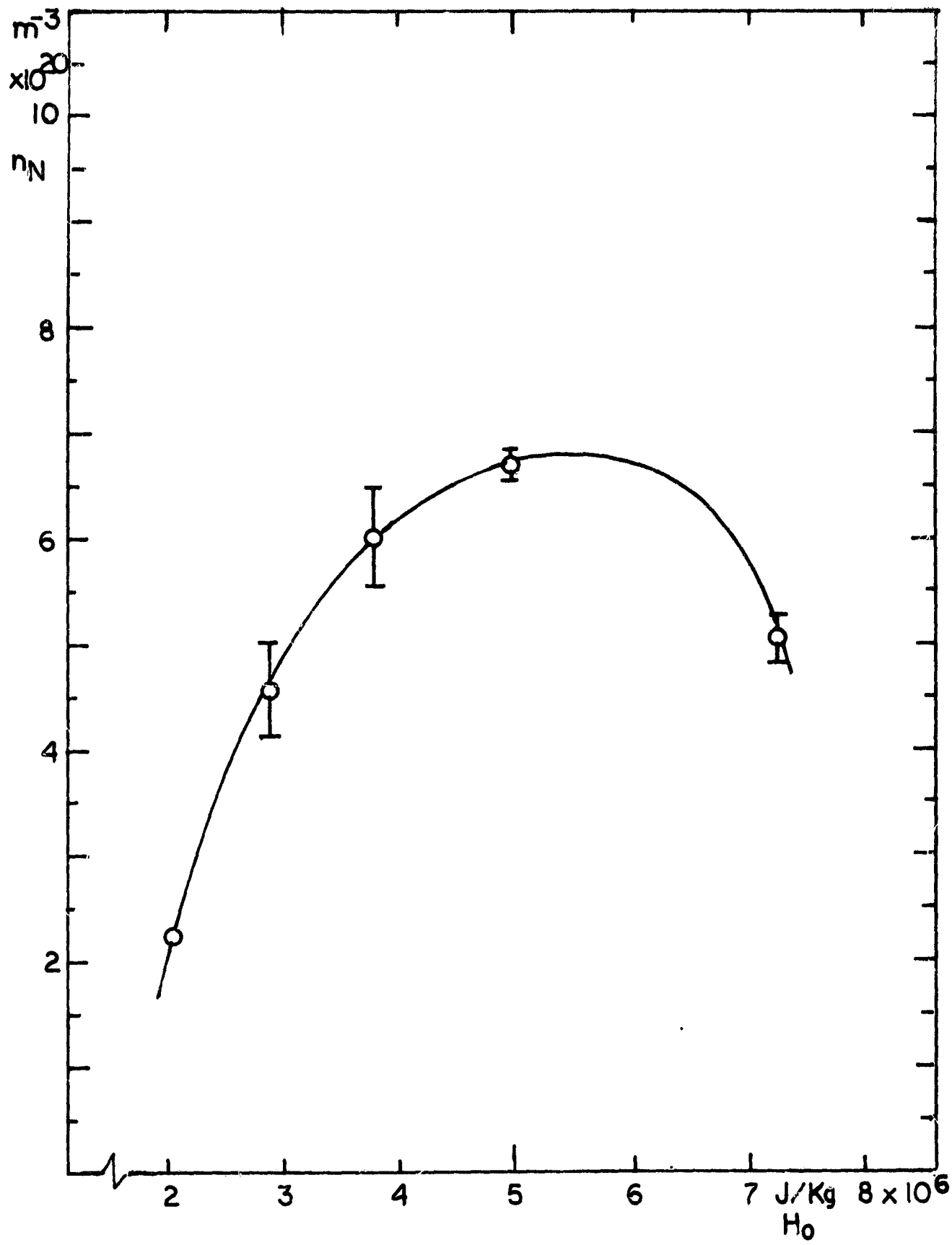

Figure C5. Number density of nitrogen atoms in nitrogen plasmajet at 0.6 Torr, as a function of stagnation enthalpy

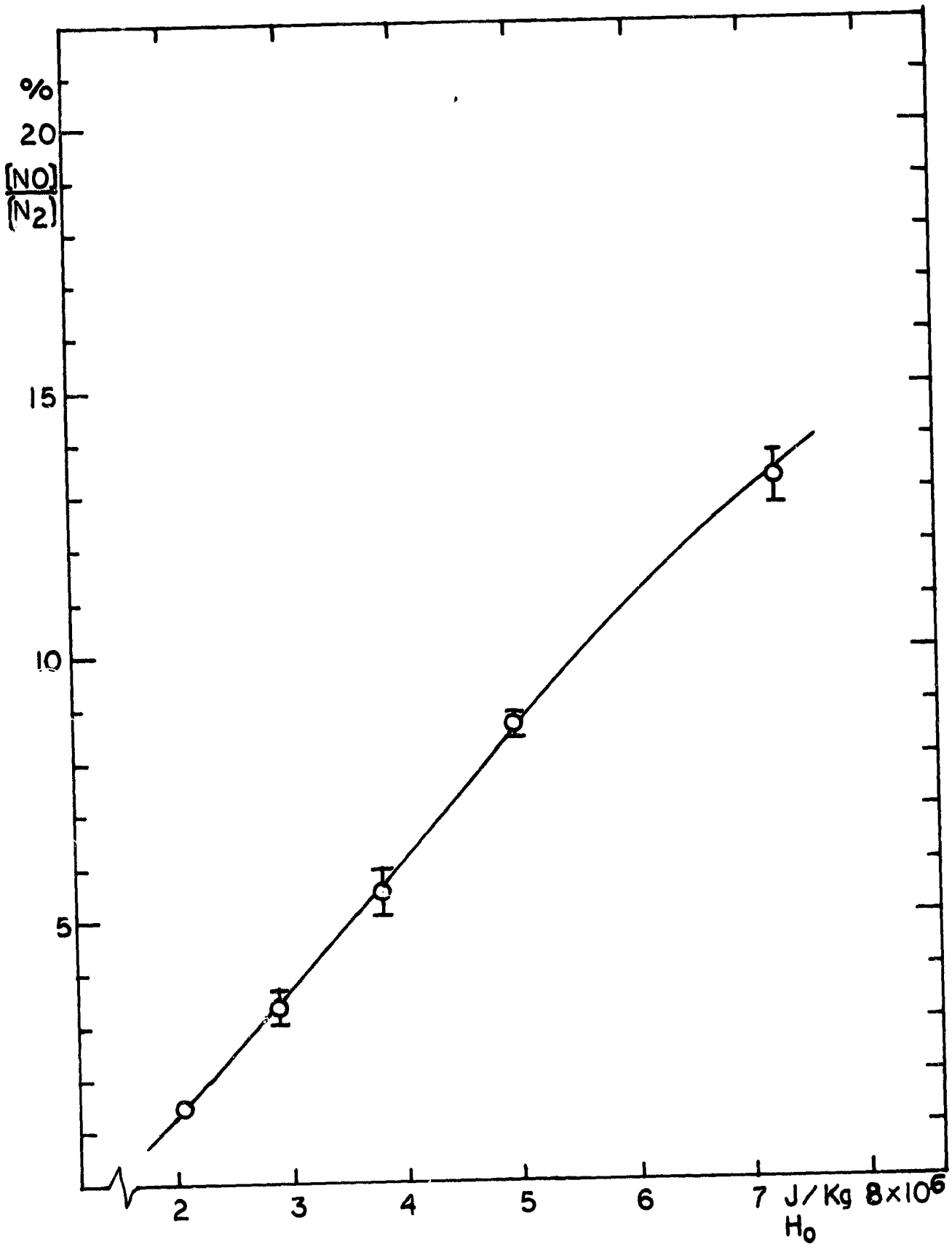

Figure C6. Ratio of flow rates of nitric oxide to nitrogen at the titration equivalence point in a nitrogen jet at 0.6 Torr, as a function of stagnation enthalpy

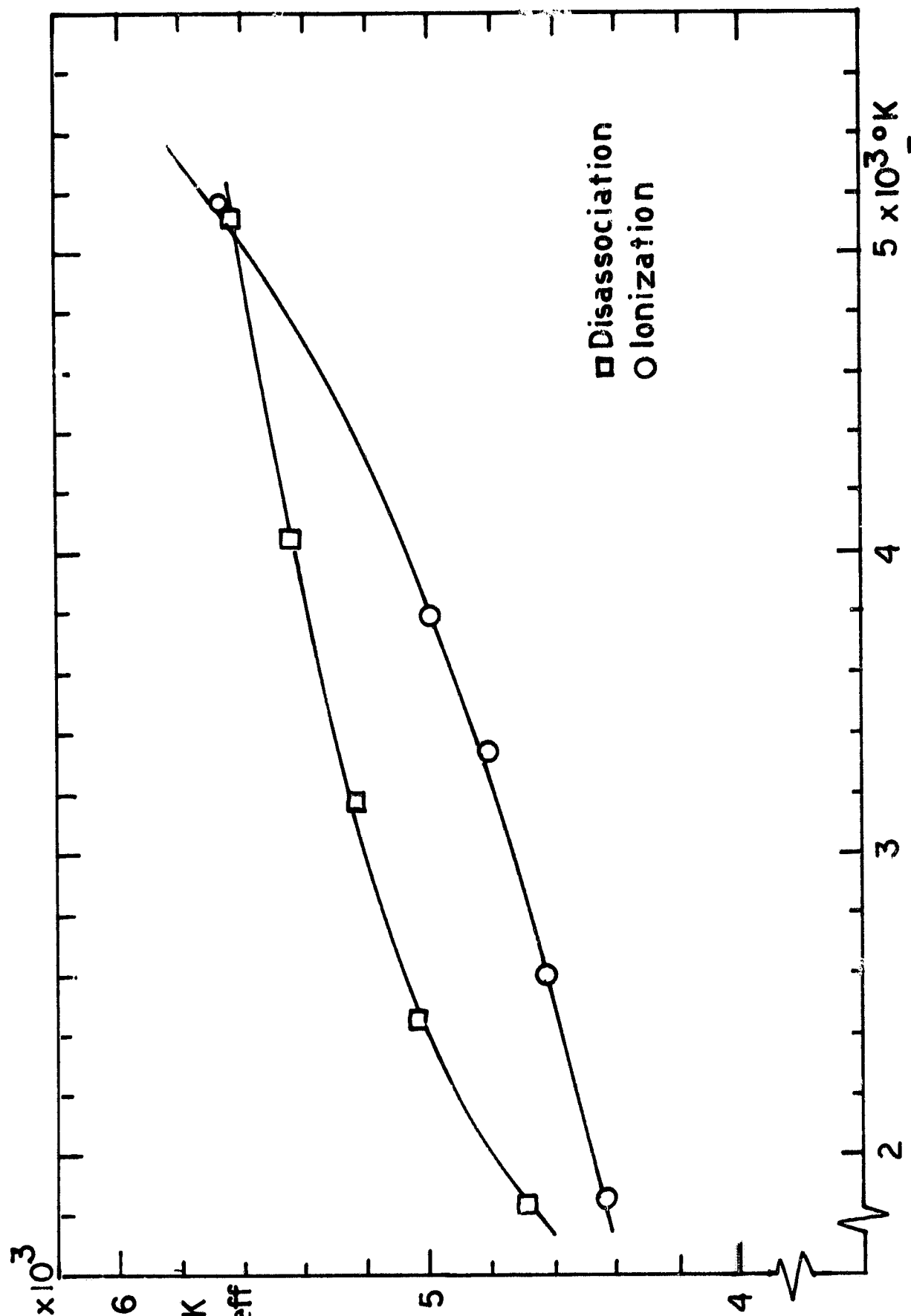

Figure C7. Effective nitrogen ionization and dissociation temperatures as a function of plasma stagnation temperature. Results derived from measurements of electron number density and dissociation in a free jet at 0.6 Torr

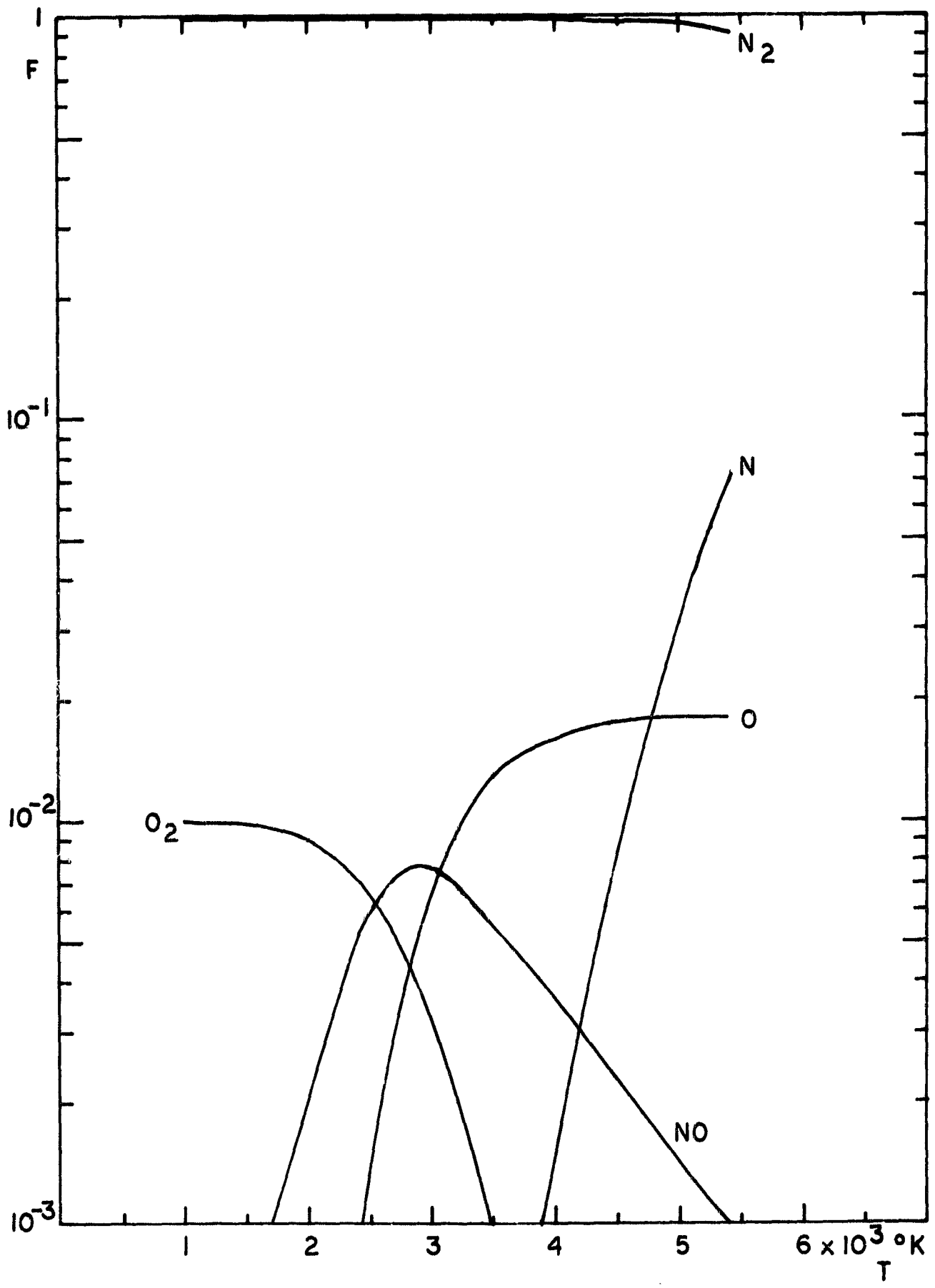

Figure C8. Equilibrium composition of a 1% O_2 - 99% N_2 mixture at 1 atmosphere pressure as a function of temperature (and enthalpy)

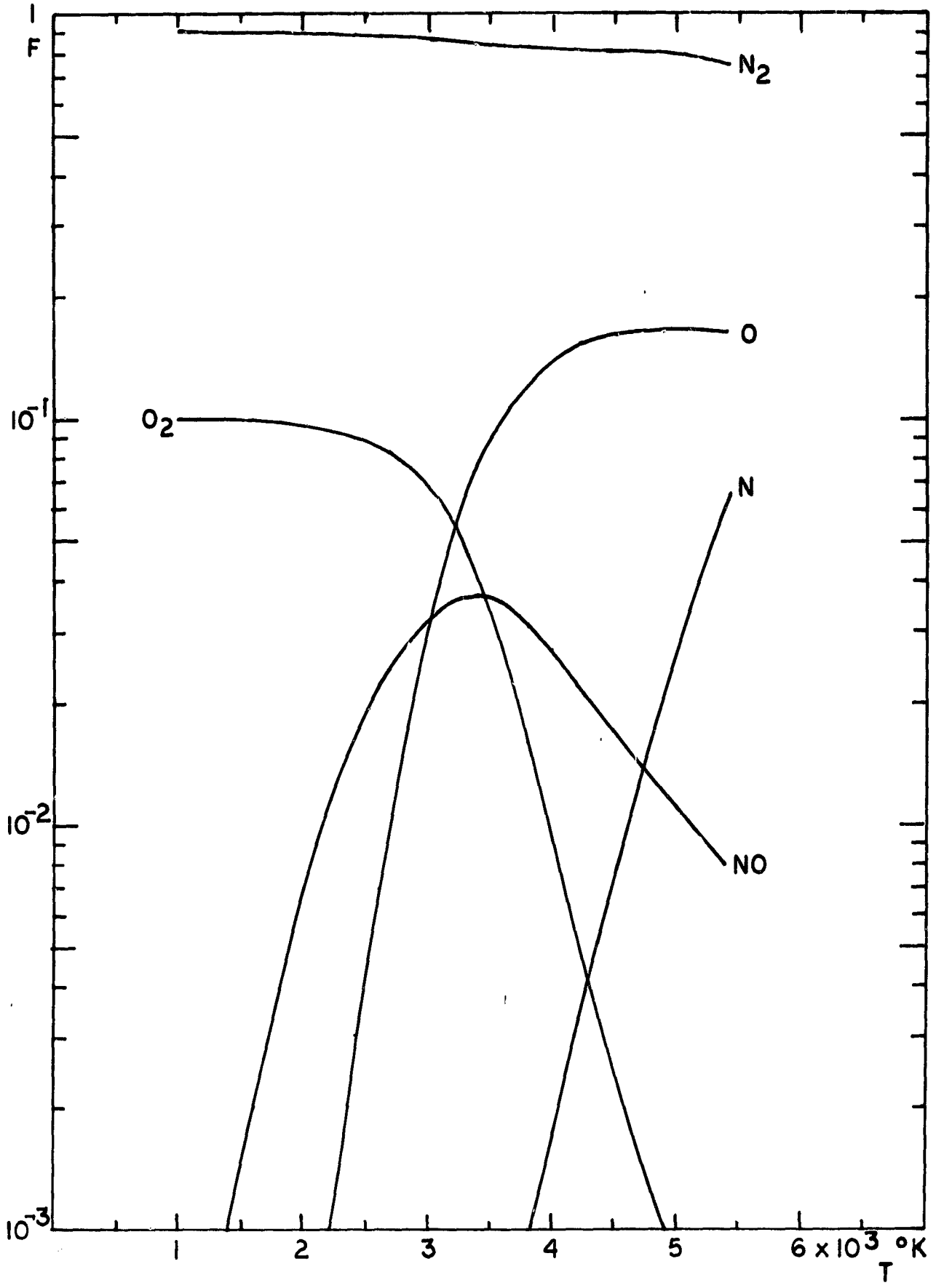

Figure C9. Equilibrium composition of a 10% O_2 - 90% N_2 mixture at 1 atmosphere pressure as a function of temperature (and enthalpy)

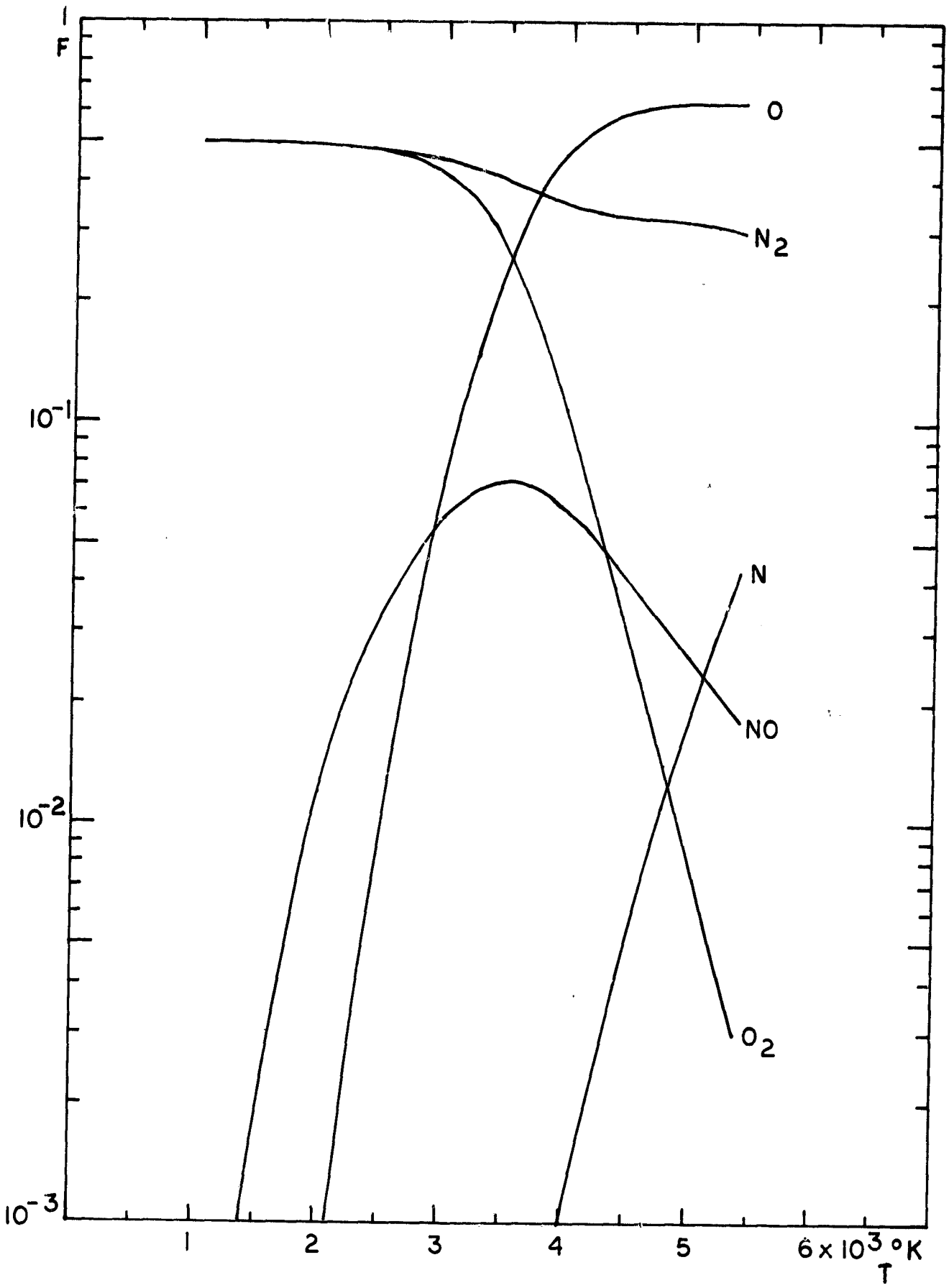

Figure C10. Equilibrium composition of a 50% O_2 - 50% N_2 mixture at 1 atmosphere pressure as a function of temperature (and enthalpy)

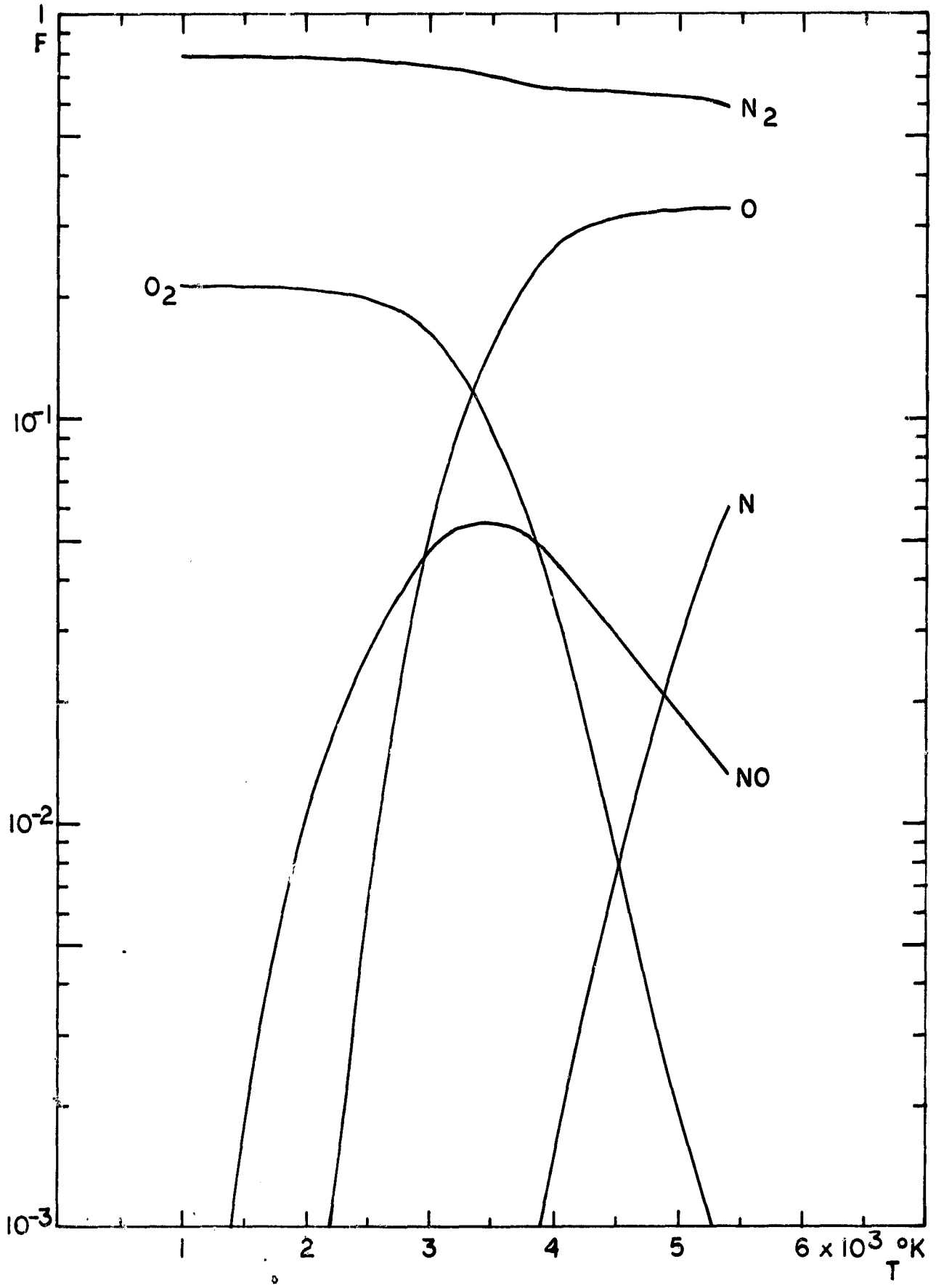

Figure C11. Equilibrium composition of a 21.4 % O_2 - 78.6% N_2 mixture at 1 atmosphere pressure as a function of temperature (and enthalpy)

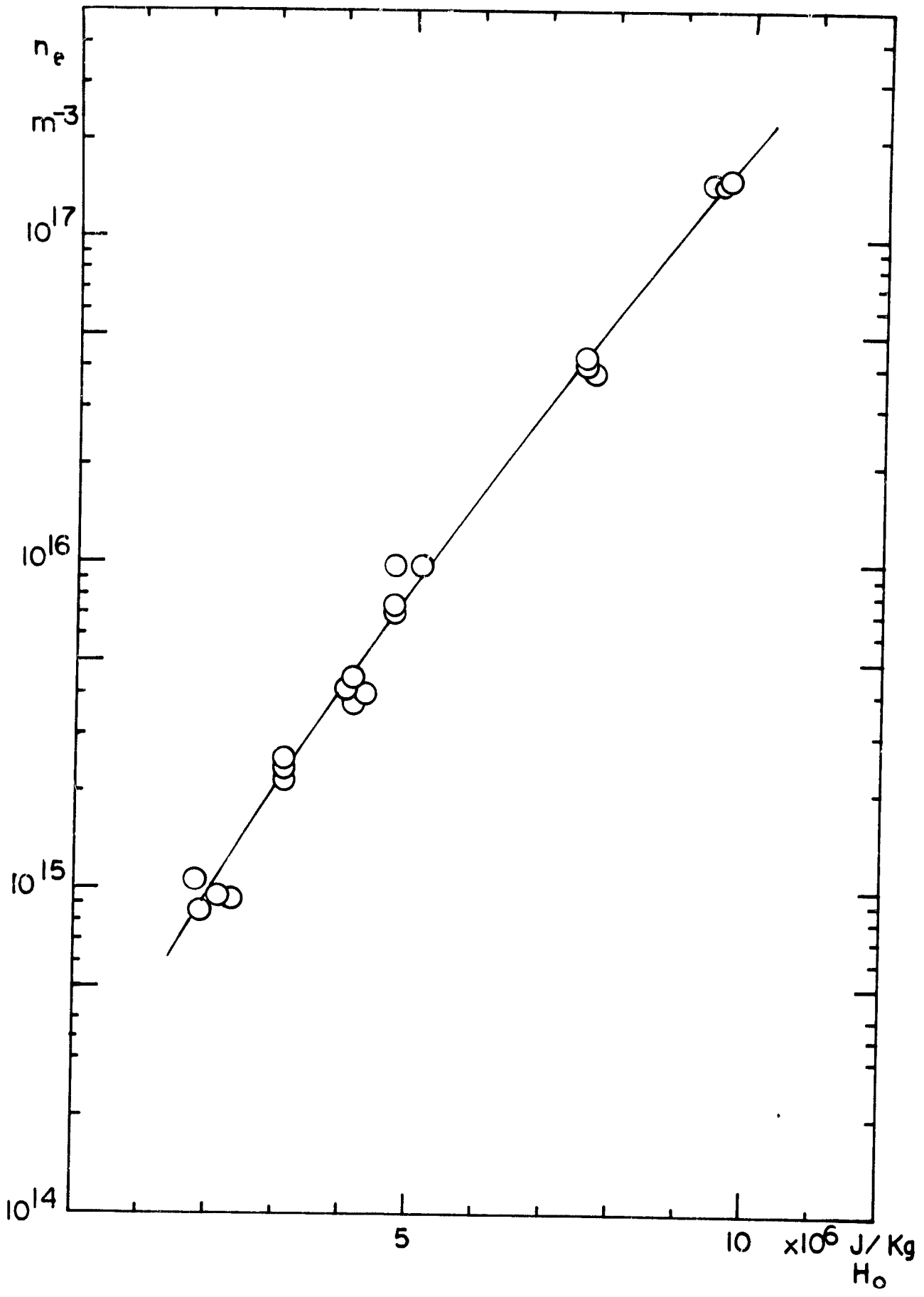

Figure C12. Electron number density as a function of nitrogen plasmajet stagnation enthalpy in a free jet at 0.6 Torr

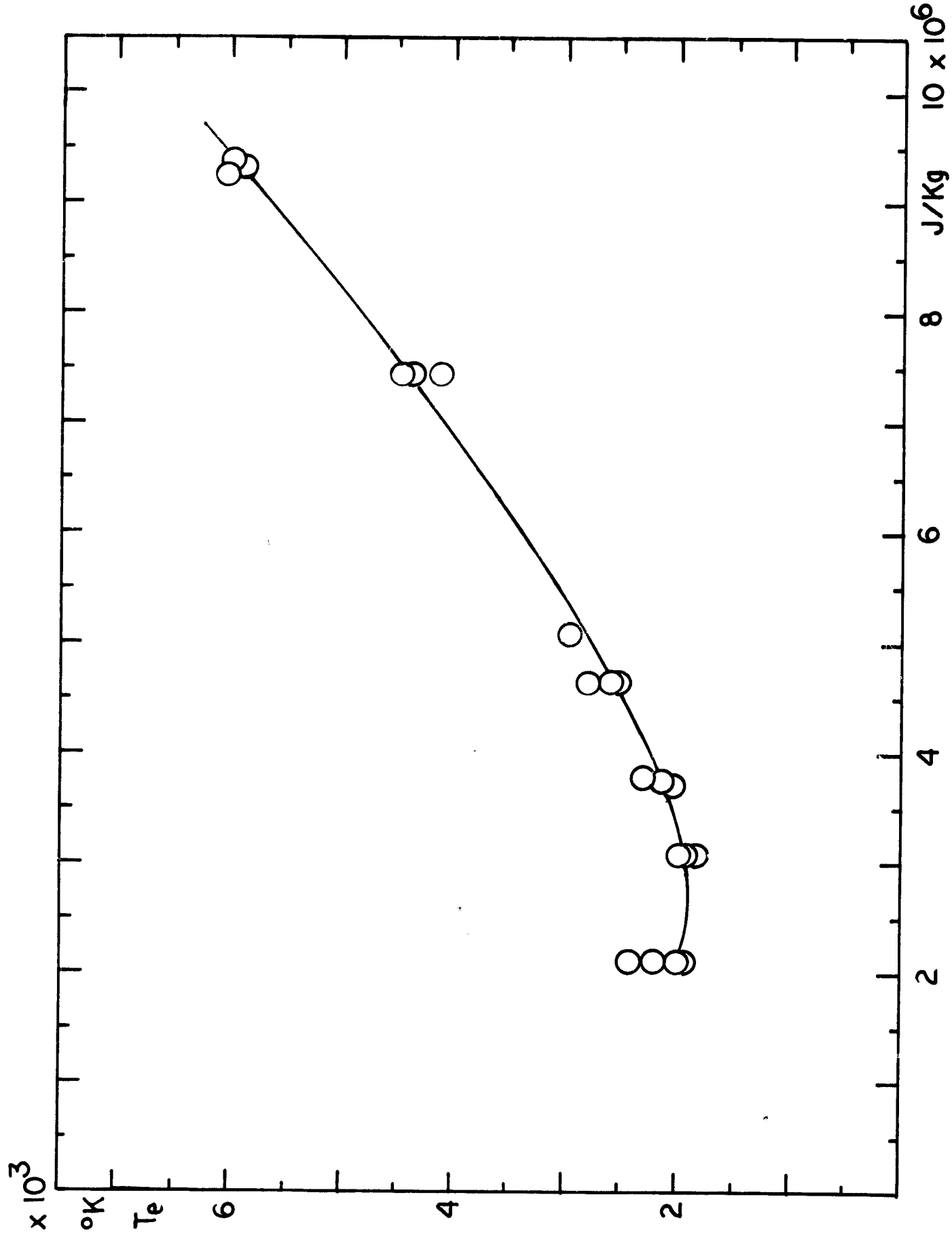

Figure C13. Electron temperature as a function of nitrogen plasmajet stagnation enthalpy in a free jet at 0.6 Torr

APPENDIX D

MEASUREMENTS OF VIBRATIONAL, ROTATIONAL, AND FREE ELECTRON TEMPERATURES IN THE NITROGEN PLASMA JET

I. Free Electron Temperatures

A Langmuir probe is used to determine free electron temperatures. A general description of the techniques we use may be found in references D1-D2.

Our Langmuir probe is a cylindrical collector consisting of a tungsten or stainless steel rod 1 mm in diameter which projects 4 - 6 mm out of a hollow quartz jacket. The probe wire is electrically isolated from the vacuum chamber and the heat exchanger, which are both grounded to a water pipe.

The current I through the probe to ground is displayed as a function of bias voltage V on a Hewlett-Packard 7000 A x-y recorder. These graphs are then manually transformed to semilogarithmic graphs with I plotted on the logarithmic scale. To find the electron temperature T_e we then use the standard result that the slope of the log I vs. V plot in the transition region between positive and negative bias is proportional to T_e. Temperatures measured in this way, without excessive noise, are reproducible to $\pm$ 100 ^{o}K, or about 3 - 5%.

Much care was taken in the design of the probe biasing circuit to insure a minimum of noise. The Langmuir probe acts as an electron or ion collector depending on the bias voltage applied between the tip and ground. We therefore obtain a current from the probe which is a function of the bias. The circuit shown in figure 1 of the main text is used to plot this current vs. voltage curve on the x-y recorder.

The electron and ion currents are given by

$$I_e = - V_e \frac{n_e}{\Delta t} e \quad ; \quad I_i = V_i \frac{n_i}{\Delta t} e \tag{D1}$$

where V_e and V_i are the effective volumes from which electrons and ions, respectively, are collected, n_e and n_i are the number densities

of electrons and ions, respectively, e the proton charge and $\Delta t = 1$ sec. Note that V_e and V_i depend on the bias voltage, and that n_e and n_i are statistical variables whose deviation from some mean gives the inherent "noise" that accompanies the measurement. This noise can unfortunately be greatly enhanced by the measuring circuit unless some care is exercised in its design.

Suppose that we were working on a portion of the I vs. V curve that looked as shown in the adjacent figure.

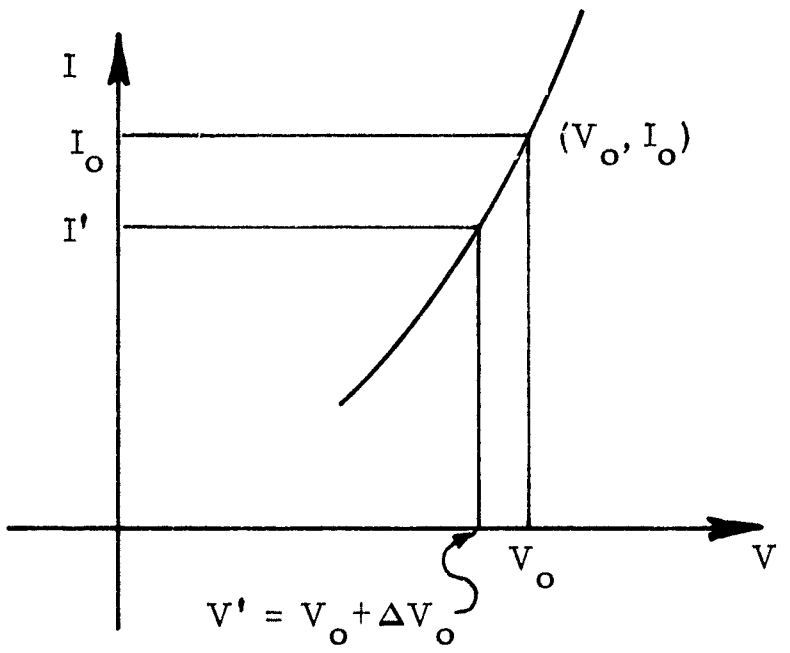

Assume that the bias voltage was set at V_o which corresponds to an ideal value for the current of I_o. Let ΔI_o be the statistical fluctuation of I at the value I_o. The bias voltage on the divider, of which the two sides have resistances R_1 and R_2, would then be given by

$$V_d = \frac{R_2 - R_1}{R_2 + R_1} \times (12 \text{ volt}) - (I_o + \Delta I_o)R_2 \qquad (D2)$$

and the probe bias by

$$V_P = V_d - (I_o + \Delta I_o)R_s \qquad (D3)$$

where R_s is the shunt resistor (see main text figure 1). If $\Delta I_o = 0$, then

$$V_P = \frac{R_2 - R_1}{R_2 + R_1} \times (12 \text{ volt}) - I_o(R_2 + R_s) = V_o \qquad (D4)$$

But because $\Delta I_o \neq 0$ we get a fluctuation of V_o given by

$$\Delta V_o \approx - \Delta I_o (R_2 + R_s) \qquad (D5)$$

Thus the probe current forces the probe bias to a new value

$$V_P' \approx V_o + \Delta V_o \qquad (D6)$$

which corresponds to a new mean value of the current

$$I' \approx I(V_o + \Delta V_o) \qquad (D7)$$

Thus the value of R_2 and R_s scale the "noise" that is generated by the measuring circuit.

The values

$$R_1 + R_2 = R_d = 200\ \Omega$$

and

$$R_s = 20\ \Omega \text{ or } 100\ \Omega$$

were found to give a "noise" of this nature which was smaller than the noise due to the statistical nature of n_e and n_i. This allowed plots of high reproducibility and precision to be obtained thus limiting the overall determination of the desired parameters to their inherent fluctuations alone.

II. Vibrational and Rotation Temperature Measurements and Electron Coupling to Vibrational States

The method described on page 40 of reference D3 was used to measure the vibrational and rotational temperatures of N_2 (prepurified gas, certified to 99.997% by manufacturer) as a function of enthalpy, and to compare them with the electron temperature. The results are summarized in table I of the main text and presented graphically in figure D1.

The rotational temperatures observed agree very well with the rotational temperatures obtained by an expansion from the plenum chamber

conditions to tank pressure when a correction is made to account for a pressure rise (above tank pressure) at the diagnostic point due to the compression waves in the jet (shock diamonds). This correction can be computed from the records of increased electron and ion densities obtained with Langmuir probe surveys of the axial region of the beam; the excellent agreement obtained by this method confirms the identification of the peaks of electron density with the compression shock diamonds observed in the jet.

The vibrational temperatures observed were always approximately 75% to 80% of the stagnation temperature in the plenum chamber, confirming the notion that the flow is vibrationally frozen.

Figure D1 also shows the electron number density n_e as a function of enthalpy. The values of n_e pertain to (a) the arcjet used, (b) operating with those current-voltage characteristics, (c) with prepurified N_2 as used, (d) clean electrodes, (e) free jet geometry, (f) averaged over the shock diamonds.

It is obvious from figure D1 that the electron temperature is very close to the vibration temperature of the molecules. This evidence is in agreement with the theoretical results (ref. D4) that the free electrons in the plasma are very nearly at equilibrium with the vibrational temperature of the nitrogen molecules and are therefore closely coupled energetically with the vibrational modes of the gas molecules. This observation is important in the interpretation of the results of the experiments of electron heating with microwave power for the measurement of the loss factor.

REFERENCES OF APPENDIX D

D1. Langmuir, I.; and Mott-Smith, H.: Theory of Collectors in Gaseous Discharges. Phys. Rev., vol. 28, 1926, p. 727.

D2. Shott, L.: Electrical Probes. In Plasma Diagnostics, W. Lochte-Holtgreven, ed., John Wiley and Sons, Inc., New York, 1968.

D3. Demetriades, S. T.: Interim Final Report on NAS2-3580, STD-68-2, 1 August 1968.

D4. Demetriades, S. T.: Determination of Energy-loss Factors for Slow Electrons in Hot Gases. Phys. Rev. 158, No. 2, June 1967, pp. 215-217.

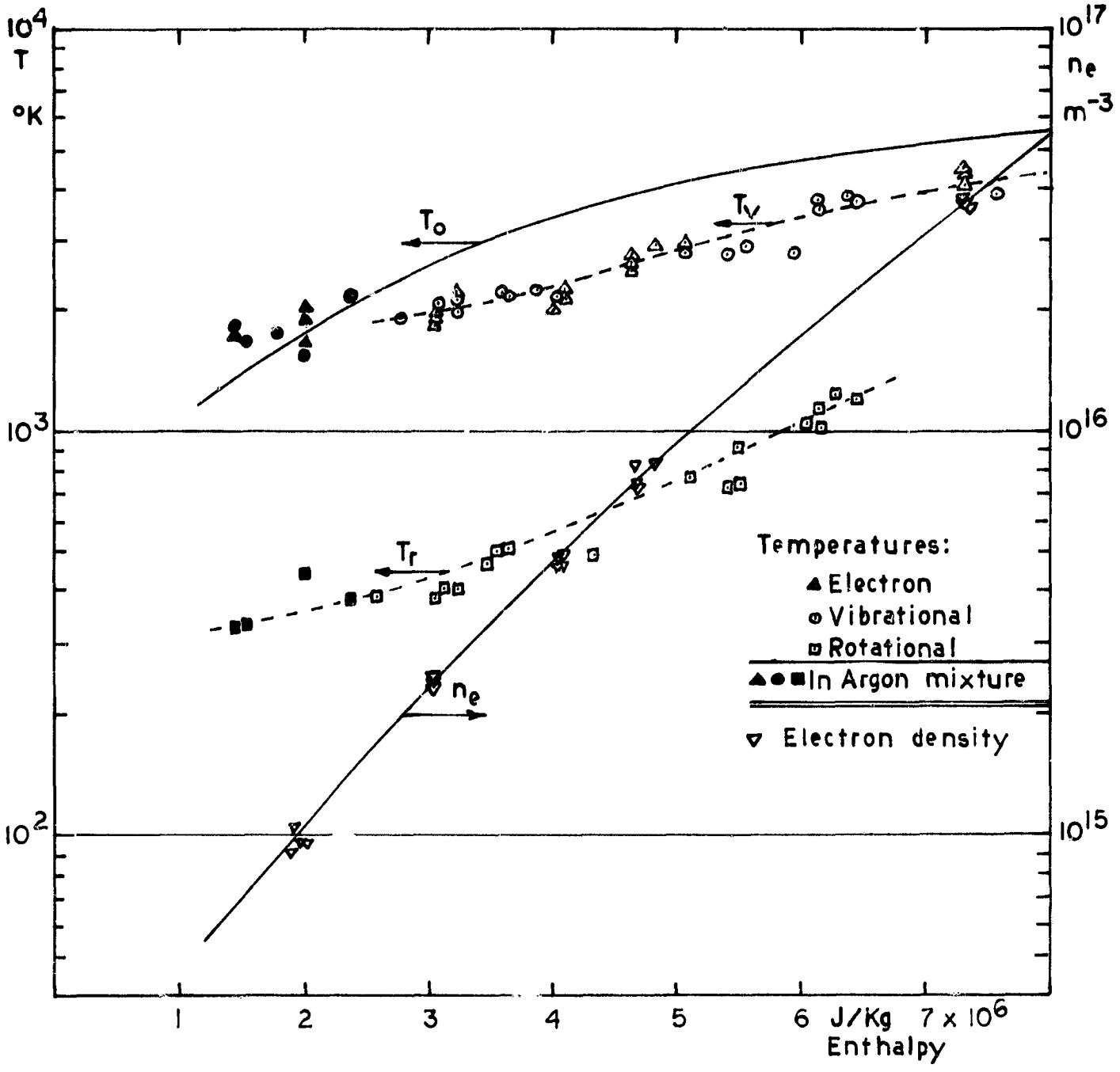

Figure D1. Measured temperatures and number densities in plasmas of pure nitrogen and nitrogen-argon mixtures (55% N_2 - 45% A, by volume), as a function of stagnation enthalpy.

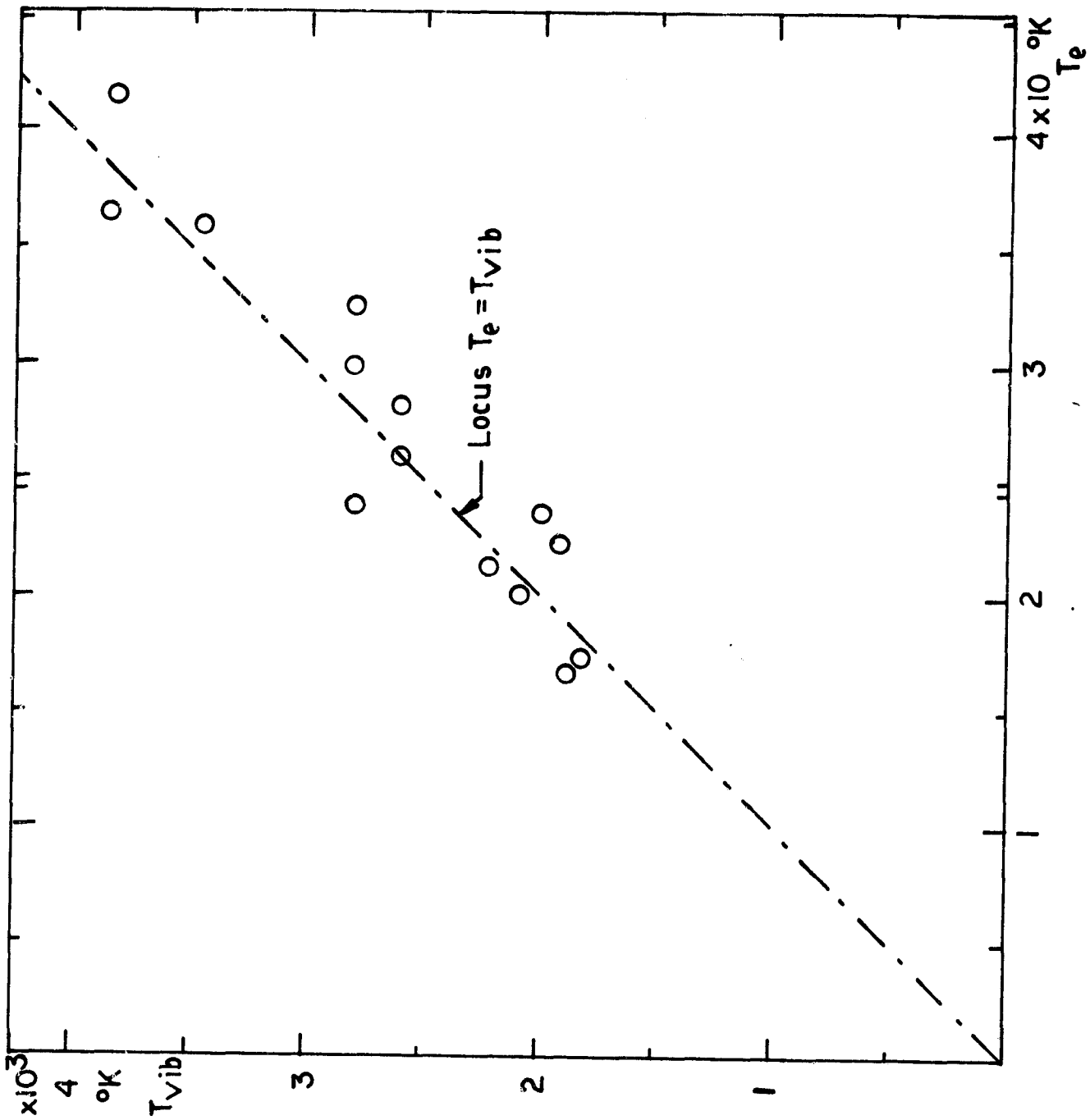

Figure D2. Comparison of measured electron temperatures and vibrational temperatures in arc heated nitrogen

APPENDIX E

RELATIVE MAGNITUDE OF CONTRIBUTIONS TO THE COLLISIONAL ENERGY EXCHANGE INTEGRAL FOR ELECTRONS IN NITROGEN

The collisional energy exchange integral, as given in the main text (equation (10)), has the form

$$Rc^{(2)} = -\frac{3}{2} kn_e \nu_t \delta_{eff} (T_e - T_n) - \dot{R} - \sum_i s_i \epsilon_i \qquad (E1)$$

and describes the total, elastic and inelastic, energy exchange between electrons and heavy particles in hot gases. The particular energy contributions contained in each term are given in some detail in the main text, and it is not necessary to repeat these definitions here. In general, however, it may be said that the last two terms, $\dot{R}$ and $\dot{S} \equiv \sum_i s_i \epsilon_i$, contain only contributions from inelastic processes, i.e., those in which the kinetic energy of the electron-target system is not conserved. On the other hand, the first term contains the entire energy contribution from elastic processes, plus possible energy contributions from inelastic processes such as electron excitation of rotational and vibrational states of polyatomic target particles.

The energy represented by the $\dot{R}$ and $\dot{S}$ terms is negligibly small in the cases of interest for nitrogen. Reference 2 of the main text demonstrates the smallness of $\dot{R}$, relative to $\frac{3}{2} kn_e \nu_t \delta_{eff} (T_e - T_n)$. The $\dot{S}$ term is known to be small at the electron energies involved. The ionization potential for nitrogen is 15.5 eV, and the dissociation energy is 9.76 eV. The average energy of an electron even at 10,000 ^{o}K is only 1.1 eV, which makes electron energy loss through ionizing or dissociating collisions extremely unlikely. Also, ion recombination will be limited since the electron temperature tends (see below) to be in equilibrium with the nitrogen vibrational temperature, which is frozen in our experiments.

Note that, in this formulation, changes in the population of vibrationally and rotationally excited states have not been included in $\dot{S}$, but are part of the inelastic contribution to the first term of $Re^{(2)}$.

$$-\phi \equiv -\frac{3}{2} kn_e \nu_t \delta_{eff} (T_e - T_n) \qquad (E2)$$

Therefore their contributions, which can be large, will be discussed when we analyze ϕ in the following. Also, collisions that create metastables in nitrogen are not included in the $\dot{S}$ term, because the metastable level (the first vibrational level of the electronic ground state) belongs to the class of transitions involving excitation of one of the degrees of freedom of the molecule (translational, rotational, and vibrational). Therefore, nitrogen metastable-creating collisions are more properly included in ϕ.

As was shown in the text, when the left side of the electron energy equation (equation (8)) is zero, it reduces to the algebraic form

$$\vec{J}_e \cdot (\vec{E} + \vec{U} \times \vec{B}) = - Re^{(2)} = \phi + \dot{S} + \dot{R} \tag{E3}$$

Since $\vec{B} = 0$ and $\dot{S} + \dot{R} \approx 0$, we write

$$\vec{J}_e \cdot \vec{E} \equiv \dot{\Omega} = \phi \tag{E4}$$

It follows from the work of Ginzburg and Gurevich (ref. 5 of the main text) that the ohmic heating by a high frequency electric field ($\omega >> \nu_t$) is given by

$$\dot{\Omega} = \frac{e^2 n_e \nu_t E_o^2}{2 m_e \omega^2} \tag{E5}$$

where $E_o^2 = (4Z/A_r)P$ for the particular configuration of the present experiments. Equating ϕ and $\dot{\Omega}$ as defined in equations (E2) and (E5) allows us to measure the effective energy loss factor of the gas in the laboratory (equation (6) of the main text), if the assumption is made that $T_n = T_{e,\,E=0}$. This assumption is justified on the grounds that it is theoretically predicted and experimentally verified that $T_{e,\,E=0} \approx T_{N_2,\,vib}$. It is argued that, since the primary contribution to the effective energy-loss factor δ_{eff} is due to vibrational excitation of the nitrogen molecules, the vibrational temperature $T_{N_2,\,vib}$, which is equal to the electron temperature in the absence of electric field $T_{e,\,E=0}$, is the appropriate reference temperature T_n. We shall show in this Appendix that the measured values of δ_{eff} are consistent with theoretical estimates of the vibrational contribution to ϕ.

To estimate the contribution of vibrational excitation of nitrogen as

a primary energy loss mechanism for electrons, let us split the term into three terms

$$\phi = \phi_{tr} + \phi_{vib} + \phi_{rot} \tag{E6}$$

where ϕ_{tr} is the elastic, translational energy exchange, ϕ_{vib} contains all the energy from vibrational excitation of the nitrogen molecule, and ϕ_{rot} contains the energy of exciting the rotational degrees of freedom of the molecule. The rotational contributions ϕ_{rot} will not be included in the following to simplify the computation (the low measured rotational temperature of the jet leads us to believe that this contribution is small, or at least of the same order of magnitude as the translational contributions). The contribution ϕ_{tr} is given by

$$\phi_{tr} = \frac{3}{2} k n_e \nu_t \delta_{N_2, el} (T_e - T_{e, E=0}) \tag{E7}$$

where $\delta_{N_2, el} = 2m_e/m_{N_2} = 3.89 \times 10^{-5}$.

The term ϕ_{vib} will now be computed from available cross sections for electron excitation and de-excitation of nitrogen. The power delivered by the electrons to the unexcited molecules is

$$\phi_{vib}^{+} = \epsilon_v n_e n_{N_2^*} R_{ex} \tag{E8}$$

where $\epsilon_v \approx 0.3$ eV $= 0.48 \times 10^{-19}$ joule is the approximated value of the transition energy from one vibration level to the next, and $R_{ex} \equiv (1/n_e n_{N_2})(dn_{N_2}/dt)$ is the normalized excitation rate. Similarly, the power delivered to the electrons by the excited molecules is

$$\phi_{vib}^{-} = \epsilon_v n_e n_{N_2^*} R_{de} \tag{E9}$$

where $R_{de} \equiv (1/n_e n_{N_2^*})(dn_{N_2^*}/dt)$ and $n_{N_2^*}$ the number density of vibrationally excited nitrogen molecules. If $\phi_{vib} > 0$, this means that energy is lost from the electrons, and is given by

$$\phi_{vib} = \phi_{vib}^{+} - \phi_{vib}^{-} = \epsilon_v n_e (N_{N_2} R_{ex} - n_{N_2^*} R_{de}) \tag{E10}$$

The absolute values for the total excitation cross section of the

vibrational levels of the N_2 molecule have been measured (see **ref.** E1) and those for the de-excitation cross section of the lowest vibrational level can be obtained by fitting the distribution **shown** in reference E2 to the absolute values given in reference 3 of the text. In both cases the cross sections are given for monoenergetic electrons. The integrated cross sections $Q(T_e)$ are found by folding in a Maxwell distribution

$$Q(T_e) = \frac{\int_o^\infty Q(\epsilon)\epsilon e^{-\epsilon/kT_e} d(\epsilon)}{\int_o^\infty \epsilon e^{-\epsilon/kT_e} d(\epsilon)} \tag{E11}$$

where $Q(\epsilon)$ is the monoenergetic cross section for electrons of energy ϵ.

If this is done for the published values, the results appear as shown in figure E1. The excitation and de-exciation rates, R_{ex} and R_{de}, are computed by multiplying each cross section by the mean electron velocity v_{ea} at each temperature T_e. The results are shown in figure E2.

The number density of excited and ground-state molecules may be found from considerations of statistical mechanics. If the nitrogen molecule is treated as a monochromatic oscillator with equally spaced vibrational energy levels $\epsilon(v) = vh\nu$ $(v = 0, 1, 2, \ldots)$, a quantity u may be defined by

$$u \equiv \frac{h\nu}{kT_{vib}} \equiv \frac{\theta}{T_{vib}} \tag{E12}$$

(for nitrogen $\theta = 3336.6\ ^oK$, ref. E4) such that

$$n_{N_2^*(v>0)} = n_{N_2, tot} \frac{\sum_{i=1}^{\infty} e^{-iu}}{\sum_{i=0}^{\infty} e^{-iu}} = n_{N_2, tot} e^{-u} \tag{E13}$$

and

$$n_{N_2(v=0)} = n_{N_2, tot} \frac{e^o}{\sum_{i=0}^{\infty} e^{-iu}} = n_{N_2, tot}(1 - e^{-u}) \tag{E14}$$

with these expressions for the number densities, equation (E10) becomes

$$\phi_{vib} = \epsilon_v n_e n_{N_2} [(1 - e^{-u}) R_{ex} - e^{-u} R_{de}] \qquad \text{(E15)}$$

The implicit assumption made in obtaining equation (E15) is that the normalized rates for de-excitation of the $(v = 1)$ state of the molecule (which were the only ones available in the literature) are the same as those for the de-excitation of any level v to the next level $v-1$. Note that de-excitation collisions involving transitions with greater energy than $\epsilon = h\nu = 0.3$ eV have been neglected.

An excellent check for both the validity of equation (E15) and the self-consistency of the excitation and de-excitation rates in figure E2 can be made by considering the case in which the electrons have reached equilibrium with all the degrees of freedom of the molecule. In particular, this means $\phi_{vib} = 0$ and $T_e = T_{vib}$. Equation (E15) then simplifies to

$$R_{ex} = \frac{1}{e^{u_o} - 1} R_{de} \qquad \text{(E16)}$$

where $u_o = 0/T_{vib} = 0/T_e$. A plot of R_{ex} and $R_{de}/(e^{u_o} - 1)$ is shown in figure E3. The two agree to within 20% over the entire range of temperatures from 2000 - 6000 ^{o}K.

By combining equations (E7) and (E15), we can give equation (E6) the form

$$\phi = \epsilon_v n_e n_{N_2} [(1 - e^{-u}) R_{ex} - e^{-u} R_{de}] + \frac{3}{2} k n_e \nu_t \delta_{N_2, el} (T_e - T_{e, E=0}) \qquad \text{(E17)}$$

In light of equation (E4), the ratio $\phi/\dot{\Omega}$ should be close to 1 for the experimental data. The value of $\phi/\dot{\Omega}$ is given in Table E-I and figure E4 for most of the pure nitrogen data obtained in our laboratory. It is seen that $\phi/\dot{\Omega}$ is actually somewhat higher than 1, on the average. This is perhaps due to the tolerances on the excitation and de-excitation rates, relating in part to the 20% inaccuracy of equation (E16).

The significance of this calculation, however, is that the major

contribution to $\phi/\dot{\Omega}$ comes from $\phi_{vib}/\dot{\Omega}$, rather than $\phi_{tr}/\dot{\Omega}$, as can be seen in table E-I. The term $\phi_{vib}/\dot{\Omega}$ amounts to at least 90% of the total in most of the cases examined. This calculation demonstrates that the measured δ_{eff} is consistent with the above independent theoretical estimate of ϕ_{vib}, verifies that the major contribution to the measured energy-loss factor comes from collisions involving vibrational transitions in the nitrogen molecule, and that $T_{e, E=0} = T_{vib}$ is indeed the correct reference temperature T_n to use in the computation of nitrogen energy-loss factors.

REFERENCES OF APPENDIX E

E1. Sobolev, N. N.; and Sokovikov, V. V.: "A Mechanism Ensuring Level Population Inversion in CO_2 Lasers," ZhETF Pis'ma 4, 8, October, 1966, pp. 303-307 - JETP lett. 4, 204, 1966.

E2. Hurle, J. R.: "On the Thermal Energy Transfer Between Free Electrons and Molecular Excitation," J. Chem. Phys. 41, 11, December, 1964, pp. 3592-3603.

E3. Engelhardt, A. G.; Phelps, A. V.; and Risk, C. G.: "Determination of Momentum Transfer and Inelastic Cross Sections for Electrons in Nitrogen Using Transport Coefficients," Phys. Rev. 135, 6A, September, 1964, pp. A1566-A1574.

E4. Mayer, J. E.; and Mayer, M. G.: Statistical Mechanics, New York, John Wiley and Sons, 1940.

Table EI. Theoretical estimates of $\phi/\dot{\Omega}$ and the non-vibrational contribution to ϕ for representative electron temperature elevation data in prepurified nitrogen.

P (watt)	$T_{e,E=0}$ (°K)	T_e (°K)	$\phi/\dot{\Omega}$	$(\phi_{tr}+\phi_{rot})/\phi$ (%)
1.70	2840	3615	1.15	5.4
1.28	3021	3609	0.73	8.6
2.56	2975	4230	2.11	3.2
5.10	2940	4725	2.02	2.4
1.54	3290	4440	3.07	3.3
2.48	3240	4580	2.53	2.9
3.60	3110	4600	2.10	2.7
4.45	3020	4460	1.59	2.8
2.60	2200	3560	2.09	3.4
1.70	2085	3165	1.95	4.5
0.85	2150	2486	0.59	9.3
0.42	2135	2471	1.21	9.0
0.42	2135	2454	1.14	9.1
0.85	2085	2825	1.95	6.2
0.85	2250	2704	0.78	9.5
1.26	2200	3022	1.58	5.6
1.69	2335	3075	0.98	6.1
2.11	2415	3657	2.27	3.6
2.54	2285	3375	1.41	4.2
3.06	2450	3610	1.38	3.8
3.20	2170	3495	1.60	3.6
0.85	2100	2739	1.52	6.8

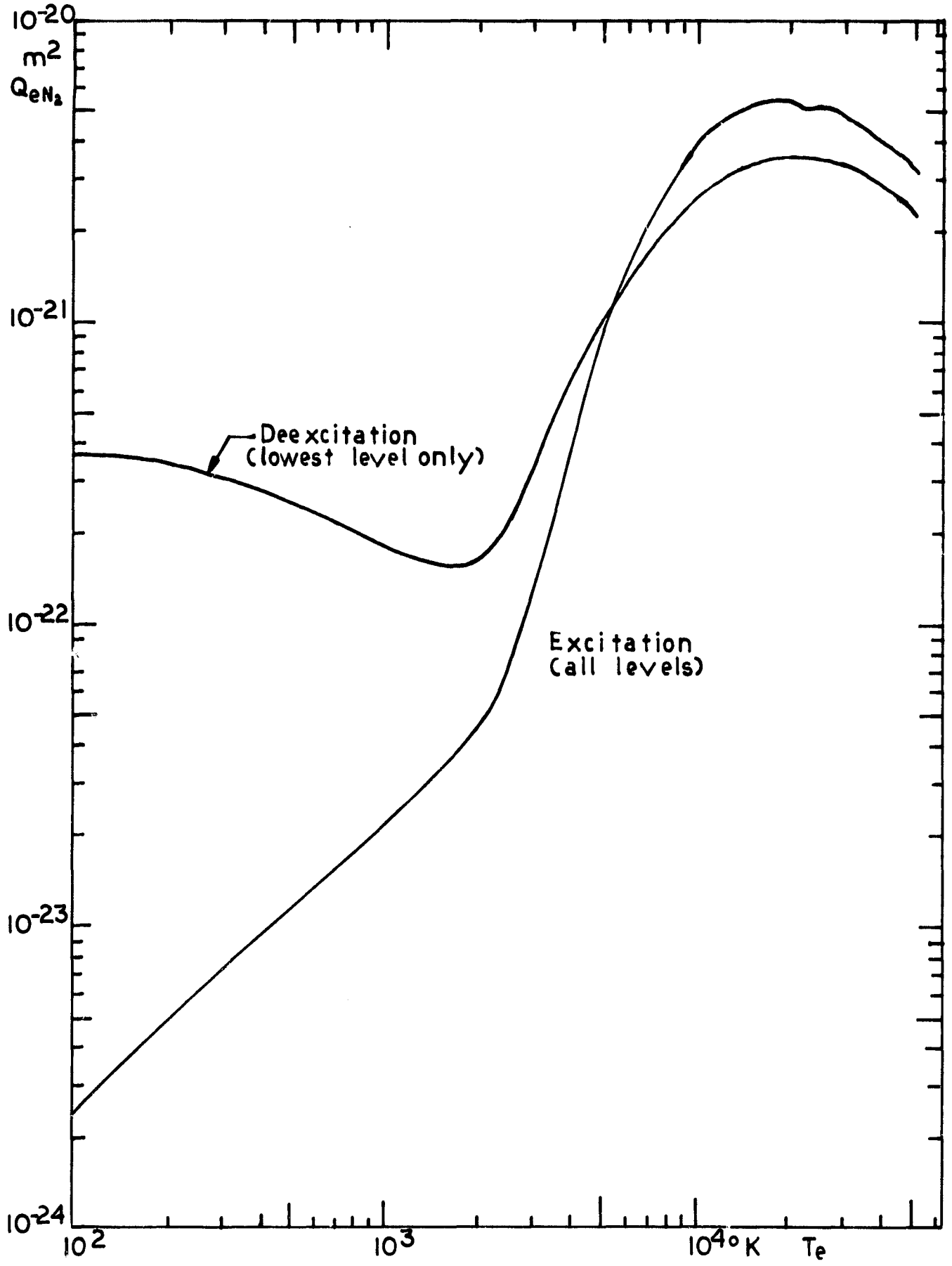

Figure E1. Excitation and de-excitation cross sections, $Q_{eN_2,ex}$ and $Q_{eN_2,de}$, as a function of electron temperature for nitrogen

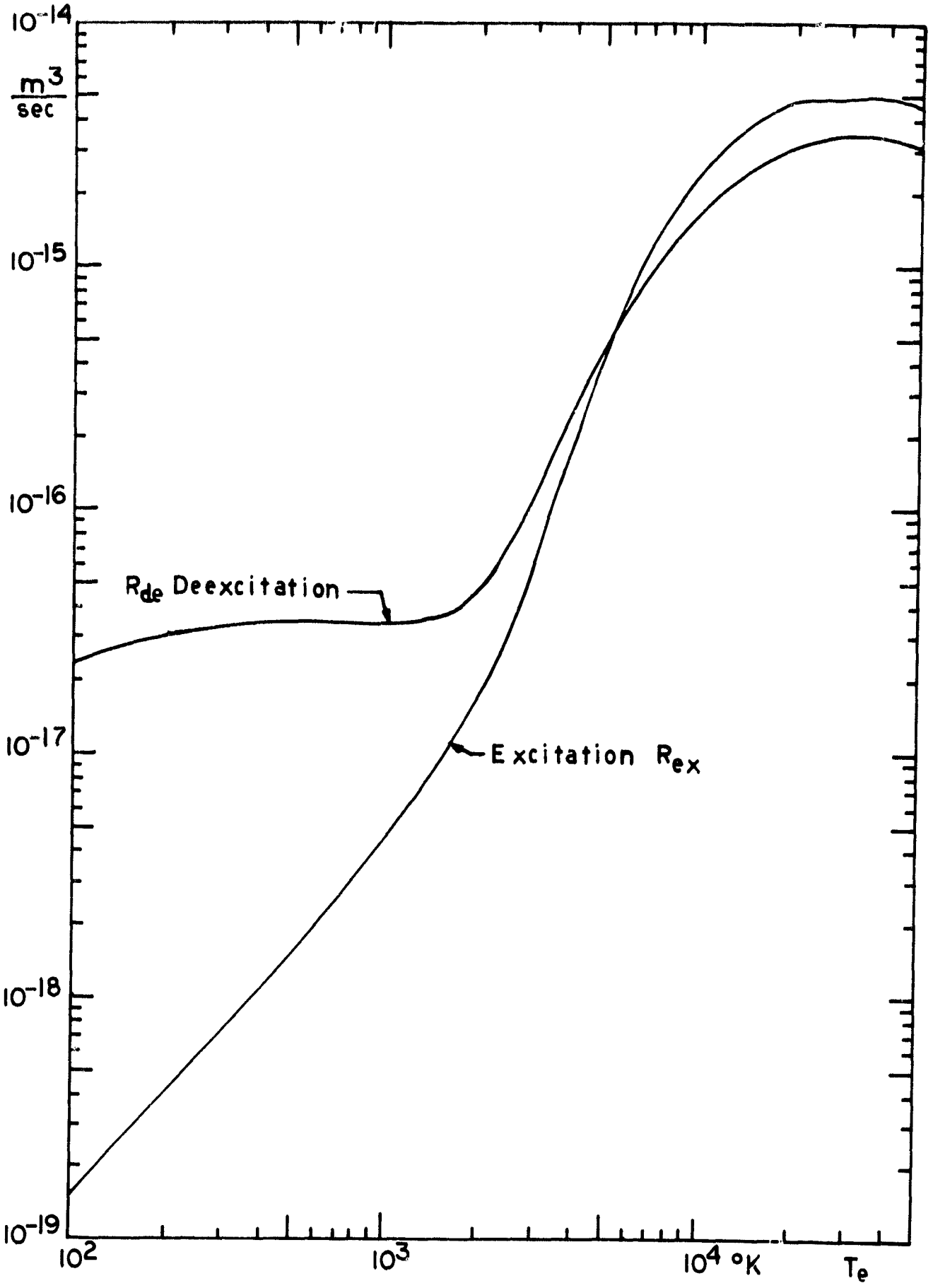

Figure E2. Normalized rates R_{ex} or R_{de} for excitation and de-excitation of nitrogen

$$R_{ex,\,de} = \frac{1}{n_{N_2} n_e}\left[\frac{dn_{N_2}}{dt}\right]_{ex,\,de}$$

Derived by integrating the cross sections for the process into a Maxwellian electron distribution

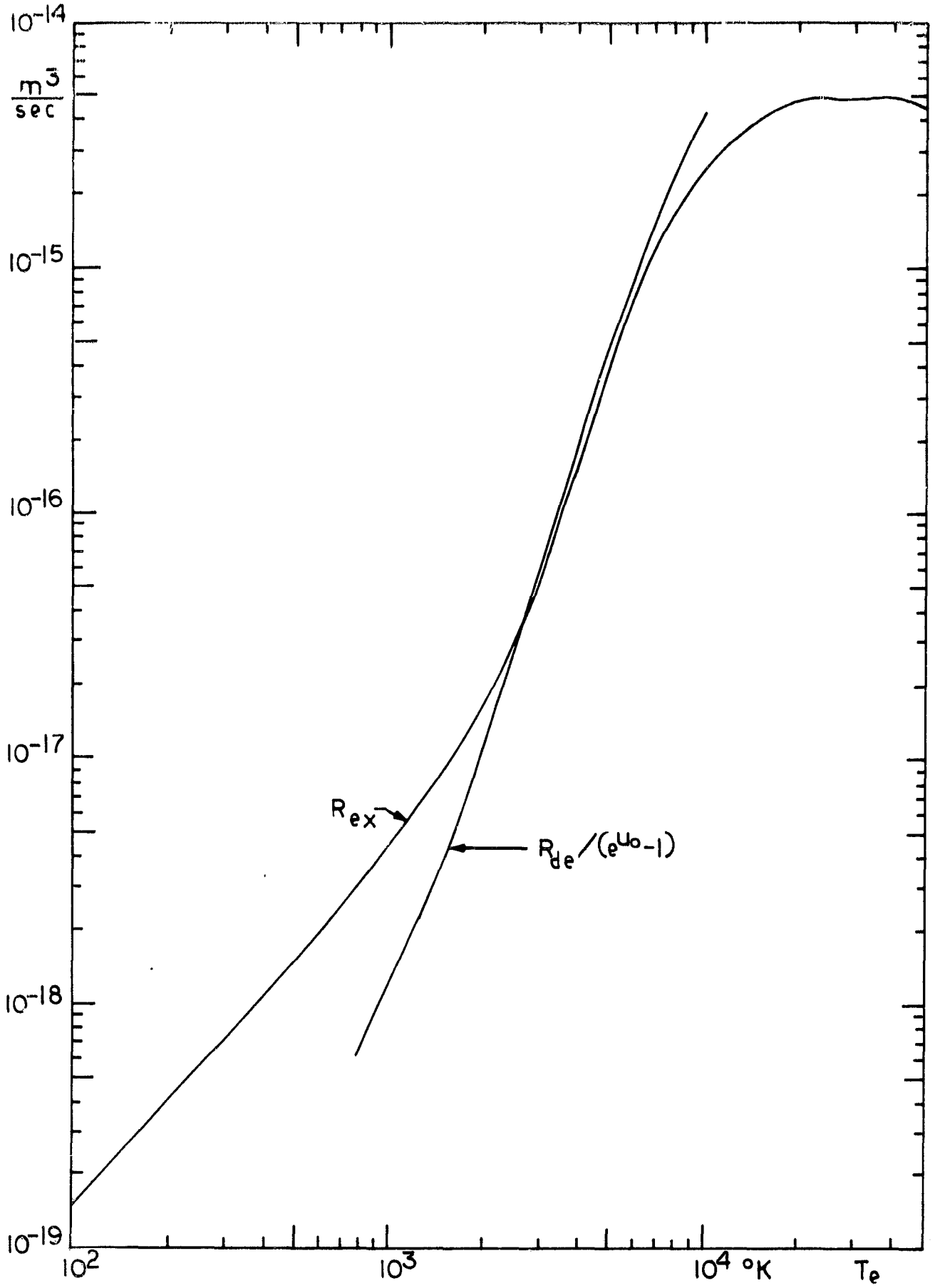

Figure E3. Excitation rate of nitrogen and de-excitation rate weighted by the ratio $n_{N_2^*(v>0)}/n_{N_2(v=0)}$ of the number densities at equilibrium ($T_{vib} = T_e$), as a function of electron temperature

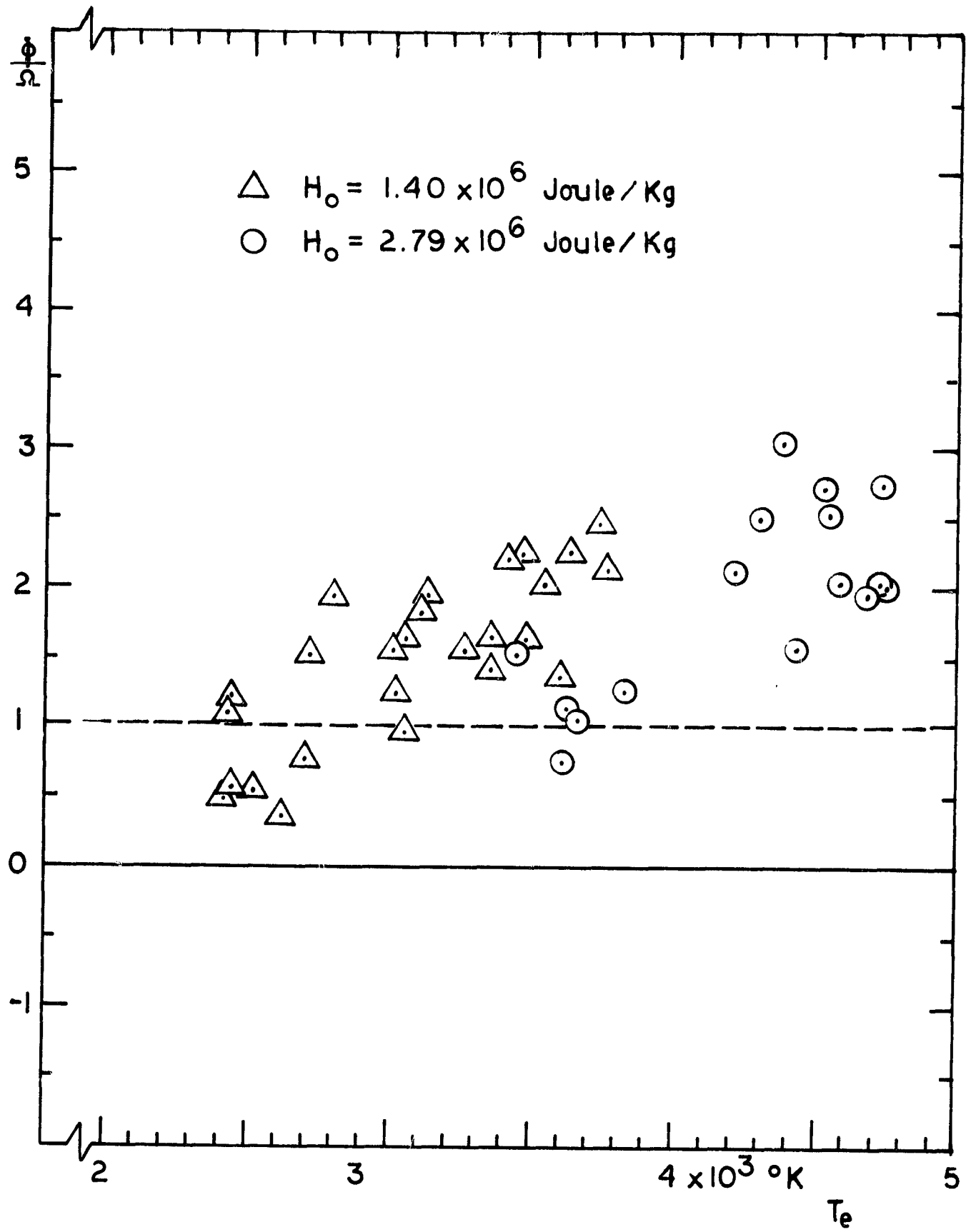

Figure E4. Ratio of theoretical estimate of the first term ϕ of the collisional energy exchange integral $R_e^{(2)}$ to experimental value of the ohmic heating in a pure nitrogen plasma, as a function of electron temperature

APPENDIX F

ELECTRON-ION RECOMBINATION AND THE SUBSEQUENT DE-EXCITATION OF RESONANT AND METASTABLE LEVELS OF ARGON

The energy level diagram of the argon atom is shown schematically in figure F1 on which some of the salient features of the collisional-radiative recombination model are indicated. Figure F1 also illustrates the de-excitation mechanism of the lower levels that are considered here.

The de-excitation of the 4s levels are not considered in detail in the recombination model because the minimum de-excitation occurs at a higher level. However, the assumption that only downward transitions occur as the electron cascades to the ground state cannot be made a priori. This is because the collisional rates are strong inverse functions of the energy difference of the transition, and the energy difference for the upward jump from level (1) to level (2) is only 0.07 eV, whereas the energy difference to the ground state is over 11.5 eV.

The collisional de-excitation rates have been determined using the classical Gryzinski cross sections * as described in reference F1 and given in units of $cm^{-3}sec^{-1}$. The transition probabilities are determined from the lifetime measurements of reference F2. At $T = 2000\ ^{o}K$, we find

$$K_{1,2} = 7.5 \times 10^{-5}$$

$$K_{1,0} = 4 \times 10^{-11}$$

$$A_{2,0} = \frac{1}{8.6 \times 10^{-9}} = 1.2 \times 10^{-8}\ sec^{-1}$$

Let $\partial n/\partial t$ represent the rate of change of population of level n due to each of the de-excitation mechanisms. We can then express

$$\partial n_1/\partial t \Big)_{1\rightarrow 2} = -n_e n_1 K_{12}$$

$$\partial n_1/\partial t \Big)_{1\rightarrow 0} = -n_3 n_1 K_{10}$$

---

* The cross sections are applicable only for allowed optical transition. The determined values of the rate constants are too large for forbidden transitions.

$$\frac{\partial n_1/\partial t)_{1\rightarrow 2}}{\partial n_1/\partial t)_{1\rightarrow 0}} = \frac{7.5\times 10^{-5}}{4\times 10^{-11}} = 10^{6}$$

Similarly, the ratio of the radiative de-excitation of the resonant level to the ground state de-excitation of the metastable level may be found. This is given by

$$\frac{\partial n_2/\partial t)_{rad}}{\partial n_1/\partial t)_{1\rightarrow 0}} = \frac{n_2 A_{2,0}}{n_e n_1 K_{1,2}} = \frac{n_2}{n_1}\ \frac{10^{18}}{n_e}$$

At $n_e = 10^{10}$ cm^{-3}, this ratio is $(n_2/n_1)\cdot 10^{8}$. Because most of the radiation is trapped, the effectiveness of the radiative transition in de-populating the resonant levels will be greatly diminished. As pointed out in other sections, the line centers will be strongly absorbed but some radiation will escape through the line wings. If this "escape factor" is as large as 10^{-5} it would appear that the resonant and metastable levels will stay closely coupled because of the rapid collisional rates between the levels as expressed by $K_{1,2}$. That is, if the metastable level tends to become over-populated from downward transitions into the level, the fast upward collisional transitions from the nearby resonant level will tend to keep the relative population of the two levels near the value specified by the Boltzmann distribution.

REFERENCES OF APPENDIX F

F1. Goldstein, R.: JPL Technical Report 32-1372, 1969.

F2. Lawrence, G. M.: Phys. Rev. 175, 1968, p. 40.

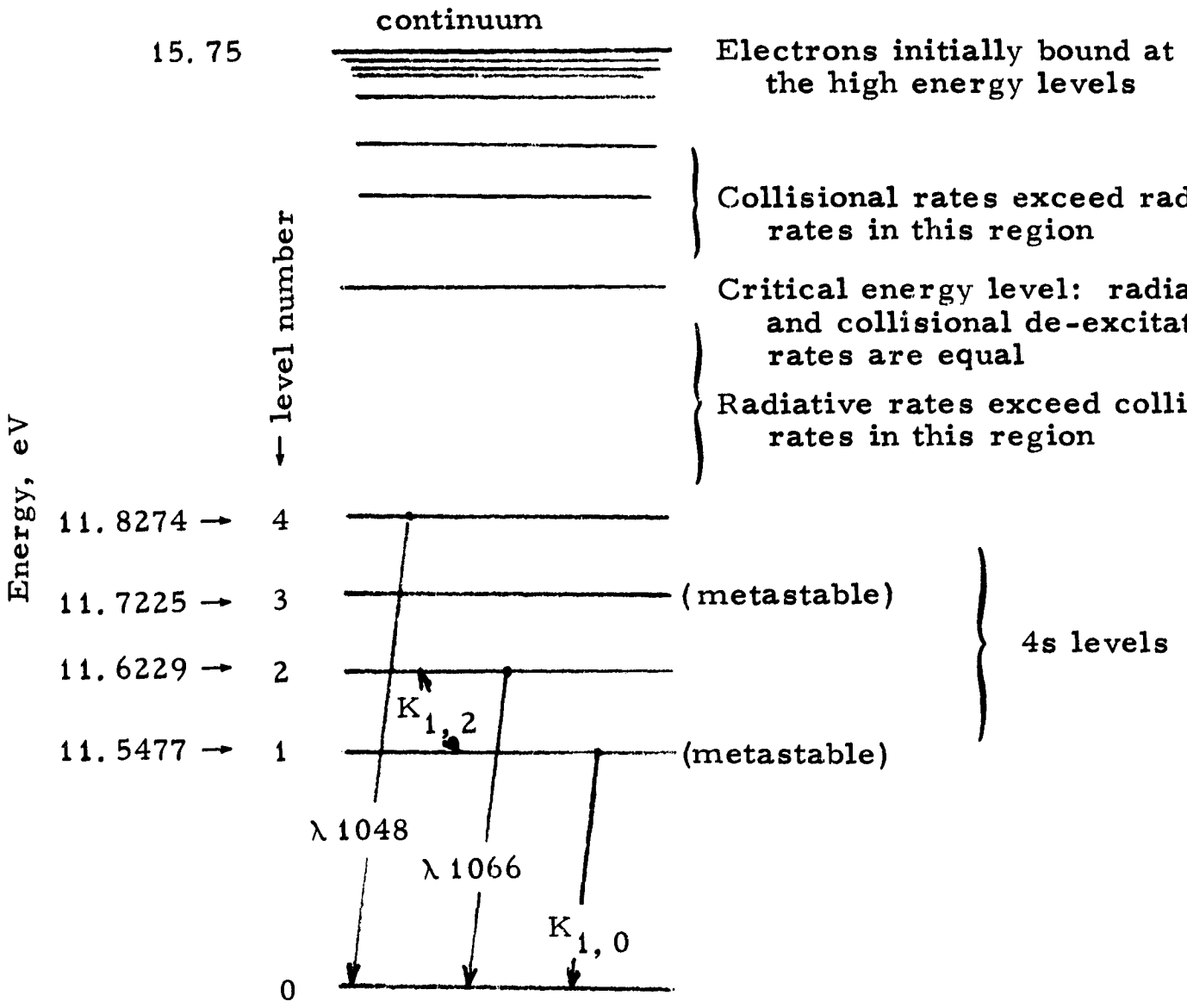

Figure F1. Schematic energy level diagram of the argon atom showing the main features of the recombination model and some of the mechanisms of de-exciting the lowest excited levels

APPENDIX G

ABSORPTION OF RESONANT RADIATION

The photon mean-free-path of an argon resonant line is estimated for the conditions of the present experiments. For this purpose, a simple planar geometry, in which the plasma properties are uniform over a distance ℓ, is considered.

The decrease of the intensity, I_ν, of a spectral line of frequency ν may be expressed as

$$(I_\nu)_2 = (I_\nu)_1 \exp(-k_\nu \ell) \tag{G1}$$

where k_ν, the absorption coefficient, depends on the line shape. The total intensity of a line is found by integrating over the full line width, $\Delta\nu$.

$$(I_{\nu_0}) = \int_{\Delta\nu} (I_\nu)\, d\nu \tag{G2}$$

Combining equations (G1) and (G2) we obtain

$$\frac{(I_{\nu_0})_2}{(I_{\nu_0})_1} = \frac{\int_{\Delta\nu_2} (I_\nu)_1 \exp(-k_\nu \ell)\, d\nu}{\int_{\Delta\nu_1} (I_\nu)_1\, d\nu} \tag{G3}$$

For a slightly ionized, low density plasma, Stark broadening and collisional broadening are small, and we may assume that only Doppler broadening is important. Consider a line centered at the frequency ν_0, where the intensity is I_0; the line profile I_ν, the absorption coefficient k_ν, and the Doppler width of the line $\Delta\nu_D$ given by (ref. G1)

$$I_\nu = I_0 \exp(-\omega^2/a^2) \tag{G4}$$

$$k_\nu = k_0 \exp(-\omega^2) \tag{G5}$$

$$\Delta\nu_D = 2 (\ln 2)^{1/2} \frac{v}{\lambda_0} = 2 (\ln 2)^{1/2} \frac{v}{c} \nu_0 \tag{G6}$$

where

$$v = (2kT/M)^{1/2} = \text{velocity of atoms in the absorber}$$

$$c = \text{velocity of light}$$

$$\omega = \frac{\nu - \nu_0}{\nu_0} \frac{c}{v} \tag{G7}$$

$$a = \frac{\text{Doppler width of source}}{\text{Doppler width of absorber}} = \left(\frac{T_{source}}{T_{absorber}} \right)^{1/2} = \frac{\Delta\nu_1}{\Delta\nu_2} \tag{G8}$$

$$k_0 = \frac{(\pi)^{1/2} e^2}{4\pi\epsilon_0 m_e v} \frac{f_{01} n_0}{\nu_0}$$

$$= \frac{2(\pi \ln 2)^{1/2} e^2}{4\pi\epsilon_0 m_e c} \frac{f_{01} n_0}{\Delta\nu_D} \tag{G9}$$

$$n_0 = \text{number density of absorbing ground state atoms}$$

$$f_{01} = \text{oscillator strength of the resonant line}$$

Equation (G3) may now be written

$$\frac{(I_{\nu_0})_2}{(I_{\nu_0})_1} = \frac{\int_{-\infty}^{\infty} \exp - (\omega^2/a^2 + k_0 \ell e^{-\omega^2}) \, d\omega}{\int_{-\infty}^{\infty} \exp (-\omega^2/a^2) \, d\omega} \tag{G10}$$

The right-hand side of equation (G10) has been evaluated by Hamberger (ref. G1) as a function of $k_0\ell$ for various a (figure G1). For our purposes we have assumed constant plasma properties and the line widths are constant throughout; hence, $a = 1$. This is a conservative assumption in the situation where a line from a hot plasma is absorbed by a colder boundary. For the AI λ1048 line, and for a plasma at a pressure of 0.3 Torr, static gas temperature 300 °K and electron temperature of, say, 5000 °K, we obtain

$$\lambda_0 = 1048 \text{ Å} = 1.048 \times 10^{-7} \text{ m}$$

$$\nu_0 = \frac{c}{\lambda_0} = 2.86 \times 10^{15} \text{ sec}^{-1}$$

$$v = \left(\frac{2 \times 1.38 \times 10^{-23} \times 300}{40 \times 1.66 \times 10^{-27}} \right)^{1/2} = 3.54 \times 10^2 \text{ sec}^{-1}$$

$$\Delta\nu_0 = 2 \times 0.833 \frac{354}{1.048 \times 10^{-7}} = 5.63 \times 10^9 \text{ sec}^{-1}$$

$$f_{01} = 0.1 \quad \text{(from ref. G2)}$$

$$n_0 = \frac{p}{kT} \frac{0.3 \times 1.333 \times 10^2}{1.38 \times 10^{-23} \times 300} = 10^{22}\ m^{-3}$$

$$k_0 = \frac{1.77 \times 2.56 \times 10^{-38} \times 9 \times 10^2}{9.11 \times 10^{-31} \times 354} \frac{10^{21}}{2.86 \times 10^{15}} = 4.42 \times 10^5\ m^{-1}$$

From figure G1 we see that, for $\ell = 1$ cm,

$$\frac{(I_{\nu_{0}})_2}{(I_{\nu_{0}})_1} \cong 10^{-4}$$

Thus, we conclude that the resonant radiation is strongly trapped at the conditions of the proposed experiments.

At lower pressures, the absorption is greatly reduced. For example, at the same temperature and at a pressure of 10^{-5} Torr, we find $k_0 = 14.7$ m^{-1} and, for $\ell = 1$ cm, $(I_{\nu_{0}})_2 / (I_{\nu_{0}})_1 = 0.95$. The proposed method of measuring the resonant radiation will make use of an evacuated tube at approximately 10^{-5} Torr, so that negligible absorption will occur in the tube.

The photon mean-free-path λ_r of an argon resonant line can now be estimated by considering it to be equal to the absorber thickness ℓ for which the intensity ratio $\tau \equiv (I_{\nu_{0}})_2 / (I_{\nu_{0}})_1$ is equal to 1/exp (1). Figure G1 shows that, for $a = 1$, τ is equal to 1/exp (1) when $k_0 \ell = 2$. We deduce that, under the conditions of our experiment, $\lambda_r = 2/k_0 = 4.5 \times 10^{-6}$ m. In terms of this mean-free-path λ_r, we can now simply estimate the ratio of the escaping resonant radiation to the total (uniform) resonant radiation: Consider the plasma jet as a cylinder of radius r (in our experiments $r \approx 2$ cm). The escaping part of the resonant radiation will all come from the skin of thickness λ_r. Therefore, the ratio of the escaping to the total resonant radiation will be given by the cross section ratio (figure G2)

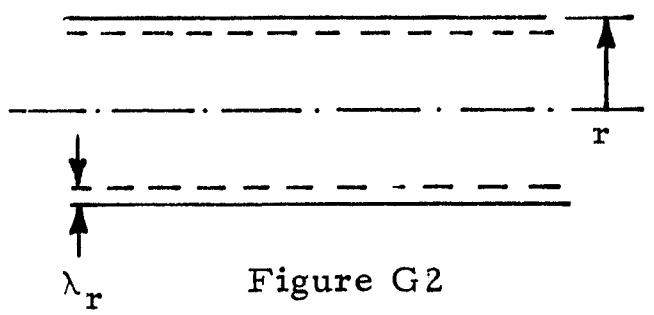

Figure G2

$$\dot{R} \equiv \frac{2\pi r \lambda_r}{\pi r^2} = 2\frac{\lambda_r}{r}$$

Thus, for the conditions of our experiments, we find that $\dot{R} = 4.5 \times 10^{-4}$. We conclude that only 4.5 parts in 10,000 of the resonant radiation escapes, and thus becomes part of $\dot{R}$ in the electron energy equation.

It would be desirable to estimate the importance of the escaping resonant radiation in the electron energy balance; in our experiments the magnitude of the terms of the electron energy balance are of the order of a few watts. The total power input in the arc is of the order of 5 kw. Of this power, approximately 1 kw is added to the gas, while the rest is carried away by the cooling water. Out of the 1 kw added to the gas, approximately 900 watts go into raising the static enthalpy and the kinetic energy of the jet. We estimate that at most 100 watts go into exciting the gas to a state from which radiative transitions can occur. Let us assume conservatively, in order to find an upper limit to the escaping resonant radiation, that all these 100 watts are available for resonant radiation. Of this power, if the assumptions used above apply, only 4.5 parts in 10,000 would escape and thus become part of $\dot{R}$. In other words, the part of $\dot{R}$ that consists of escaping resonant radiation could be, at most, of the order of 4.5×10^{-2} watts. This term would be very small compared to the other terms of the electron energy balance, since these terms, as mentioned above, are of the order of a few watts. In fact, it would even be small compared to the rest of $\dot{R}$ (namely to the radiation loss in the visible and infrared range), since the latter has been found to be indeed significant in the higher rf-power range of our experiments (see figure 3 of main text).

We conclude that the escaping part of the resonant radiation can be expected to give a negligible contribution to the electron energy balance equation under the conditions leading to the result $\lambda_r = 4.5 \times 10^{-6}$.

REFERENCES OF APPENDIX G

G1. Hamberger, S. M.: "Measurement of neutral atom density in a highly ionized plasma by absorption of line radiation," Proceedings of the Fifth International Conference on Ionization Phenomena in Gases (Munich, 28 August - 1 September 1961); edited by M. Maecher, North-Holland Publishing Company, Amsterdam, 1962.

G2. Gruzdev, P. F.: "Oscillator strengths of resonance lines in the spectra of NeI, ArI, KrI, XeI atoms and NaII and RbII ions," Optics and Spectroscopy 22, 1967, p. 170.

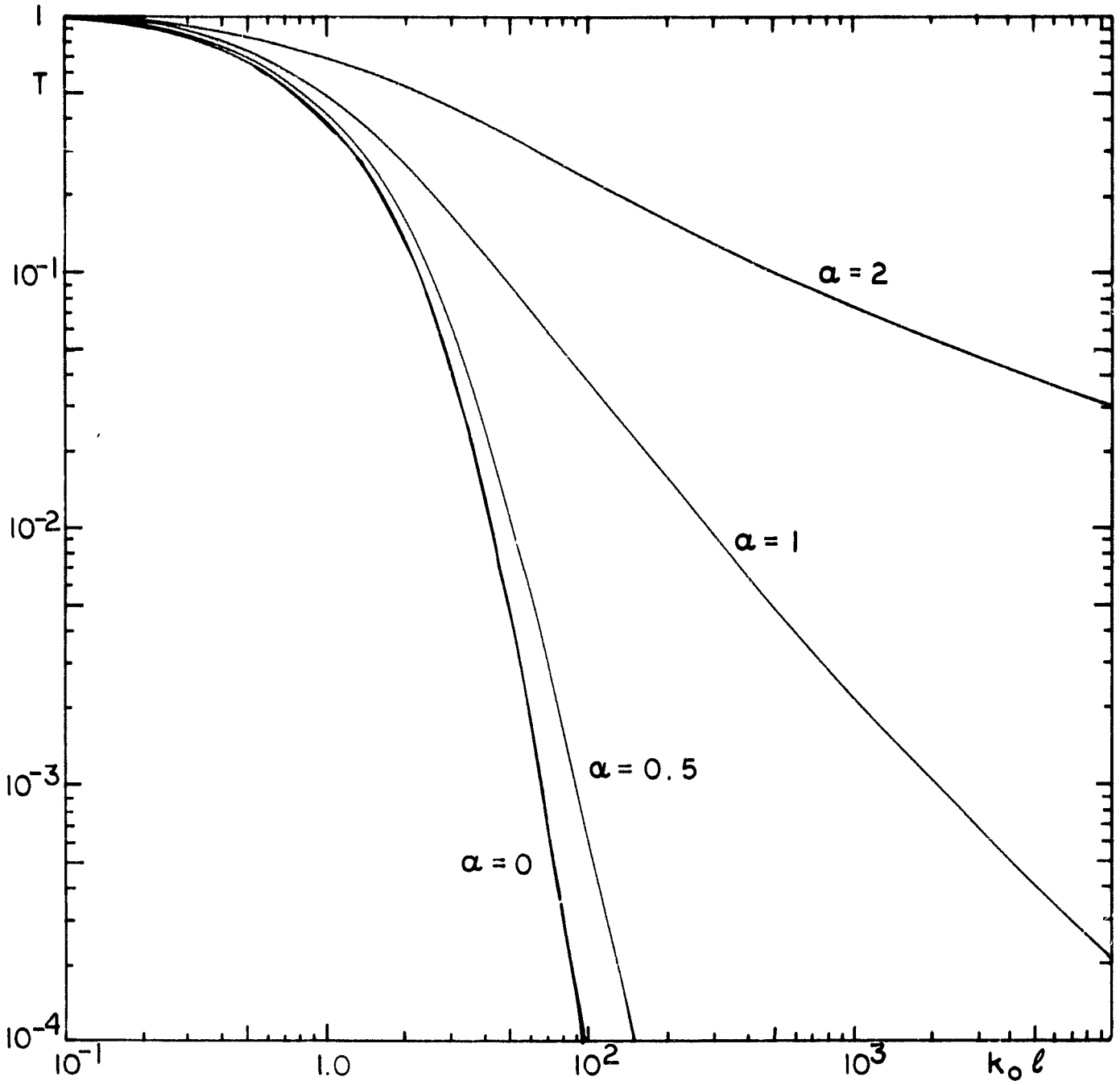

Figure G1. The transmission of a Doppler broadened line (Ref. G1)